

Biofilm morphogenesis on soft hydrogels

Présentée le 3 mars 2023

Faculté des sciences de la vie
Unité du Prof. Persat
Programme doctoral en science et génie des matériaux

pour l'obtention du grade de Docteur ès Sciences

par

Alice CONT

Acceptée sur proposition du jury

Prof. A. Mortensen, président du jury
Prof. A. L. A. Persat, directeur de thèse
Prof. A. Dal Co, rapporteuse
Dr E. Secchi, rapporteuse
Prof. E. Amstad, rapporteuse

Acknowledgements

It is now time to thank all the people that were by my side in the past 5 years.

First of all, I want to thank my thesis supervisor Prof. Alexandre Persat for giving me the opportunity to explore the fascinating world of bacteria, despite my different educational background. He believed in me and he encouraged me throughout the years. He supported me both scientifically, by engaging with me in scientific discussion, providing valuable comments and stimulating my critical thinking, and at the human level.

I would like to thank the jury members Prof. Esther Amstad, Prof. Alma Dal Co and Dr. Eleonora Secchi for taking the time to review my work.

I want to express my full gratitude to what has been a big family for me during these 5 years: the Persat lab. I want to mention every member of the lab, present and past, as everyone contributed in creating an amazing workplace environment, characterized by mutual help and enjoyable scientific conversations, but, most of all, many laughs. In order of arrival: Zainebe, Lorenzo, Xavier, Tamara, Jeremy, Sophia, Marco, Alessandra, Pascal, Sourabh, Sofya, Tania, Alix, Lucas, Hanyi and Gani. A particular thanks goes to Tamara and Jeremy, for having been close friends, desk neighbors and flatmates, to Marco for his special humor and to Sourabh and Tania for the many after-work beers and long personal discussions. The relationship we built over the years goes well beyond being simply good colleagues. We shared joys, sorrows and many special moments that are not restricted to the lab space. Board games, dinners and drinks, hikes and sport, are just some examples of the activities we did together. We are dear friends and I hope it will stay that way in the future.

I would like to thank my students Joseph and Florent, because I probably learned more from them than they did from me.

I am grateful to the many other people that I met along the way inside and outside EPFL, as everyone left me with a good memory. In particular, I want to thank my flatmates and ex-flatmates Hugo, Jarka, Guanhao, Rachel and Claudia for all the time spent together chatting, watching movies,

cooking and having fun. A big thank you goes to my ex colleagues from the SMaL lab, especially Mathias, for inspiring scientific collaborations and discussions and for the nice time spent together as friends. I would like to thank Vance and the crowd of the 'Soirées ludiques'. A special thanks goes to Fabio, for his friendship and for being a person I can always count on. I thank Alex for having been part of my life.

I would like to express my gratitude to Amir for the precious time we spent together in the past months and for being so supportive and understanding.

Finally, I want to thank my family and the friends of a lifetime back in Italy. The biggest thanks go to my parents and my brother, for always being there for me with their unconditional love. Distance was not easy for both sides. Feeling so much loved and welcomed every time I went back home has always been reinvigorating.

Abstract

Bacteria often colonize their environment in the form of surface attached multicellular communities called biofilms. Biofilms grow from surface-attached cells that undergo division while self-embedding in a viscoelastic matrix. Biofilms grow at the surface of biotic and abiotic materials with a wide range of mechanical properties. In particular, during infections and in microbiota, the association of the bacterial cells with the surface of soft tissues is of fundamental importance for successful colonization. For a long time, the field of microbiology has focused on biochemical aspects of infection and biofilm formation. There is now evidence that mechanical forces play critical roles in bacterial physiology and impact biofilm formation and stability. For example, evidence is emerging that fluid flow and physicochemical substrate material properties impact biofilm formation. We are however still missing a rigorous investigation of how the mechanical properties of a substrate material impacts biofilm morphogenesis and its relevance in the context of infection.

In the laboratory, bacteria are traditionally grown in liquid cultures, on agar plates or in flow cells with glass or hard plastic as a surface. However, these systems do not recapitulate the mechanical complexity of a real infection environment, where bacteria most often colonize soft tissues while experiencing flow. To solve these technical limitations, I combined synthetic PEGDA hydrogels with microfluidics which enabled high-resolution live imaging of single bacteria and biofilm formation while interacting with soft substrates in flow.

In chapter 2, I show that the pathogens *Vibrio cholerae* and *Pseudomonas aeruginosa* deform the synthetic soft gels. This behavior is the result of a buckling instability generated by the buildup of compressive mechanical stress inside the growing biofilm and its adhesion to the substrate. By using mutants in matrix components and comparing overproducer strains with wild type ones we showed that cell-cell cohesion and cell-substrate adhesion simultaneously drive deformation. In addition, we found that buckling biofilms can exert forces that compromise the integrity of soft epithelial cells monolayers, thus suggesting that biofilm can mechanically compromise host integrity.

In chapter 3, I investigated the effect of substrate mechanical properties on *P. aeruginosa* biofilm morphology. We showed that biofilms take different shapes as a function of substrate mesh size due to differences in exploratory twitching motility. The mechanical control of single-cell twitching speed, gives rise to a range of architectures that vary from compact, dome shaped biofilms to flat and dispersed ones, ultimately influencing both their tolerance to antibiotics and the spatial structure of different lineages.

Overall, our results show that the mechanical coupling with soft substrates impacts bacterial phenotypes such as surface motility and biofilm architecture and can play a role in the outcome of an infection both by modulating the biofilm susceptibility to antibiotics or by actively becoming a source of virulence.

Keywords

Pseudomonas aeruginosa, *Vibrio cholerae*, microbiology, hydrogels, biofilm, biofilm morphomechanics, mechanobiology, twitching motility

Sommario

I batteri spesso colonizzano il loro habitat sotto forma di comunità multicellulari attaccate alla superficie chiamate biofilm. I biofilm si sviluppano a partire da cellule che si dividono e che allo stesso tempo si amalgamano con una matrice viscoelastica da loro stessi prodotta. I biofilm crescono sulla superficie di materiali biotici e abiotici che hanno un'ampia gamma di proprietà meccaniche. In particolare, durante le infezioni e nel microbiota, il contatto delle cellule batteriche con la superficie di tessuti molli è di fondamentale importanza per il successo dell'insediamento. Per molto tempo il campo della microbiologia si è concentrato sugli aspetti chimici legati all'infezione e alla crescita di biofilm. Ora ci sono prove che le forze meccaniche svolgono ruoli critici nella fisiologia batterica e che influiscono la formazione e la stabilità dei biofilm. Ad esempio sta diventando sempre più chiaro che il flusso di liquidi e le proprietà fisico-chimiche del substrato abbiano un impatto sullo sviluppo del biofilm. Tuttavia ci manca un'indagine rigorosa di come le proprietà meccaniche di un materiale determinino la morfogenesi dei biofilm e la sua rilevanza nel contesto di un'infezione.

In laboratorio i batteri vengono tradizionalmente coltivati in colture liquide, su piastre di agar o in celle a flusso con vetro o plastica dura come superficie. Tuttavia, questi sistemi non riassumono la complessità meccanica presente in un' infezione dove i batteri colonizzano maggiormente tessuti molli e sono soggetti al flusso di fluidi corporei. Per risolvere questi limiti tecnici ho combinato idrogel sintetici con microfluidica : ciò ha consentito la visualizzazione dal vivo e ad alta risoluzione di singoli batteri e biofilm che interagiscono con substrati morbidi alla presenza di una corrente.

Nel secondo capitolo mostro che i patogeni *Vibrio cholerae* e *Pseudomonas aeruginosa* deformano i soffici gel. Questo comportamento è il risultato di un'instabilità meccanica generata dall'accumulo di sollecitazioni meccaniche di compressione all'interno del biofilm in crescita e dalla sua adesione al substrato. Utilizzando mutanti che producono matrici di diversa composizione e in diversa quantità abbiamo dimostrato che la coesione cellula-cellula e l'adesione cellula-substrato guidano assieme la deformazione. Inoltre abbiamo scoperto che il buckling dei biofilm può esercitare

forze che compromettono l'integrità di monostrati di cellule epiteliali, suggerendo così che il biofilm può danneggiare meccanicamente tessuti umani.

Nel terzo capitolo ho studiato l'effetto delle proprietà meccaniche del substrato sulla forma del biofilm del batterio *P. aeruginosa*. Abbiamo dimostrato che i biofilm assumono architetture diverse in funzione della dimensione del reticolo del substrato a causa di differenze nella motilità. Il controllo meccanico della velocità di singole cellule dà origine a biofilm con architetture molto diverse a lungo termine, influenzando sia la loro tolleranza agli antibiotici che la distribuzione di diversi lignaggi.

Nel complesso i nostri risultati mostrano che l'accoppiamento meccanico tra i batteri e il substrato molle incide su fenotipi quali la motilità superficiale e l'architettura del biofilm e può svolgere un ruolo nell'esito di un'infezione, sia modulando la suscettibilità del biofilm agli antibiotici, sia diventando attivamente una fonte di virulenza.

Parole chiave

Pseudomonas aeruginosa, *Vibrio cholerae*, microbiologia, idrogels, biofilm, meccanobiologia, motilità contrattile

Contents

Acknowledgements	iii
Abstract	v
Sommario	vii
List of Figures	xii
List of Supplementary Figures	xiii
List of Tables.....	xiv
Chapter 1. Introduction	2
1.1 Motivation	2
1.2 Bacterial surface colonization	4
1.2.1 Adhesion	4
1.2.1.1 Effects of environmental mechanics on adhesion	5
1.2.2 Mechanosensing	10
1.2.2.1 Mechanosensing in <i>P. aeruginosa</i>	11
1.2.3 Twitching motility	12
1.2.3.1 Effects of environmental mechanics on twitching motility	13
1.2.4 Biofilms.....	17
1.2.4.1 Matrix composition and biofilm mechanical properties	18
1.2.4.2 Self-generated forces and morphomechanics.....	21
1.2.4.3 Effects of environmental mechanics on biofilm morphogenesis.....	24
1.3 Aims and organization of the thesis	28
Chapter 2. Biofilms deform soft surfaces and disrupt epithelia.....	29
2.1 Abstract	29
2.2 Introduction.....	30
2.3 Results	32
2.3.1 Biofilms deform soft substrates.....	32
2.3.2 Biofilms deform soft substrates after reaching a critical diameter	34
2.3.3 Biofilms push their substrate in the growth direction	36
2.3.4 Wild-type and rugose biofilms deform soft-substrates.....	36
2.3.5 EPS composition drives biofilm and substrate deformations.....	37
2.3.6 Biofilms generate large traction forces	40
2.3.7 Biofilms deform and disrupt epithelial cell monolayers	41
2.4 Discussion	43
2.5 Acknowledgements	47
2.6 Methods.....	47

2.6.1	Cell culture	47
2.6.2	Cell culture on collagen/Matrigel gels	47
2.6.3	Bacterial strains and culture conditions	48
2.6.4	Infection of tissue-engineered epithelia by <i>Vibrio cholerae</i>	48
2.6.5	Fabrication of PEG hydrogels and mechanical characterization	49
2.6.6	Fabrication of thin PEG hydrogel layers and implementation with PDMS microfluidic chip	50
2.6.7	Biofilm growth in microfluidic chambers.....	50
2.6.8	Staining procedures	51
2.6.9	Visualization	52
2.6.10	Image analysis and computation of deformation profiles	52
2.6.11	Digital volume correlation and traction force microscopy	53
2.7	Supplementary information	54
2.7.1	Supplementary figures	54
2.7.2	Movies	59
2.7.3	Tables	59
Chapter 3. Mechanical control of biofilm architectures promotes <i>Pseudomonas aeruginosa</i> antibiotic tolerance.....		63
3.1	Abstract	63
3.2	Introduction.....	64
3.3	Results	66
3.3.1	<i>P. aeruginosa</i> biofilm architecture depends on substrate mechanics	66
3.3.2	Mechanical modulation of twitching motility	68
3.3.3	Substrate mechanics impact antibiotic tolerance of biofilms	72
3.3.4	Material mechanics mediate biofilm heterogeneity.....	74
3.4	Discussion	76
3.5	Acknowledgements	79
3.6	Methods.....	79
3.6.1	PEG hydrogels fabrication	79
3.6.2	PEG hydrogels characterization	80
3.6.3	Assembly of hydrogel-coated coverslips with microfluidic chips	82
3.6.4	Bacterial strains	83
3.6.5	Single cell twitching and adhesion	83
3.6.6	Biofilm formation	84
3.6.7	Quantification of cAMP and c-di-GMP during surface growth	84
3.6.8	Image processing and analysis	85
3.7	Supplementary information	89

3.7.1	Supplementary Figures	89
3.7.2	Movies	93
3.7.3	Tables	94
Chapter 4.	Conclusion.....	97
References	103
Curriculum Vitae	115

List of Figures

Figure 1.1 Bacteria experience mechanical forces in their environment.	2
Figure 1.2 Environment encountered by bacteria during host colonization.	3
Figure 1.3 Biofilm development at a solid-liquid interface.....	4
Figure 1.4 Schematic illustration of physicochemical factors affecting bacterial adhesion.	5
Figure 1.5 Mechanosensing in bacteria.	10
Figure 1.6 Twitching motility.....	13
Figure 1.7 Effects of environmental mechanics on twitching motility.....	16
Figure 1.8 Matrix composition of <i>V. cholerae</i> and <i>P. aeruginosa</i> biofilms.	20
Figure 1.9 Buckling instabilities in biofilm morphogenesis.....	24
Figure 1.10 Effects of environmental mechanics on biofilm formation.	26
Figure 2.1: Biofilms deform soft substrates.....	33
Figure 2.2: Biofilms deform their substrate by buckling.	35
Figure 2.3: Wild-type and rugose biofilms deform soft-substrates.....	37
Figure 2.4: EPS composition drives biofilm and substrate deformations.....	39
Figure 2.5: Biofilms generate large traction forces.	40
Figure 2.6: Biofilms deform and disrupt epithelial cell monolayer.....	42
Figure 3.1: Hydrogel elastic substrates regulate <i>P. aeruginosa</i> biofilm architecture.....	67
Figure 3.2: Hydrogel mesh size modulates biofilm architecture by regulating twitching motility.	70
Figure 3.3: Mechanical control of biofilm architecture promotes <i>P. aeruginosa</i> 's tolerance to antibiotics.	73
Figure 3.4: Hydrogel substrates regulate the spatial organization of heterogeneous <i>P. aeruginosa</i> biofilms.	76
Figure 4.1 Bacterial clusters growing inside PEG hydrogels formed via thiol-ene photoclickchemistry.	99

List of Supplementary Figures

Supplementary Figure 2.1: Biofilm diameter-dependence of δ_{max} and λ .	54
Supplementary Figure 2.2: Hydrogel deformation field computed at different growth stages, superimposed with a brightfield image of the biofilm.	55
Supplementary Figure 2.3: Biofilm diameter-dependence of maximum deformation for the smooth variant of different <i>V. cholerae</i> strains grown in M9.	55
Supplementary Figure 2.4: Deformation behaviour for <i>vpsL</i> deletion mutant and complementation strains.	56
Supplementary Figure 2.5: <i>P. aeruginosa</i> biofilms on substrates with different stiffness.	56
Supplementary Figure 2.6: Biofilm diameter-dependence of λ for substrates with different moduli.	57
Supplementary Figure 2.7: Power-law relationship between deformation δ_{max} and substrate moduli (E).	57
Supplementary Figure 2.8: Confocal images of uninfected (i) and infected (ii-iv) monolayers of Caco-2 cells.	57
Supplementary Figure 2.9: Biofilms perturb the viability of MDCK cell monolayers.	58
Supplementary Figure 2.10: Biofilms increase the permeability of MDCK cell monolayers.	59
Supplementary Figure 3.1: Hydrogel substrates regulate <i>P. aeruginosa</i> biofilm architecture.	89
Supplementary Figure 3.2: <i>P. aeruginosa</i> initial attachment and adhesion strength are independent of hydrogel mesh size.	90
Supplementary Figure 3.3: Flagella are not affecting the mechanoregulation of twitching motility.	91
Supplementary Figure 3.4: Twitching motility of the mutant Δpel is sensitive to the mechanical properties of the gels.	91
Supplementary Figure 3.5: <i>P. aeruginosa</i> does not increase intracellular levels of cAMP and c-di-GMP on hydrogels of different compositions during early times of surface colonization.	92
Supplementary Figure 3.6: Hydrogel mechanical properties impact cell density of biofilms.	92
Supplementary Figure 3.7: Hydrogel substrates regulate the spatial organization of heterogeneous <i>P. aeruginosa</i> biofilms.	93

List of Tables

Table 1.1 Summary of studies which investigated the effect of material stiffness on bacterial adhesion	8
Table 1.2 Summary of studies which investigated the effect of material stiffness on <i>P. aeruginosa</i> mechanosensing	12
Table 1.3 Summary of studies which investigated the effect of material stiffness on twitching motility	16
Table 1.4 Summary of studies which investigated the effect of material stiffness on biofilm formation	27
Table 2.1: Molecular weight and concentrations of the precursors used for the generation of the hydrogels and resulting elastic modulus	60
Table 2.2: Key Resources Table. Bacterial strains, cell lines, plasmids, chemicals, others.....	60
Table 3.1: Summary of mechanical properties of PEGDA hydrogels	94
Table 3.2: Numerical values of biofilm aspect ratio h/r from Figure 3.1C	94
Table 3.3: Numerical values of twitching speed from Figure 3.2D-E	94
Table 3.4: Numerical values of alive biomass and biofilm surface to volume ratio from Figure 3.3(A, D).....	95
Table 3.5: Numerical values of 1st NND from Figure 3.4B	95
Table 3.6: Numerical values of initial cell number and attached cells under a shear stress of 0.2 and 2 Pa from Supplementary Figure 3.2	95
Table 3.7: Numerical values of YFP/mKate and GFP per cell from Supplementary Figure 3.5	95
Table 3.8: Numerical values of biofilm density from Supplementary Figure 3.6.....	96
Table 3.9: List of bacterial strains	96

Chapter 1. Introduction

1.1 Motivation

To survive in diverse and fluctuating environmental conditions, bacterial cells have evolved mechanisms of attaching to surfaces and forming multicellular communities called biofilms (1–3). This lifestyle presents advantages relative to free living planktonic cells, such as protection from predators and environmental challenges (1). For this reason, biofilms dominate in all habitats on the surface of the Earth, accounting for nearly 80% of bacterial cells: we can find them in soil, in oceans, on water pipes, river rocks, ship hulls, inside animals and humans (4).

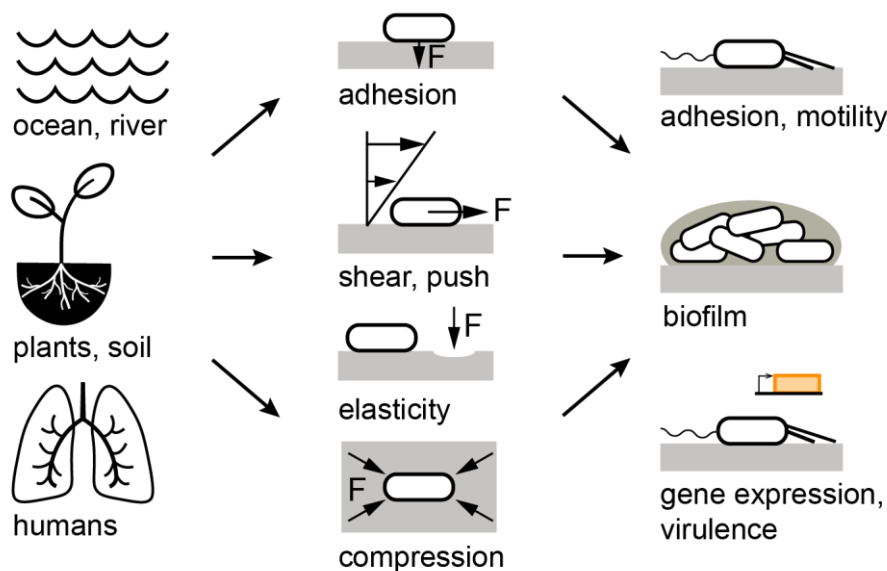


Figure 1.1 Bacteria experience mechanical forces in their environment.

Bacterial phenotypes are influenced by mechanical forces which arise from their interaction with flow, pressure, surfaces and each other.

Bacteria have been mostly studied in a biochemical context, assuming that they can exclusively sense and respond to chemical stimuli. However, the environment experienced by the bacteria is diverse, and it is not only characterized by the presence of chemical cues, but also by an array of mechanical forces generated by flow, pressure and their interactions with surfaces and with each other (5). This aspect has traditionally been vastly overlooked and it only recently emerged as a possible regulator of bacterial behavior (Figure 1.1). Yet, despite the growing evidence for

mechanically regulated phenotypes, whether these are important in a realistic context of infection remains to be investigated.

In our body, bacteria can be found in the form of beneficial biofilms, such as in the case of commensal microbiota, or in the form of pathogenic biofilms that cause recurrent and chronic infections (6). During infections, pathogens can be located at the surface of abiotic indwelling medical devices, such as catheters and prosthetic implants, or they can be directly in contact with human tissues (Figure 1.2). Human tissues are heterogeneous materials composed of cells and extracellular matrix. Despite the heterogeneity in mechanical properties for the different subcomponents, the bulk elastic moduli of tissues span from 11 Pa to 20 GPa, for intestinal mucus and cortical bone respectively (7). However, most of our tissue have moduli below 1 MPa.

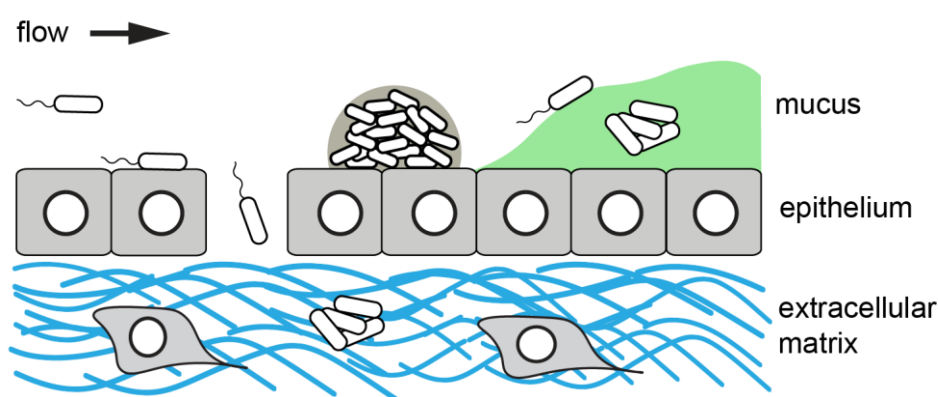


Figure 1.2 Environment encountered by bacteria during host colonization.

During infection and in microbiota bacteria experience flow of body fluids and are in contact with soft substrates such as cells, extracellular matrix and secretion. Adapted from (5).

Multiple studies have shown how substrate stiffness impact the physiology of eukaryotic cells (8). We now know that mechanical properties of material substrates regulate migration (9), proliferation (10), stem cell differentiation (11), development (12) and cancer progression (13). In contrast, despite the importance of bacterial interaction with soft tissues during host colonization, only a few have attempted to test the effect of substrate mechanical properties on bacterial physiology. Most of these studies focused purely on the relationship between surface stiffness and bacterial adhesion in order to explore alternative material properties to reduce biofouling. However,

whether material stiffness plays a role in other bacterial phenotypes and whether they are relevant in the context of host infection, has yet to be determined.

1.2 Bacterial surface colonization

Biofilms are dynamic and highly regulated systems, both at the biological and architectural level. The typical biofilm cycle starts with bacterial adhesion to a surface, followed by division and formation of clusters during which cells produce a matrix made of polymeric substances (Figure 1.3). After maturation, biofilms ultimately disperse so that cells can colonize elsewhere (14). In the following paragraphs I will discuss the effects of the mechanical environment on the different steps of biofilm formation, with a particular focus on the influence on substrate stiffness.



Figure 1.3 Biofilm development at a solid-liquid interface.

Planktonic cells first approach the surface and reversibly attach to it. They then start to secrete a matrix that promotes firm adhesion to the substrate and between the proliferating cells. The community develops in an organized three-dimensional structure and eventually disperse, allowing the colonization of new surfaces.

1.2.1 Adhesion

Bacterial adhesion depends on multiple physicochemical properties of the fluid environment, the surface and the bacterium itself (15–22) (Figure 1.4). At first the bacterium must be able to approach the surface. Thermodynamic classical or extended DLVO theory captures the interaction force between cell and surface (15, 21). In particular, the attractive/repulsive forces involved are Van der Waals, electrostatic, acid-base and steric interactions. Once the bacterium initiates surface contact by overcoming repulsive forces, they have to strengthen adhesion. To achieve this, cells reorient their body (for example from polar to longitudinal position to maximize the contact area), progressively remove interfacial water, engage surface appendages and adhesins (e.g. flagella, pili,

curli), and secrete extracellular polymeric substances (EPS) (16). In some cases, the production of adhesins and EPS is stimulated by the surface contact itself, through surface sensing (5, 16).

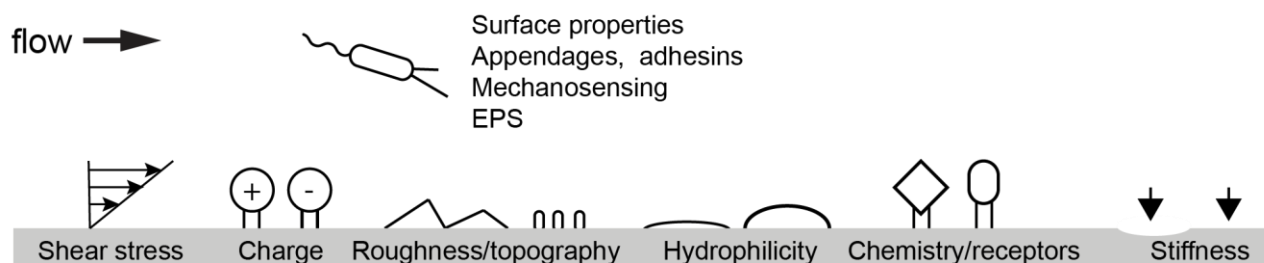


Figure 1.4 Schematic illustration of physicochemical factors affecting bacterial adhesion.

The interplay between hydrodynamic forces, material surface properties and the properties of the bacterium itself is of fundamental importance in determining the transition from a free-swimming cell to a surface attached one. Adapted from (19).

1.2.1.1 Effects of environmental mechanics on adhesion

In most environments bacteria experience fluid flow. This is true for both abiotic conditions, like on moving ships, catheters and riverbeds, and in biotic ones, like during colonization of intestine and airways, blood vasculature and urinary tract (5). Cells need to first approach the surface to initiate attachment: they can do that passively, for example through sedimentation and Brownian motion, or actively, using swimming motility generated by flagellar rotation (16). Fluid flow dramatically impacts the ability of a cell to reach the surface or to remain stably attached. Flow that is too strong may prevent the cells to reach the surface. Moreover, in flow, single surface-attached cells experience a drag force generated by shear stress, which may overcome adhesive forces and consequently detach cells from the surface. In some instances, increasing shear stress can counterintuitively enhance bacterial adhesion. For example, *Escherichia coli* attaches to mannose with an adhesin called FimH with a force dependent bond, called catch-bond, that is strengthened under tension (23). In *Pseudomonas aeruginosa*, the residence time of the cells on the surface increased with shear stress through an unresolved mechanism (24).

Bacteria can colonize a variety of surfaces, abiotic and biotic, but the efficiency changes with chemical and physical properties of the substrate. The influence of different materials on bacterial

adhesion has been studied mainly in the context of antifouling strategies (15, 17–19). Surface charge, chemistry, hydrophobicity, roughness and topography are the main properties which influence bacterial adhesion.

Surface chemistry, for example, can hinder bacterial adhesion by exposing biocidal groups or enhance it by exposing specific receptors (25). Appendages and adhesins in general interact non-specifically with a wide range of substrates. However, in biotic contexts, many pathogens use their appendages to specifically bind to the membrane of eukaryotic cells. For example, *E. coli* specifically binds to mannose residues on the cell surface with its type I pili (26), while *P. aeruginosa* adheres specifically to the glycolipid Asialo-GM1(27) with its type IV pili and to mucin with its flagellar cap FliD (28). As most bacteria are negatively charged, in general they tend to attach more tightly and rapidly on positively charged surfaces (15). Positive charges also induce cell death by damaging the cell membrane (15).

The effect of surface hydrophobicity on adhesion depends on the hydrophobicity of the cell itself: hydrophobic bacteria will attach better on apolar surfaces, while hydrophilic bacteria prefer hydrophilic surfaces (15, 20). However, in most cases bacteria prefer hydrophobic surfaces (20). The wettability of a surface can be determined both by its chemical properties and/or its topography. It has been shown that both superhydrophilic and superhydrophobic surfaces, with extreme contact angles, hinder bacterial adhesion (17, 18). On superhydrophilic surfaces, obtained for example using zwitterionic polymers, the tightly bound hydration layer can block bacterial adhesion. On superhydrophobic surfaces, that can be fabricated by changing the topography of the surface, air pockets trapped in between the structures can reduce the surface available for bacterial adhesion. In general, surface roughness promotes bacterial attachment both due to an increase in contact area and the protection from the hydrodynamic shear stress (15). The topography of the surface can impact bacterial adhesion in several ways. In general, if surfaces have a characteristic feature size which is similar to the one of the bacteria, adhesion is enhanced because the bacteria are provided with shelter and a higher available surface area (18). If the surface characteristic feature is at the

nanometer scale, bacterial adhesion is in general reduced because of superhydrophobic or bactericidal effects (15, 18).

The possibility that material stiffness could play a role in bacterial adhesion and biofouling has gained attention in the last years (15, 18). Lichter *et al.* showed that *S. epidermis* and *E. coli* adhere better to stiffer substrates made of polyelectrolyte multilayers (PEM) (29). Similarly, Kolewe *et al.*, Guegan *et al.* and Saha *et al.* observed that various species attached better to stiffer substrates regardless of the hydrogel chemistry using poly(ethylene glycol)dimethacrylate (PEGDMA) (30), agar gels (30, 31), photocrosslinked polyelectrolyte multilayer (31) and poly-*N*-isopropylmethacrylamide P(NIPMAM) microgels (32). Other studies used polyacrylamide gels to study the interaction between substrate stiffness and bacteria (33, 34), and revealed an inverse trend where cells attach better to softer substrates (34). Overall, for hydrophilic materials bacteria tend to adhere more on stiffer substrates. However, studies that used hydrophobic PDMS as a substrate observed the opposite behavior. Song *et al.* noticed that *E. coli* and *P. aeruginosa* attach better, grow faster and are more susceptible to antibiotics on softer substrates (35). They attributed these differences to the ability of bacteria to sense differences in substrate stiffness (36, 37). Siddiqui *et al.* showed that PDMS substrates with different stiffnesses did not affect initial bacterial adhesion, but it drastically impacted the adhesion strength (38). Other groups observed higher adhesion on softer PDMS substrates as well, but they attributed the difference to physicochemical properties of the substrates rather than to an active surface sensing mechanism (39–41). In particular, Straub *et al.* showed that the same adhesion trend could be obtained using carboxylated beads. Valentin *et al.* attributed the difference to differences in viscosity of the PDMS and the presence of free mobile polymer chains at the interface that increase the adhesive properties of softer substrates (40), while Pan *et al.* showed that by coating the different PDMS substrate with a 2 nm thick highly cross-linked PDMS layer, which did not alter the substrate stiffness, differences in adhesion were no longer observed (41).

Another aspect which is not yet clear is “how deep” the bacteria would be able to sense the substrate (18). Lichter *et al.* showed that just by masking stiff PEM substrates with a compliant layer

would reverse the effect on adhesion, suggesting that bacteria would be sensitive to the first tens of nanometers of the substrate (29). However, other studies showed that the thickness of the substrate appeared to influence bacterial adhesion despite no differences in Young's modulus (32, 42). These studies suggest that material stiffness can play a role in bacterial physiology. However, these studies don't lead to an unambiguous conclusion on the effect of substrate stiffness on bacterial adhesion, both in terms of adhesion or of mechanism involved (active surface mechanosensing or pure physicochemical interactions). Differences in materials used, bacterial species, flow conditions and stiffness range could explain at least partially the contrasting results. We note that the materials used in these studies are polymeric substrates which feature a nano or sub-nanoporous topography which is strictly related to their stiffness (18). In general, stiffer polymeric substrates have a higher network density and therefore a higher density of functional groups that can interact with bacterial cells. For example, Kolewe *et al.* showed that higher PEG concentrations, both in hydrogels and polymer brushes, lead to longer runs of surface rolling in *S. aureus* (43). A summary of the studies about the influence of substrate stiffness on bacterial adhesion can be found in Table 1.1.

Table 1.1 Summary of studies which investigated the effect of material stiffness on bacterial adhesion

Material	Behavior	Bacteria	Modulus	Results
PEM (29)	Adhesion	<i>S. epidermis</i> <i>E. coli</i>	0.8 MPa- 80 MPa	Cells adhere more to stiffer substrates; masking stiff PEM with a bilayer of compliant PEM and viceversa reverses the trend
Photocrosslinked PEM (31)	Adhesion, growth	<i>L. lactis</i> <i>E. coli</i>	30-150 kPa	Cells adhere more to stiffer substrates; <i>E. coli</i> grows slower on stiffer substrates
Agarose hydrogel (44)	Adhesion	<i>Bacillus 4J6</i> <i>Pseudoalteromonas D41</i>	7 -110 kPa	D41 adheres more to stiffer substrates; 4J6 clusters on soft substrates
PEGDMA and agar gels (30)	Adhesion	<i>E. coli</i> <i>S. aureus</i>	44-1495-5152 kPa	Cells adhere more to stiffer substrates
Polyacrylamide gels (33)	Growth	<i>P. aeruginosa</i> <i>E. coli...</i>	1.4-50 kPa	PAAm gels can be used for studying bacteria
Polyacrylamide gels (34)	Adhesion	<i>S. aureus</i>	17-654 Pa	Cells adhere more on softer gels

PEGDMA gels (42)	Adhesion	<i>E. coli</i> <i>S. aureus</i>	30-400-1000 kPa	More bacteria adhere on thinner hydrogels compared to thicker hydrogels with the same modulus
Glass coated with P(NIPMAM) microgel (32)	Adhesion	<i>S. aureus</i>	21-117-346 kPa	Bacterial adhesion decreased with a lower cross-linking density at equal coating thickness Bacterial adhesion decreased and at equal cross-linking density with a thicker microgel coating
PEGDMA hydrogels and PEG brushes (43)	Flow driven surface motion	<i>S. aureus</i>	2-1300 kPa	On higher PEG concentrations <i>S. aureus</i> exhibits long runs of surface rolling
PDMS (35)	Adhesion, growth, antibiotic resistance	<i>E. coli</i> <i>P. aeruginosa</i>	0.1-2.6 MPa	Cells attach more and grow faster on softer substrates; cells on stiffer substrates are smaller and less susceptible to antibiotics
PDMS (36)	Flagellar motility	<i>E. coli</i>	0.1-2.6 MPa	Cells on stiff surfaces are more motile, <i>motB</i> involved in the response
PDMS (39)	Adhesion	<i>P. aeruginosa</i> <i>E. coli</i> <i>S. aureus</i>	0.06-4.52 MPa	<i>P. aeruginosa</i> and <i>E. coli</i> adhere more on soft substrates, no difference for <i>S. aureus</i> ; trend replicated by using carboxylated or amine modified PS beads
PDMS (40)	Adhesion	<i>E. coli</i>	565-186-21 kPa	<i>E. coli</i> adheres more and is more resistant to desorption on viscous PDMS
PDMS (38)	Adhesion and adhesion strength	<i>E. coli</i>	0.26-124 kPa	Similar number of initially attached cells; cells exhibit stronger adhesion on soft substrates
PDMS (45)	Adhesion, 3D motion	<i>Pseudomonas sp.</i> <i>E. coli</i>	3.4-278.1 MPa	Cells adhere more on stiffer substrates and is correlated with both adapted response (tumble/flick frequencies) and bacteria-surface interaction; cells move more on softer pdms
PDMS – coated PDMS (2 nm)	Adhesion	<i>P. aeruginosa</i> <i>E. coli</i>	64-2326 kPa	Cells adhere more to soft substrates on uncoated

thick layer of hard PDMS) (41)		<i>S. epidermis</i>		substrates; no difference in adhesion on coated substrates
--------------------------------	--	---------------------	--	--

1.2.2 Mechanosensing

Bacteria can sense forces generated by fluid flow and their contact with the surface (5). This process involves cell membrane and appendages like flagella and pili as mechano-transmitting elements. The presence of a surface can inhibit or abolish flagellar rotation, it can perturb pili dynamics or conformation, while the adhesion forces can deform the cell membrane. Mechanosensors such as two-component systems and second messenger molecules transduce the mechanical signal into cellular responses such as adhesin production, motility, virulence or activation of biofilm formation (46) (Figure 1.5).

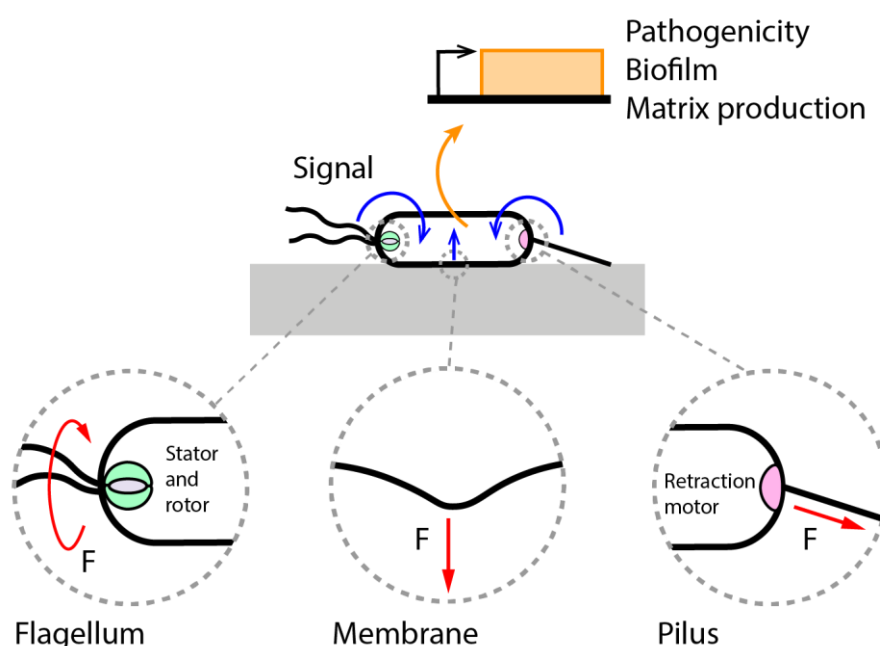


Figure 1.5 Mechanosensing in bacteria.

Bacterial components such as flagella, pili and cell membranes experience external forces and transmit the mechanical signal to sensory systems. These induce a variety of downstream mechanoresponses, including transcriptional regulation. Adapted from (5).

For example, *Bacillus subtilis* senses increased load on flagellar rotation to promote the production of adhesins. Similarly, increased load on the flagellar motor and/or obstruction of pili

retraction on surface stimulate the production of an adhesive holdfast in *C. crescentus* (16). When *E. coli* is in contact with hydrophobic or nanopatterned surfaces, the membrane perturbation activates the Cpx two-component system, and therefore the expression of factors maintaining periplasmic protein integrity (47, 48). The enterohemorrhagic *Escherichia coli* O157:H7 initiates transcription of its type III secretion system upon contact and attachment to epithelial cells. The expression of these virulence factors is further enhanced by physiological shear force (49). The mechanism is still not completely clear, but it is probably involving the Cpx system.

1.2.2.1 Mechanosensing in *P. aeruginosa*

P. aeruginosa has at least two distinct surface sensing mechanism: the Pil-Chp and the Wsp systems. The Pil-Chp system initiates a hierarchical cascade of second messenger signaling. Upon surface contact, T4P activate the Chp system inducing an increase in cAMP levels (50). cAMP stimulates the transcription of hundreds of genes via the transcription factor Vfr (virulence factor regulator), including genes encoding type III secretion system, and therefore pathogenicity. At the same time, high level of cAMP increases the expression of genes involved in T4P biogenesis, including the minor pilin PilY1. It has been proposed that this protein is involved in mechanosensing and later causes an increase in c-di-GMP levels (5). High levels of c-di-GMP stimulate production of biofilm matrix components. The Wsp system, on the other end, is sensitive to chemicals and mutations that perturb the cell envelope as well as to surface-induced cell envelope stress and provides an additional input for regulation of c-di-GMP levels during long-term surface contact (51, 52).

c-di-GMP levels depend on the magnitude of shear force acting on the cell (53). The shear force was tuned by increasing either the flow rate or the adhesion strength of the cells to the surface. This output required T4P and PilY1. Recently, Jones and coworkers showed that *P. aeruginosa* initiates a transcriptional response early after surface attachment (5-60 minutes) (54). The response appeared to be surface specific, with very few genes being regulated in response to surfaces in general when silicone, glass and plastic were compared. Separate work has shown that flow can tune gene expression in a force-independent manner (55). Cells upregulate the *fro* operon in flow,

but the magnitude of the response depends on the fluid velocity rather than the shear force it generates.

Koch *et al.* showed that *P. aeruginosa* can distinguish the agarose and polyacrylamide stiffness using its T4P (56). The levels of cAMP do not linearly increase with stiffness, but peaked at a stiffness of about 100 kPa. By using both agarose and polyacrylamide gels they show that this response is specifically due to the stiffness of the material and not to differences in chemistry or mesh size. Song and coworkers showed that the stiffness of PDMS substrates influences attachment, growth, and size of the attached cells, as well as c-di-GMP levels (37). These differences were abolished in mutants of the *oprF* gene, which encodes for an outer membrane protein. Blacutt *et al.* showed the potential of using PEGDA hydrogels in measuring c-di-GMP levels in *P. aeruginosa* (57). A summary of the studies about the influence of substrate stiffness on *P. aeruginosa* mechanosensing can be found in Table 1.2.

Table 1.2 Summary of studies which investigated the effect of material stiffness on *P. aeruginosa* mechanosensing

Material	Behavior	Bacteria	Modulus	Results
Agarose/polyacrylamide (56)	cAMP	<i>P. aeruginosa</i>	0.1-1000 kPa	T4P can sense stiffness, cAMP levels are peaked
PEGDA (57)	c-di-GMP	<i>P. aeruginosa</i>	44-3600 kPa	Method paper
PDMS (37)	c-di-GMP	<i>P. aeruginosa</i>	0.1-2.6 MPa	Cells on soft substrates have higher levels of c-di-GMP

1.2.3 Twitching motility

In liquid environments bacteria can propel themselves and swim using flagella. However, when bacteria attach to a surface, they engage surface-associated motility systems. These include sliding, swarming, gliding and twitching (58). Sliding consists in a passive spreading of cells due to the push from other dividing cells. Swarming is a collective mode of motility on semi-solid surfaces mediated

by flagella. Gliding involves the translation of substrate adhesion sites along the cell body (58). During twitching, cells pull themselves using filaments called type IV pili (T4P) via cycles of extension, attachment of the pilus tip and retraction (Figure 1.6). T4P extend and retract by polymerization and depolymerization of the pilin subunits. They extend a few microns, are about 5-8 nm thick and exert forces that can exceed 100 pN (59). Due to their dimensions, pili cannot be visualized by traditional transmitted light microscopy. T4P in live cells have been recently visualized either by interferometric scattering microscopy (iSCAT) (60) or by fluorescently labeling cysteine mutated pili with a thiol-reactive maleimide dye (61). Several species perform twitching motility: *P. aeruginosa*, *Myxococcus xanthus*, *Neisseria gonorrhoeae* and *Acinetobacter baumannii*. In *N. gonorrhoeae* T4P are randomly distributed around the round cell body, while in the rod-shaped *P. aeruginosa* they are localized at the poles. *P. aeruginosa* can twitch either by ‘crawling’ or ‘walking’. While the first mode consists in a highly directional persistent motion where cells lie flat on the surface, the second is nearly a random walk and it is specific to cells that stands upright on the surface (62). Recent work showed that twitching direction in *P. aeruginosa* is controlled by the mechanical input of T4P in a process called mechanotaxis (63). T4P are not only involved in surface motility, but also in DNA uptake (64), adhesion to host cells (65), microcolony and biofilm formation (66, 67), and mechanosensing (50).

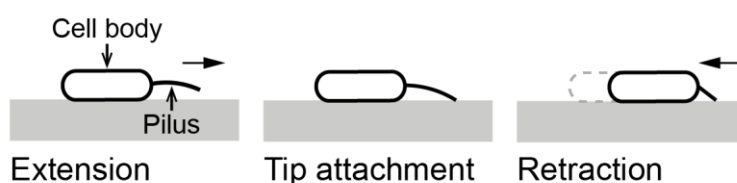


Figure 1.6 Twitching motility.

Pili extend and attach with their tip at the surface. The retraction of the pili pulls the cell body forward.

1.2.3.1 Effects of environmental mechanics on twitching motility

Flow can direct *P. aeruginosa* to twitch upstream by aligning the cells in the direction of the fluid motion while the piliated pole faces upstream. This promotes a movement against the current (68) (Figure 1.7A).

While in some instances T4P can adhere specifically to host receptors (65), during twitching they mainly interact non-specifically with the surface. *P. aeruginosa* showed stronger binding to hydrophobic surfaces compared to hydrophilic ones (69). Similarly, gonococcal pili bind more strongly to polystyrene than glass and their binding strength is reduced by BSA (70). For *M. xanthus* the retraction of the pili during twitching is mediated by the self-produced EPS and chitin (71). Similarly, T4P in *P. aeruginosa* were observed to adhere strongly to one of its matrix component Pel: twitching was enhanced on a glass slide covered with this polysaccharide (72). The polysaccharide Psl influences *P. aeruginosa*'s twitching motility as well: the cells deposit a web of Psl as they move on a surface which in turn influences the motility of the cells that encounter these trails leading to further Psl accumulation (73). Landry *et al.* showed that surfaces coated with mucins inhibit surface motility because the flagellar cap protein FliD binds to the mucin anchoring the cells to the surface (74). This resulted in the formation of large biofilm aggregates on mucin-coated surfaces. A similar behaviour was observed on surfaces with different charges, where mushroom like structures formed on negatively charged surfaces, while flat biofilms developed on positively charged ones (75). Even in this case, the difference in morphology was attributed to differences in surface motility. Recently, single cell tracking on polymer microarrays displaying different chemistries showed that twitching speed correlated with surface chemistry independently from surface stiffness, topography and water contact angle (76).

Topography can influence twitching as well. Surface motility is guided by elevations with dimensions and depths corresponding to the size of bacteria (77–79). The availability of attachment sites for the pili, both in terms of 'how much' area is available for pili attachment and 'how easy' it is to reach an attachment site, might be the reason for this behaviour (78). Kühn *et al.* showed that when *P. aeruginosa* cells encounter an obstacle, be that either another cell or non-biological material, they reverse in response to the mechanical signal (63). The effect of subcellular nanotopography has also been explored. Rosenzweig *et al.* explored the influence of nanopillared surfaces on *P. aeruginosa* twitching motility: displacement and velocity decreased with decreasing

pillar tip packing fractions, and therefore with a decreased surface area available to T4P contact (80) (Figure 1.7B).

Bacteria use T4P to interact with host cells, soft biological tissues and secretions (81–86). However, only few studies have tried to elucidate the role of substrate viscosity and stiffness in twitching motility. Holz *et al.* tried to mimic the physical properties of the membrane of eukaryotic cells by using supported lipid membranes (87). They showed that the speed of *N. gonorrhoeae* negatively correlates with lipid fluidity (Figure 1.7C). In addition, on microstructured surfaces with alternating fluidity, bacteria clustered on top of non-fluid areas. These phenomena are explained with the fact that on fluid membranes the force generated by the pilus are not translated into movement since the pilus-bound lipids slip within the membrane (87). Zhang *et al.* studied the twitching behaviour of *P. aeruginosa* on surfaces grafted with a layer of thermally sensitive poly(N-isopropylacrylamide) (PNIPAAm) chains that transition from a soft brush-like conformation to a stiffer collapsed conformation as a function of temperature (88). They saw that twitching trajectories were straighter on stiffer substrates. In addition, they noticed that *P. aeruginosa* slingshot more on soft surfaces that has longer relaxation time. Slingshots are translation movements due to the release of single T4P and are 20 times faster than translations due to pull actions (89): it is therefore thought that slingshots at a shear-thinning condition facilitate surface motility by reducing energy dissipation. Sabass *et al.* performed traction force microscopy (TFM) experiments on *M. xanthus* using very soft polyacrylamide gels ($E \sim 121$ Pa) coated with chitosan (90). It was possible to observe local traction in small hotspots with forces on the order of 50 pN due to twitching. In addition, these forces appeared amplified in groups of twitching bacteria. Koch *et al.* performed TFM experiments on *P. aeruginosa* with polyacrylamide gels with substrate stiffnesses ranging from 4.5 to 132 kPa (56). They could observe that the traction force applied to deform the substrate increases with substrate stiffness. The effect of substrate stiffness on twitching speed has been recently modelled by Simsek *et al.* (91). They describe the bacterium as an ideal twitcher characterized by a pilus that binds onto the surface to pull the cell forward and a passive rear adhesion of the cell body. They show that the migration speed depends on the force-sensitivity of the adhesion bonds: upon tension build-up, if

the rear adhesions are more force sensitive, the twitching speed increases with increasing substrate rigidity. The contrary is true if the front adhesions are more force sensitive. On soft substrates, as there is not a significant build-up of tension forces, the migration is not dependent on the force sensitivity of the adhesion. However, this model is applicable only in the case where the substrate is 'sticky', with binding rates being an order of magnitude larger than unbinding rates in absence of force. Very recently, experiments performed on polyacrylamide gels with moduli ranging from 3 to 80 kPa showed that the twitching speed increases with substrate rigidity (92). A summary of the effect of surface stiffness on twitching motility can be found in Table 1.3.

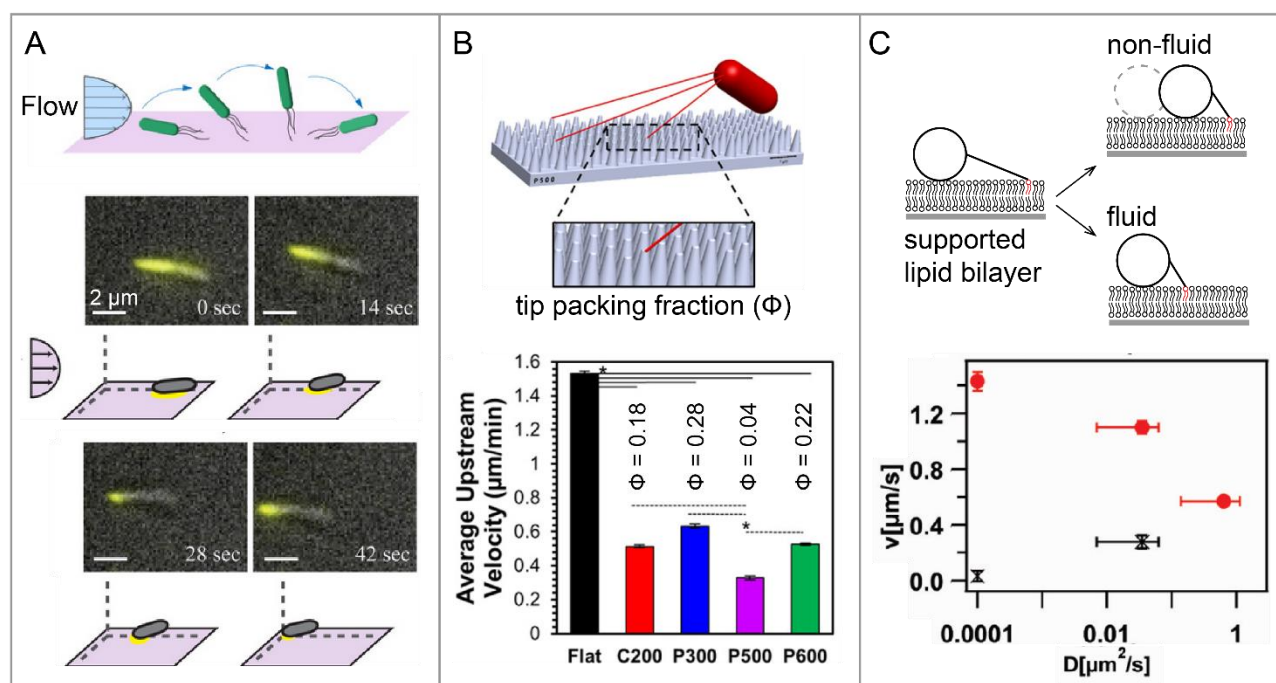


Figure 1.7 Effects of environmental mechanics on twitching motility.

(A) Fluid motion aligns *P. aeruginosa* cells in the direction of the flow, promoting an upstream migration. Adapted from (68). (B) Low tip packing fraction in nanopillared surfaces decreases twitching speed in *P. aeruginosa* because of lower surface availability for pili attachment. Adapted from (80). (C) *N. gonorrhoeae* twitches more slowly on fluid membranes (higher membrane diffusion coefficient D) compared to non-fluid ones. In the graph red and black data points are values for *wt* and *pilT*- (no pili retraction) respectively. Adapted from (87).

Table 1.3 Summary of studies which investigated the effect of material stiffness on twitching motility

Material	Behavior	Bacteria	Modulus	Results
Supported lipid bilayer (87)	Twitching	<i>N. gonorrhoeae</i>	Diffusivity $D = 10^{-4}$ -0.6 $\mu\text{m}^2/\text{s}$	Speed negatively correlates with lipid fluidity

PMIPAAm Brush (88)	Twitching	<i>P. aeruginosa</i>	Relaxation time $\tau = 10-100$ s	Cells slingshot more on soft brushes with longer relaxation time
Polyacrylamide gels (90)	Twitching/TFM	<i>M. xanthus</i>	121 Pa	Groups of bacteria exert more force
Polyacrylamide gels (56)	TFM	<i>P. aeruginosa</i>	4.5-132 kPa	Applied force increases with substrate stiffness
Ideal elastic substrate (91)	Twitching	<i>P. aeruginosa</i>		Migration speed depends on the force-sensitivity of the adhesion bonds
Polyacrylamide gels (92)	Twitching/biofilm	<i>P. aeruginosa</i>	3 -80 kPa	Twitching speed increases with substrate rigidity

1.2.4 Biofilms

The presence of a self-produced matrix of extracellular polymeric substances is a characteristic feature of bacterial biofilms (1). The matrix is a hydrated polymeric network that mediates the adhesion of bacteria to the surface and that promotes the cohesion and immobilization of cells inside the biofilm (2). This confers mechanical stability and therefore protection against environmental challenges like shear flow, phagocytosis by the immune system and grazing by protozoa. The polymeric substances that constitute the matrix are mainly polysaccharides, proteins and extracellular DNA (eDNA). The matrix can also maintain a hydrated environment that protects biofilms from desiccation and it can host extracellular enzymes which can degrade biopolymers and therefore acts as an external digestive system. In addition, the matrix can hinder the penetration of antibiotics by binding and reacting with them or physically limiting their diffusion (6). For example, cationic antibiotics such as tobramycin and colistin can bind to negatively charged components of the matrix such as polysaccharides and extracellular DNA, while some antibiotics can be inactivated by β -lactamases enzymes present in the matrix. As the cells are immobilized and spatially confined

by the matrix, stable gradients of oxygen, nutrients and other molecules arise across the biofilm (1). This can lead, for example, to the formation of metabolically diverse subpopulations depending on the ease of access to nutrients and oxygens (6). This contributes to the biofilms' tolerance to antibiotics, as metabolically inactive, slow-growing cells do not offer many targets compared to metabolically active, fast-growing ones.

The phenotypes of biofilm-dwelling cells are heterogeneous. In addition, in most natural environments, microbial communities are composed of different strains and species (1, 93). These different populations interact with each other and can engage in social interactions, such as the exchange of metabolic by-products, signalling molecules and degrading enzymes, or competitive interactions including toxin secretion and surface protection (1). As these interactions are strictly dependent on the distance between cells, the initial spatial structure and arrangements of the different populations is of critical importance to determine the community dynamics (93).

1.2.4.1 Matrix composition and biofilm mechanical properties

Biofilms are soft active materials that exhibit both elastic (instantaneous reversible deformations) and viscous (time dependent irreversible deformations) characteristics (94). In particular, biofilms behave like an elastic solid at short time scales and like a fluid at longer ones. The ability of biofilms to 'flow' over long time scales enables the dissipation and relaxation of mechanical stress generated by growth or by external forces such as shear stress (5). The relaxation in a biofilm results from multiple rearrangement processes, including the rearrangement of the EPS matrix and of the bacterial cells themselves that have to find a new stable position upon an imposed deformation (94). Over a wide sample of biofilms, the shear modulus and the viscosity range from 10^{-2} to 10^6 Pa and from 10 to 10^9 Pa·s respectively (95). However, the relaxation time is almost the same with a value of about 18 min. As this value is of the same order of magnitude as the cells doubling time, this time might have a survival significance as the period over which a biofilm can respond to external stresses (94).

The composition, the concentration and the properties of the individual components of the matrix influence the biofilm mechanical properties and way of living. In *V. cholerae*, the polysaccharide VPS serves as the main scaffold of the extracellular matrix for this bacterium. Three accessory proteins, namely RbmA, Bap1 and RbmC, depend on VPS to function (96) (Figure 1.8). RbmA connects neighbouring cells by dimerizing and interacting with VPS. Bap1 and RbmC have partially redundant functions in ensuring cell to surface adhesion and contributing to the biofilm strength. Bap1, more than RbmC, localizes at the interface between the biofilm and the substrate, therefore acting as an anchor, while RbmC is mainly found in the bulk of the biofilm where it provides additional crosslinks with VPS (97). Additionally, RbmC seems to play a role in the adhesion to host intestinal surfaces. *V. cholerae* biofilm has been described as a double network: one network is composed of stiff bacterial cells interconnected through short-range interactions mediated by RbmA, the other one is composed of soft secreted polymers reinforced by crosslinks mediated by RbmC and Bap1 (98). Each matrix component contributes to the mechanics of the biofilm (98, 99). Starting from a mutant that doesn't produce any matrix with a low storage modulus G' (~120 Pa) and yield stress σ_s (~10 Pa), the addition of VPS increases the yield strain while the addition of RbmA, Bap1 and RbmC increases the modulus, leading to a WT biofilm with a G' ~1 kPa and a σ_s ~100 Pa. The expression of the genes encoding these components is controlled by c-di-GMP levels and quorum sensing (100). *V. cholerae* can develop into phenotypically different colonies, smooth and rugose colony variants, depending on the amount of matrix produced (increased matrix production for the rugose variant).

In *P. aeruginosa* the EPS consists of 3 major polysaccharide: Pel, Psl and alginate, which are positively, neutral and negatively charged respectively (97). Other important structural components are eDNA and the protein CdrA (Figure 1.8). In non-mucoid strains, Pel and Psl are the main polysaccharides. Psl plays the major role during attachment. It is anchored to the cell surface in a helical pattern and it promotes adhesion with strong, long ranged adhesive force (101, 102). Pel mediates adhesion through weak, short-range forces that promotes a symmetrical adhesion of the rod-shaped cell. There is a strain-to-strain variability in the contribution of Pel and Psl to the structure

of mature biofilms. For example, the strain PA14 relies only on Pel, while PAO1 mainly relies on Psl, with very few differences in the resulting biofilms, indicating that the two polysaccharides have a redundant role in regards to structure and cell-cell interactions (103).



Figure 1.8 Matrix composition of *V. cholerae* and *P. aeruginosa* biofilms.

In *V. cholerae* the polysaccharide VPS is the main structural component. The proteins Bap1, RbmA and RbmC interact with VPS to promote cell-substrate adhesion, cell-cell adhesion and crosslinking. For *P. aeruginosa* the main scaffold is provided by the polysaccharides Psl and Pel. The protein CdrA acts as a crosslinker by interacting with Pel and Psl, while eDNA can ionically bind to Pel.

At early stages, Psl forms a matrix that holds bacterial cells together, but it accumulates on the periphery of the colonies at later stages, preparing for biofilm dispersal with the formation of a cavity where cells lyse releasing DNA (102). Pel, on the contrary, localizes at the centre of the colony near the attachment surface, where it ionically binds to eDNA (104). eDNA, plays also a role in initial adhesion and in streamer formation (105, 106). The protein CdrA promotes aggregation both by binding to the Psl and Pel, therefore acting as a crosslinker for the polysaccharide matrix, but also through direct CdrA-CdrA interactions (107, 108). The moduli of *P. aeruginosa* have reported values that vary between few Pa to tens of kPa, depending on the technique used for the measurement and the strain studied (109). Since the role of the different components of the matrix is redundant, it is difficult to isolate their individual effects on the mechanical properties of the biofilm. Microrheology studies have shown that Δ psl strains are more relatively viscous and more compliant than biofilms of WT strains and Δ pel mutants (110). Bulk rheology measurements showed that the biofilm modulus is on the order of 1 kPa and that increased expression of either Pel or Psl increases yield stress, however Psl does that increasing the modulus, while Pel by increasing the yield strain (109). In addition, they show that the stiffening caused by Psl requires the presence of CdrA, which therefore

acts as a crosslinker. *P. aeruginosa*, like *V. cholerae*, can be found in smooth or rugose variants (111). Rugose variants constitutively produce more matrix, autoaggregate in liquid cultures, are hyperadherent and display high level of c-di-GMP. The increase in EPS production results in biofilms which are less compliant and exhibit increased relative elasticity (more elastic than viscous) compared to the WT strain (110).

1.2.4.2 Self-generated forces and morphomechanics

Self-organization in space and time is a fundamental developmental process in multicellular organisms as well as in bacterial communities (112). This process is governed by both cellular processes (growth, division, death, matrix production, differentiation) and physical forces (113). When surface-attached bacteria start growing and dividing while gluing themselves to each other and to the substrate, mechanical forces and instabilities arise. Self-generated internal forces and interactions with the substrate control biofilm morphogenesis in terms of local cellular order, transition from 2D to 3D colonies and global biofilm architecture. The physics behind this process involves repulsive forces between bacteria (steric cell-cell interactions and osmotic pressure resulting from a high concentration of matrix component in the intercellular space), friction forces between bacteria and the substrate, cell-cell attractions and elastic forces exerted on bacteria growing in a confined environment (114, 115). When bacteria grow sandwiched between glass and agarose, they first expand in a horizontal plane but eventually invade the agarose to form a three-dimensional community. This happens when microcolony ‘squeezing’ causes cells to move out of the horizontal plane, overcoming the vertical forces resulting from compression of the agarose and the extension of the elastic links with the substrate (116, 117). The colony shape and the size at the onset of the second layer depends on the adhesion of the bacterial cells to the substrate (earlier onset and more circular shape with higher adhesion) (117).

Advances in microscopy enabled live single-cell resolution imaging of natural *V. cholerae* biofilms as they develop from one founder cell to mature 3D clusters and the discovery of the forces that promote their architectural development (100, 118, 119). At first cells grow in a 1D line attached to the substrate, and this line eventually buckles in a 2D arrangement, presumably when cell-surface

adhesion becomes stronger than bacterial pole-pole adhesion. The colony keeps growing horizontally until when the combination of expansion and confinement due to the peripheral cells generates a stress that overpowers the cell-to-surface adhesion causing cells to align vertically and triggering the transition from a 2D to a 3D growth (120) (Figure 1.9A). Because of the orientation of the division along the cell line and the compression due to the increase in cell density (driven by proliferation and cell-cell adhesion), the biofilm core is packed in a nematically ordered structure with cells perpendicular to the surface. Cells at the periphery instead align radially and remain horizontal. Biofilms can therefore be considered as self-replicating active liquid crystals (115). Mutagenesis of the main matrix components revealed that surface adhesion mediated by Bap1/RbmC is necessary for the transition into the 3rd dimension and the instauration of both vertically and radially ordered regions (100). Cell-cell cohesion mediated by RbmA controls the biofilm growth mode: the absence of RbmA increases cell-to-cell distances and establishes a growth mode driven by matrix expansion which is no longer resisted by cell-to cell-connections. The loose structure of the $\Delta rbmA$ mutant makes the biofilms more susceptible to mechanical disruption, shear flow, outcompetition and invasion from phages and other cells (100, 115, 121). Recently, light sheet microscopy combined with intracellular puncta labelling technology enabled the tracking of single cells inside the growing biofilm. The cell trajectories revealed that a set of cells is trapped at the surface while another set expand outward in fountain-like flow driving 3D expansion. In addition, they showed that the coherence of the trajectories requires RbmA and that the substrate friction alters biofilm morphology (increased height-to-radius aspect ratio with increasing friction).

The magnitude of forces generated by growing biofilms is underexplored. Preliminary work has shown that *E. coli* colonies growing in a confined environment exert pressures higher than 10 kPa, while Yeast colonies can generate stress in the order of MPa (5, 122, 123). These forces would be sufficient to rupture eukaryotic cells membranes from inside. Micropillars embedded in microchambers were used to study the forces generated by *P.aeruginosa* biofilms: the deflection of the pillars revealed that the applied pressures were in the range of 1-25 kPa (124). The growth of pellicles (biofilms floating on top of liquid) under confinement induces a compressive force of about

80 Pa: this growth-induced pressure helps maintaining the biofilm integrity, contributes to its self-repair and trigger the buckling and wrinkling of the elastic pellicle (125, 126) (Figure 1.9B). The production of matrix is required for the production of this force as it maintains the pellicles connected and elastic. Biofilms growing on surfaces are confined due to adhesion with the substrate. Biofilms growing at the agar-air interface exhibit rich surface patterns including concentric rings, radial ridges, labyrinthine networks, branches, and their combinations (127) (Figure 1.9B). These patterns vary widely, even within the same species, depending on physiological conditions and environmental cues (128). Experimental and theoretical studies have tried to reveal the origin of these morphologies (113, 127–137). It has been proposed that the formation of wrinkles might be a strategy adopted by the biofilm to facilitate transport of nutrients and oxygen (135–137). Gradients of environmental cues (nutrient limitation in the centre), heterogeneity in gene expression and matrix production (stiffness gradients), anisotropic expansion (due to directional cell division) and differential cell growth/proliferation along the radial direction combined with the interaction with the substrate participate in the generation of compressive stresses (127, 128, 130–133, 138). If these stresses are large enough they can destabilize the biofilm, leading to the different patterns.

Strain mismatch between bonded layers with different expanding or shrinking rates induce mechanical instabilities. This phenomenon represents a potential universal mechanism for the formation of morphological patterns in growing tissues, organs, plants and microorganisms (131). The compressive stress generated by mismatch leads to various morphologies such as wrinkles, folds or delaminated blisters depending on the amount of mismatch strain, the modulus of the biofilm and the substrate and the interfacial adhesion energy. A biofilm growing on agar can be described as a growing layer attached to a non-growing one. When the growth strain reaches a critical value, the accumulated stresses may destabilize the biofilm layer, and depending on the parameters of the systems, the initially flat biofilm can for example release the compressive stress by wrinkling and subsequently delaminating as growth gradually builds up compressive stress (132). Material properties of the biofilm (viscoelasticity, modulus, adhesion, amount and type of matrix component) are important in determining the resulting pattern. For example, rugose colonies (high levels of matrix

production), are named this way because of the formation of morphological patterns, as opposed to their smooth counterpart. Rugose *V. cholerae* form radial blisters, while the absence of Vps hinders this process; the absence of RbmA or Bap1 and RbmC leads respectively to smaller blisters and a curious star shaped pattern (139). Dead cells and defects can focus mechanical forces, facilitating the onset of buckling and blister formation (113, 132). Overall, genetic and regulatory features and their spatial organization, coupled with mechanical instabilities, control the origin of these patterns (140).

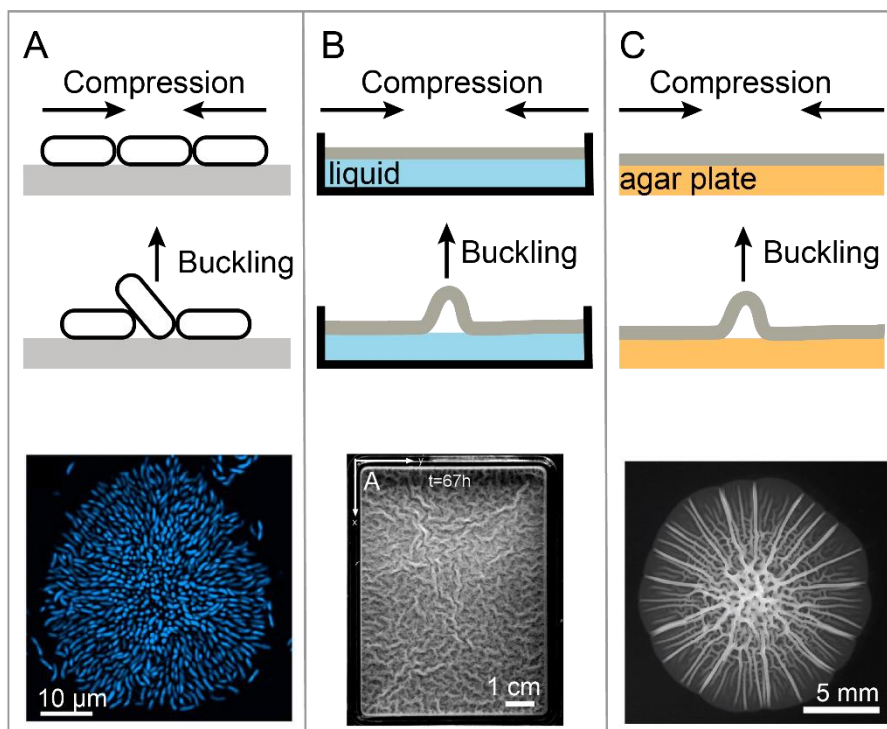


Figure 1.9 Buckling instabilities in biofilm morphogenesis.

(A) In *V. cholerae* immersed biofilms, surface attached peripheral cells compress cells growing in the inside region, triggering their buckling and verticalization. Adapted from (120). (B) Pellicles of *B. subtilis* growing at the air liquid interface wrinkle when they are laterally confined. Adapted from (126). (C) *V. cholerae* colonies growing at the agar-air interface are confined by their adhesion to the substrate. Compressive stresses destabilize the biofilm and lead to the formation of various patterns. Adapted from (132).

1.2.4.3 Effects of environmental mechanics on biofilm morphogenesis

Flow can influence the distribution of nutrients, signaling molecules and antimicrobials that surface-attached cells experience (22). This mediates the behavior of single bacteria and the development of multicellular communities. For example, in the absence of flow, *Vibrio cholerae* ‘cheater’ mutants

(not able to digest chitin as they cannot produce chitinase) can take advantage of diffusing nutrients released by the wild type strain (141). However, this cannot happen under flow, as the nutrients are dispersed. Irregular flow geometries, like the ones found in bends of curved channels or at the corners of pillars, create the conditions for the formation of streamer biofilms (106, 142). As streamers are in the bulk of the flow, they tend to clog the channels and create zero flow conditions, that in the case of *P. aeruginosa* for example, can allow non-producing matrix cells to accumulate (143). In addition, the interplay between advection and diffusion can determine the lineage mixing in biofilm communities: low flow promotes swimming-dependent mixing, while strong flow favors the formation of larger, more segregated colonies (144) (Figure 1.10A). Flow can also influence the mechanical strength of the biofilms. In general, biofilms grown under higher flow tend to be more elastic, more resistant, denser and with higher content of matrix proteins and EPS (15). This behavior has been associated to a shear-induced EPS production (115). Overall, flow can influence biofilm architecture, composition and mechanical strength.

Most investigations of the effects of material properties on bacterial colonization focus on the initial steps of adhesion, but studies on long-term effects of materials on biofilm formation are lacking. Few studies related to surface motility, described in section 1.2.3.1, showed differences in biofilm morphology: large biofilm aggregates would form when motility was inhibited, opposed to flat and dispersed biofilms (74, 75) (Figure 1.10B). Studies describing differences in architecture and morphologies focused on biological or chemical factors. For example, the carbon source can determine biofilm formation in *P. aeruginosa*: flat biofilms form with citrate, while heterogeneous mushroom-shaped structures would form with glucose (145). Iron limitation was shown to trigger twitching motility and therefore limit the formation of cell clusters (146). Δ pilA mutants (deficient in pili formation) form protruding microcolonies at fixed locations as they cannot spread on the surface (145). Geisel *et al.* recently showed that tuning the adhesive strength between a PDMS substrate and PAO1 biofilms impacts buckling-delamination instabilities and therefore induce or impede biofilm delamination and channel formation (147). Martinez-Garcia and co-workers modelled the combined effect of adhesion and flow on the biofilm spatial structure: highly-adhesive strains form larger

coherent clonal clusters than the weakly-adhesive ones; however, when flows are weak or the population density is high the opposite behaviour is expected (148).

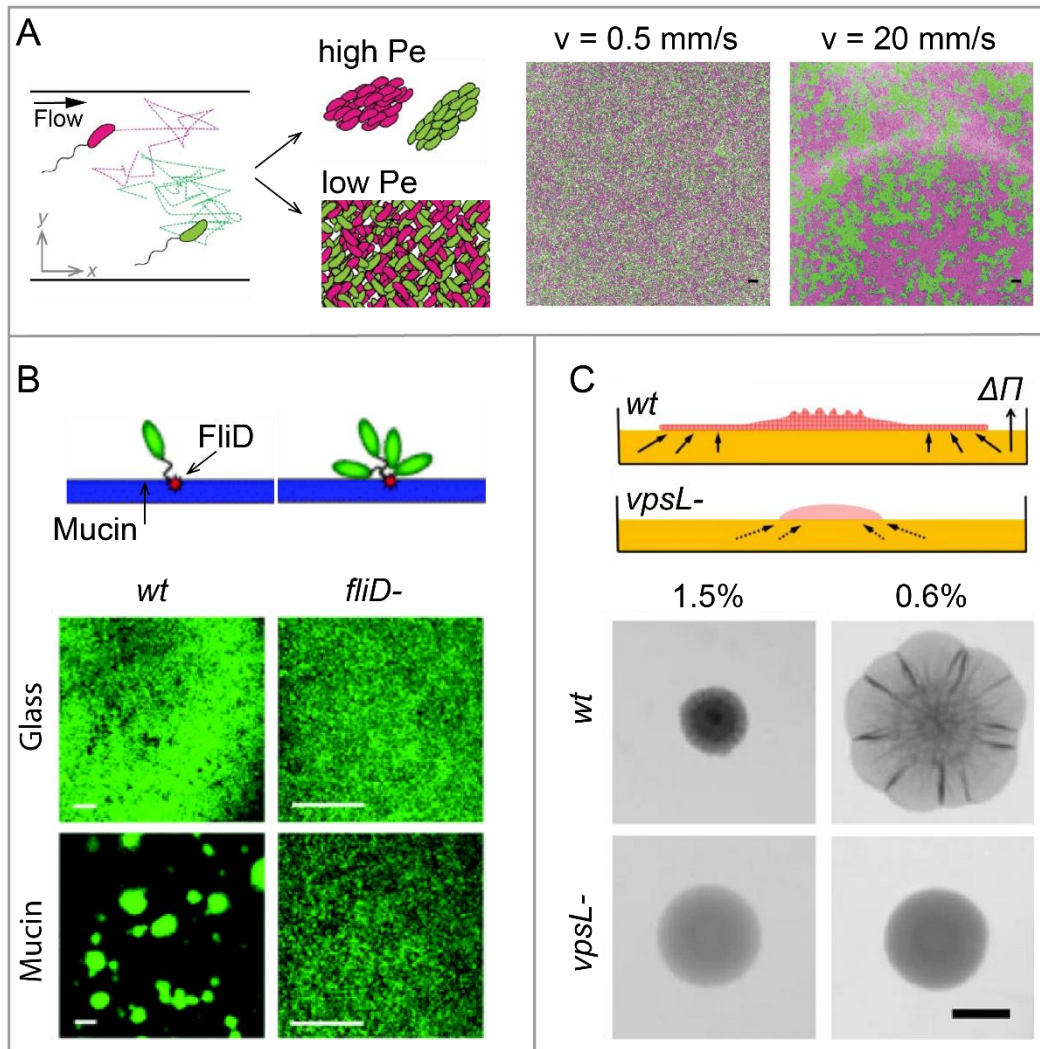


Figure 1.10 Effects of environmental mechanics on biofilm formation.

(A) The relative contribution of advective and diffusive transport (described by the Péclet number Pe) influences the mixing of different lineages in *C. crescentus*. Adapted from (149). (B) Binding of the flagellar cap FliD to mucin coated surfaces inhibits twitching and flagellar motility in *P. aeruginosa*, leading to the formation of clustered biofilms. Adapted from (74). (C) Osmotic pressure differences $\Delta\Pi$ between the agar and the matrix of the biofilm drives biofilm expansion in *V. cholerae* colonies grown at the agar-air interface. Stiffer substrates (higher agar concentration) inhibits swelling and nutrient uptake, limiting biofilm expansion. Adapted from (139).

Despite host-associated biofilms ubiquitously forming on soft surfaces, the mechanisms by which mechanical properties of a substrate impacts the structure and organization of a biofilm have been overlooked. Only few studies, limited to biofilms grown at the solid-air interface, have tried to address this question. When biofilms are grown on agar of different stiffnesses, the general

observation across studies is that biofilm expansion decreases with increasing agar concentration (139, 150). However, this trend has been mainly associated to differences in the mesh size of the agar gel and the subsequent osmotic pressure differences between the biofilm matrix and the substrate and the nutrient uptake: a higher osmotic difference (on lower concentrations of agar) promotes swelling of the colony and nutrient uptake and therefore more expansion (139, 151) (Figure 1.10C). However, Asp *et al.* recently showed that colony growth increases with substrate stiffness when using polyacrylamide gels, independent from the mesh size of the gel or the bacterial species and motility (150). Stiffness doesn't only influence the expansion rate of the colonies, but its morphology as well. Indeed, Yan *et al.* showed that in *V. cholerae* the wavelength of wrinkles and the wrinkling to delamination transition varies with the substrate stiffness, as predicted by the mechanical instability theory (132). Fey *et al.* studied the morphodynamics of colonies growing on agar of different concentrations and observed that on soft substrates (low friction) the wrinkles initially appear in the peripheral region and propagate inward, while on stiff substrates (high friction) the wrinkles first appear in the central region and propagate outward (133). A summary of the effect of surface stiffness on biofilm formation can be found in Table 1.4.

Table 1.4 Summary of studies which investigated the effect of material stiffness on biofilm formation

Material	Behavior	Bacteria	Modulus	Results
Agar (139)	Biofilm expansion	<i>V. cholerae</i>	0.5-12 kPa	Expansion decreases with substrate stiffness
Polyacrylamide (150)	Biofilm expansion	<i>S. marcescens</i> <i>P. aeruginosa</i> <i>P. mirabilis</i> <i>M. xanthus</i>	0.1-10 kPa	Expansion increases with substrate stiffness
Agar (132)	Biofilm morphology	<i>V. cholerae</i>	0.14-67 kPa	Stiffness impact wavelength of wrinkles and the wrinkling to delamination transition
Agar (133)	Biofilm morphodynamics	<i>V. cholerae</i>	0.1-10 kPa	Stiffness and friction influence the origin of wrinkle formation

1.3 Aims and organization of the thesis

The association of the bacterial cells with the surface of host cells and tissues and the presence of fluid flow are fundamental characteristics of a host-colonization environment. There is a growing evidence of mechanically regulated bacterial phenotypes. However, the role of substrate stiffness has been investigated mainly with respect to initial adhesion. Adhesion studies have explored different materials such as hydrogels and PDMS, and studies of biofilm morphogenesis are still confined to agar-air and glass-agar systems or to immersed biofilms growing on glass or plastic. To recapitulate the mechanics of the infection environment it is necessary to combine soft substrates with flow.

During my thesis I combined microfluidics with synthetic PEGDA hydrogels in order to investigate the effect of substrate stiffness on biofilm formation and its implications in infections. The thesis is organized in 2 main chapters:

In chapter 2 I show how we discovered that biofilms can deform soft substrates and damage monolayers of epithelial cells. We demonstrate that this phenomenon is due to a buckling instability and it relies on both the mechanical properties of the substrate as well as to the material properties of the growing biofilm.

In chapter 3 I show how the mechanical properties of the substrate can influence twitching motility and thus the subsequent biofilm architecture, resulting in biofilms with different tolerance to antibiotics and with different spatial structures.

Finally, I will discuss the significance of my findings and I will provide inputs for future work.

Chapter 2. Biofilms deform soft surfaces and disrupt epithelia

This chapter has been published in eLife (152):

<https://doi.org/10.7554/eLife.56533>

Authors:

Alice Cont, Tamara Rossy, Zainebe Al-Mayyah, Alexandre Persat*

Affiliations:

Institute of Bioengineering and Global Health Institute, EPFL, Lausanne, Switzerland

*Corresponding author: alexandre.persat@epfl.ch

My contributions: Design of the experiments, data acquisition and data analysis.

2.1 Abstract

During chronic infections and in microbiota, bacteria predominantly colonize their hosts as multicellular structures called biofilms. A common assumption is that biofilms exclusively interact with their hosts biochemically. However, the contributions of mechanics, while being central to the process of biofilm formation, have been overlooked as a factor influencing host physiology. Specifically, how biofilms form on soft, tissue-like materials remains unknown. Here we show that biofilms of the pathogens *Vibrio cholerae* and *Pseudomonas aeruginosa* can induce large deformations of soft synthetic hydrogels. Biofilms buildup internal mechanical stress as single cells grow within the elastic matrix. By combining mechanical measurements and mutations in matrix components, we found that biofilms deform by buckling, and that adhesion transmits these forces to their substrates. Finally, we demonstrate that *V. cholerae* biofilms can generate sufficient mechanical

stress to deform and even disrupt soft epithelial cell monolayers, suggesting a mechanical mode of infection.

2.2 Introduction

In their natural environments, bacteria commonly grow and self-organize into multicellular structures called biofilms (1). Biofilms form when bacteria attach onto a solid surface and divide while embedding themselves in a matrix of extracellular polymeric substances (EPS) (153). The biofilm matrix is a viscoelastic material generally composed of a mixture of polysaccharides, proteins, nucleic acids and cellular debris (2). EPS maintains cell-cell cohesion throughout the lifecycle of a biofilm, also making the resident cells more resilient to selective pressures. The biofilm lifestyle provides resident cells with fitness advantages compared to their planktonic counterpart, for example by increasing their tolerance to external chemical stressors such as antimicrobials and host immune effectors. In addition, its mechanical strength and cohesion promotes biofilm integrity against physical challenge such as flow and grazing (154).

Bacteria often colonize the tissues of their host in the form of biofilms. For example, they are a common contributor of infections, as in cystic fibrosis patients who are chronically infected by biofilms of the opportunistic pathogen *P. aeruginosa* (155, 156). Biofilms are also widespread in microbiota, for example as commensals seek to stably associate with host intestinal epithelium (157). As they grow on or within a host, biofilms must cope with a battery of chemical and physical stressors. In particular, they must inevitably form at the surface of soft biological material composed of host cells or extracellular matrix (ECM). Multiple biophysical explorations have demonstrated the importance of biofilm internal mechanics in morphogenesis (100, 113, 125, 132). However, and despite host-associated biofilms ubiquitously forming on soft surface, we still lack a rigorous understanding of how the mechanical properties of a substrate impacts the physiology of a biofilm, and reciprocally how biofilms impact the mechanics of soft biological surfaces.

The growth of single cells embedded within self-secreted EPS drives biofilm formation. During this process, cells locally stretch or compress the elastic matrix, thereby exerting mechanical

stress (125, 140). This local action at the level of single cells collectively generates mechanical stress across the whole biofilm structure. Thus, the combination of biofilm growth and matrix elastic properties imposes buildup of internal mechanical stress (5). As a consequence of this stress, bacterial colony biofilms form folds and wrinkles when growing on agar plates or at an air-liquid interface (126, 132). These mechanics also influences the spatial organization of single cells within *V. cholerae* immersed biofilms (115, 118, 120). Internal mechanical stress can also arise by a combination of cell-surface adhesion and growth, influencing the architecture of submerged biofilms and microcolonies. Friction force between the microcolony and the surface opposes biofilm expansion, generating an inward internal stress that leads to a buckling instability verticalizing or reorienting contiguous cells (117, 120). These studies demonstrate the importance of mechanics in biofilm morphogenesis and spatial organization, but their function in the context of host colonization remains unknown.

Here, we investigate how biofilms form at the surface of soft material whose mechanical properties replicate the ones encountered *in vivo*. We show that biofilms from the model pathogens *V. cholerae* and *P. aeruginosa* can deform soft synthetic hydrogel substrates they grow on. By spatially and quantitatively measuring substrate morphology, we propose a model where biofilms buckle to initiate deformations. By comparing wild-type, EPS matrix hypersecreting and mutant strains, we demonstrate that matrix components maintaining cell-cell cohesion and cell-surface adhesion contribute to the mechanism of substrate deformation. The magnitude of the deformations depends on the stiffness of the material in a range that is physiologically-relevant. Using traction force microscopy, we show that biofilms can generate large mechanical stress reaching up to 100 kPa. Finally, we demonstrate that biofilms can deform and even damage tissue-engineered soft epithelia whose mechanics reproduce the ones of a host tissue. These insights suggest that forces generated by growing biofilms could play a role not only in their morphogenesis, but also in mechanically compromising the physiology of their host.

2.3 Results

2.3.1 Biofilms deform soft substrates

To understand how biofilms interact with soft surfaces, we first explored their formation on synthetic hydrogel substrates. We generated polyethylene glycol (PEG) hydrogel films via photoinitiated polymerization of PEG diacrylate precursors at the bottom surface of microfluidic channels. These polymeric films are covalently bound to the glass surface to avoid drift and delamination. By using a “sandwich” method for polymerization, we could fabricate flat ~100 μm -thin PEG films that allowed us to perform high resolution live confocal imaging of biofilm formation under flow (Figure 2.1A). We first used a rugose variant of *V. cholerae* A1152 strain (referred to as *V. cholerae* Rg) which constitutively secretes EPS matrix, thereby forming robust and reproducible biofilms. On soft hydrogels, *V. cholerae* Rg formed biofilms whose bottom surfaces appeared bell-shaped (Figure 2.1B), in striking difference with the typically flat-bottom biofilms that form on hard surfaces such as glass and plastic. To distinguish whether this shape was a result of the deformation of the hydrogel or of the detachment of the biofilm from the surface, we embedded fluorescent tracer particles within the hydrogel film by mixing them with the pre-polymer solution before the cross-linking step. We could observe that the fluorescent tracer particles filled the apparent bell-shaped void at the biofilm core and that the hydrogel surface and the biofilm remained in contact (Figure 2.1C). This demonstrates that the soft hydrogel substrate deforms under *V. cholerae* biofilms.

We then wondered whether these deformations were specifically induced by *V. cholerae* or could represent a common feature of biofilms across species. We thus tested whether *P. aeruginosa* biofilms could deform soft hydrogels. We found that biofilms of *P. aeruginosa* *wspF* mutant (*P. aeruginosa* Rg), which constitutively produces EPS matrix and robustly forms biofilms, could similarly deform soft PEG hydrogels (Figure 2.1D-E). In summary, *V. cholerae* and *P. aeruginosa*, two model biofilm-forming species with distinct EPS composition are both able to deform soft substrates. This is consistent with a mechanism where biofilms generate mechanical stress on the material they grow on.

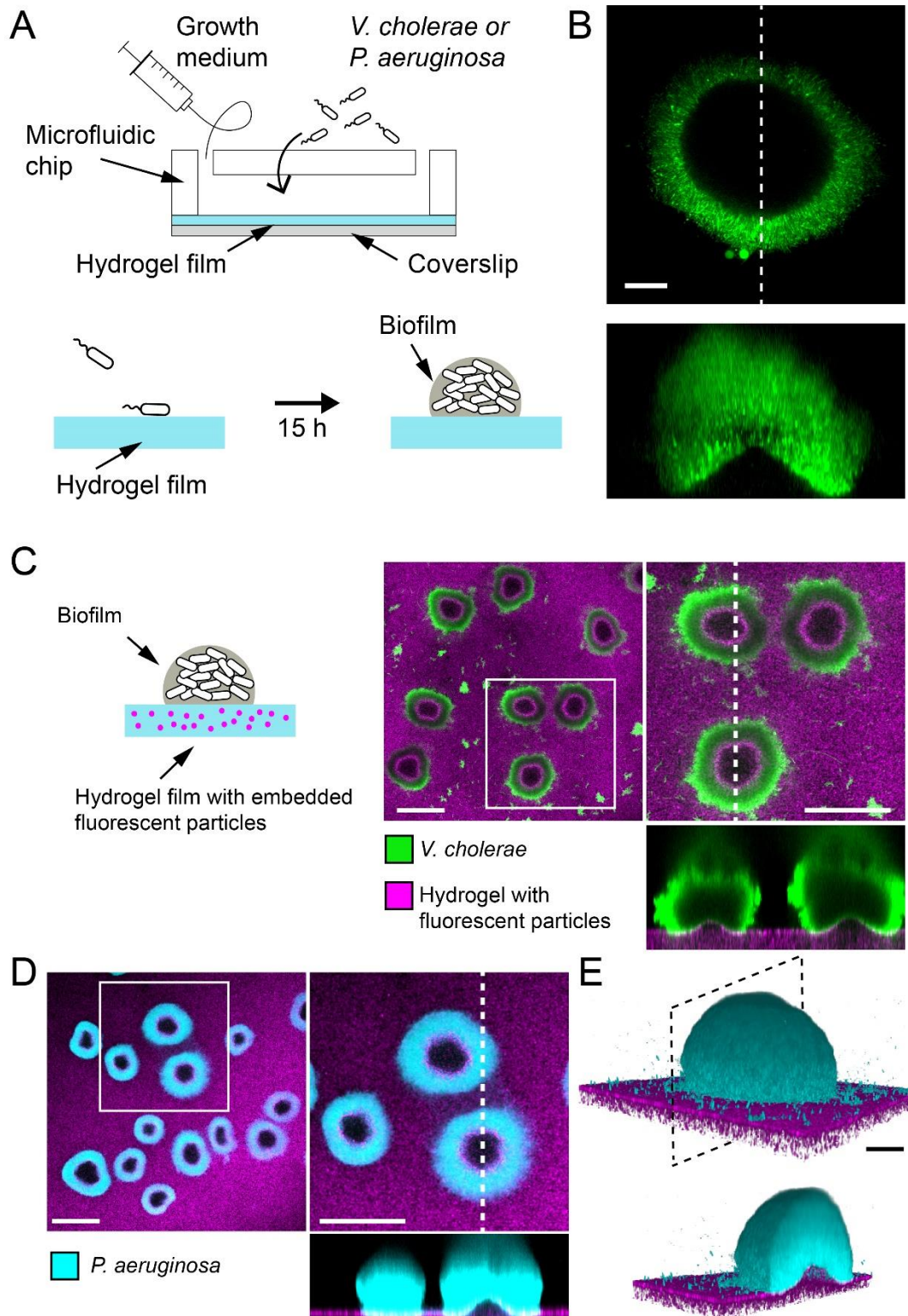


Figure 2.1: Biofilms deform soft substrates.

(A) Illustration of experimental setup where we generate thin hydrogel films at the bottom surface of microchannels. These devices allow us to study biofilm formation on hydrogels reproducing mechanical properties of host tissues. (B) In-plane and cross-sectional confocal visualizations show that *V. cholerae* *Rg* biofilms growing on hydrogels display large gaps at their core. (C) Embedding fluorescence tracer particle in the hydrogel films allow for visualization of deformations. *V. cholerae* *Rg* biofilms formed at the surface of the films deform the substrate. (D) *P. aeruginosa* *Rg* biofilms similarly deform the soft substrates. Hydrogel elastic modulus: (B and C) $E = 12$ kPa, (D and E) $E = 38$ kPa. Scale bars: (C and D) 100 μm , (B and E) 20 μm .

2.3.2 Biofilms deform soft substrates after reaching a critical diameter

How do biofilms mechanically deform hydrogel films? Given the influence of growth-induced internal mechanical stress on biofilm morphology and architecture, we hypothesized that biofilms could deform soft substrates by transmission of internal stresses to the substrate they grow on. To test this hypothesis, we performed dynamic visualizations of the deformations of hydrogel films as biofilms grew. To obtain an accurate deformation profile, we performed a radial re-slicing and averaging around the biofilm center. We could thus extract the deformation profile δ , its maximum deformation amplitude δ_{max} and full-width at half maximum λ (Figure 2.2A). We thus recorded surface profiles for many biofilms. By reconstructing hydrogel surfaces for biofilms of different sizes, we found that δ_{max} and λ linearly scaled with the diameter d of the biofilm (Supplementary Figure 2.1), indicating that biofilm expansion promotes surface deformation.

We went further and dynamically tracked these deformations for single biofilms. Deformations increased as biofilms grew, even displaying a slight recess near the biofilm edges (Figure 2.2B-C, Movie 2.1). In these visualizations, we noticed that there was a lag between the increase in biofilm diameter and the onset of deformation, with a finite deformation only appearing after 7 h of growth. This was further confirmed by following the deformations generated by many biofilms. Measurable morphological changes of the surface appeared after 6 to 7 h of growth (Figure 2.2D). Rescaling these measurements with the diameter of the biofilm collapsed δ_{max} measurements, highlighting a critical biofilm diameter (35 μm) above which deformations emerged (Figure 2.2E). The existence of a critical diameter is reminiscent to buckling instabilities of rigid bodies subject to compressive stress, as in Euler buckling.

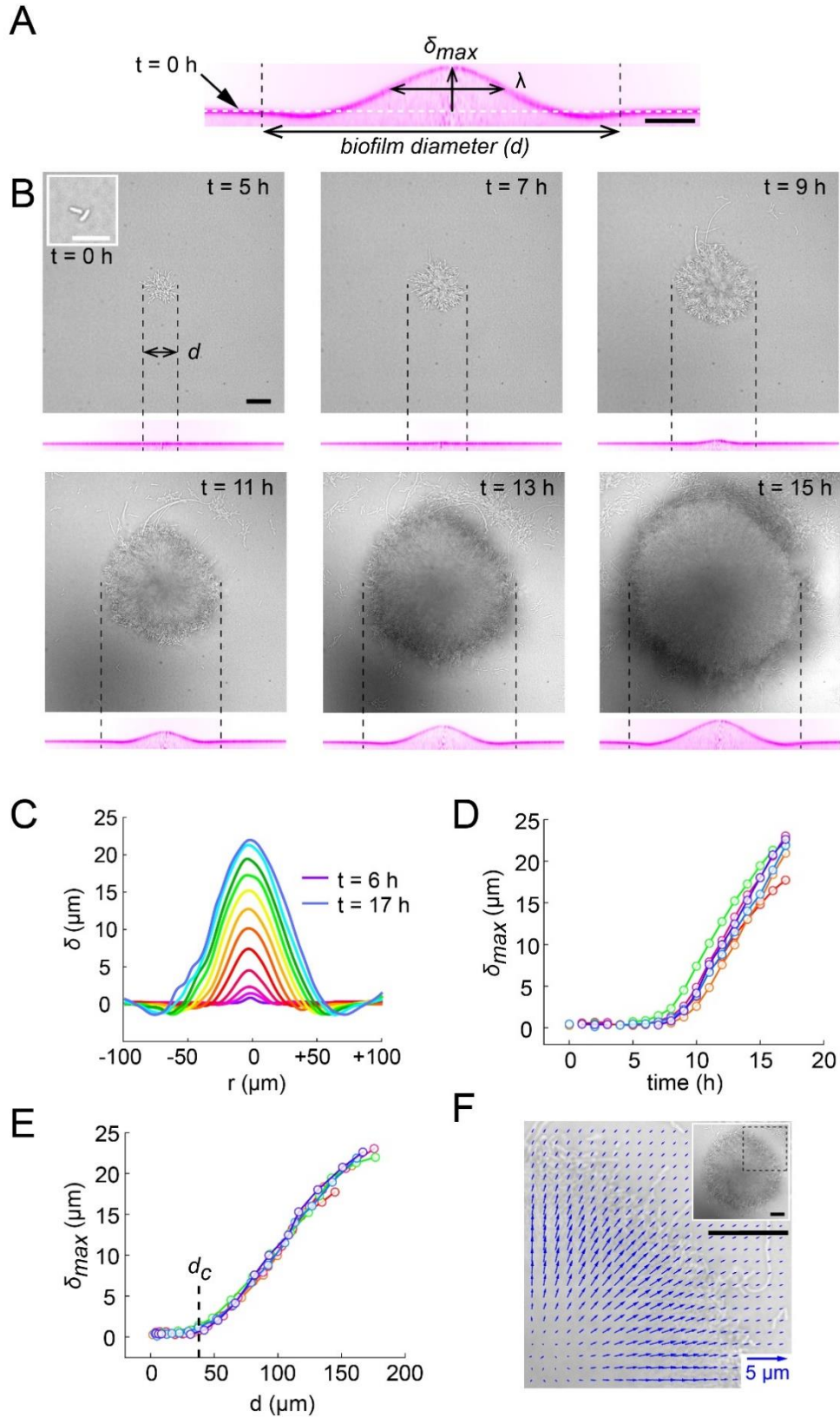


Figure 2.2: Biofilms deform their substrate by buckling.

(A) Morphological parameters δ_{max} (maximum deformation amplitude) and λ (half max full width) computed from resliced deformation profiles. Dashed line indicates the baseline position of the gel surface. (B) Timelapse visualization of *V. cholerae* Rg biofilm growth (brightfield, top) with deformation (reslice, bottom). Dashed lines

indicate biofilm position and size on the corresponding hydrogel profile. (C) Superimposition of these profiles shows the rapid deformation and the emergence of a recess at biofilm edges. Each color corresponds to the same biofilm at different times. (D) Time evolution of δ_{max} shows a rapid increase after 6 to 7 h of growth. (E) The dependence of δ_{max} on biofilm diameter highlights a critical biofilm diameter d_c above which deformation occurs. For D and E each line color corresponds to a different biofilm. (F) Hydrogel strain field computed by digital volume correlation between 11 h and 12 h of growth. We superimposed the vector strain field with a brightfield image of the biofilm. For visualization purposes we only display data for the top right quarter of the biofilm shown in inset (dashed lines). $E = 38$ kPa. Scale bar: 10 μm for inset $t = 0$ h in (B), else 20 μm .

2.3.3 Biofilms push their substrate in the growth direction

To further investigate the mechanism by which biofilms deform surfaces, we quantified the hydrogel substrate strain during growth. To achieve this, we tracked the displacements of the fluorescent tracer particles embedded within the hydrogel in 3D using a digital volume correlation algorithm (158). At the early stages of hydrogel deformation, we found that in the plane defined by the initial surface at rest, the particles under the biofilm move in the direction of growth. Thus, the strain field shows that the biofilm stretches its substrate radially in the outward direction in addition to vertical deformations (Figure 2.2F and Supplementary Figure 2.2). In other words, a biofilm applies an in-plane stress on the substrate in its growth direction, which is most likely generated by a friction between the biofilm and the surface (117, 120). As a result, the elastic biofilm experiences a force in the opposite direction, towards its center. This result is consistent with observations of growth of colony biofilms (132). In summary, the opposition between biofilm growth and friction with the surface generates an internal mechanical stress within the biofilm oriented radially, towards its center.

2.3.4 Wild-type and rugose biofilms deform soft-substrates

Given its importance in generating internal stress with the biofilm, we anticipate that the EPS matrix plays a role in the onset of substrate deformations. Rugose strains constitutively produce copious amounts of matrix compared to wild-type (100, 111, 115, 132, 159–161). To verify whether WT can deform substrates and to probe the contribution of matrix hypersecretion, we quantitatively compared the deformations of WT strains of *V. cholerae* and *P. aeruginosa* with their *Rg* forms. First, WT *P. aeruginosa* deformed hydrogel films under the same growth conditions as *Rg*. The amplitude of the deformation δ_{max} was substantially lower than *Rg* (Figure 2.3A). Then, we visualized smooth WT *V. cholerae* A1552 under multiple growth conditions which are known to influence its ability to form

robust biofilms. WT biofilms deformed the hydrogel substrate when grown in M9 medium, but not in LB where biofilms are rare and WT *V. cholerae* essentially spread as a monolayer of cells on the surface (Figure 2.3B). The deformation amplitude δ_{max} of WT biofilms in M9 could reach the magnitude of R_g (Figure 2.3C), but were however more heterogeneous between biofilms. Finally, we went on to compare the ability of smooth WT *V. cholerae* strains A1552, N16961 and C6706, to deform hydrogel substrates. These strains are commonly used as models for biofilm formation, build biofilms with identical matrix components, but likely regulate them distinctly. We found that all three strains could deform the substrate (Supplementary Figure 2.3). The magnitudes of deformation however differed between isolates: N16961 and C6706 deform the substrate more dramatically than A1552. In summary, WT and rugose *V. cholerae* and *P. aeruginosa* biofilms deform soft substrates. The quantitative differences in deformation amplitudes observed across growth conditions and strains, plus the established role of the EPS in biofilm morphogenesis suggests that matrix production plays a fundamental role in generating internal forces and in subsequently deforming soft substrates.

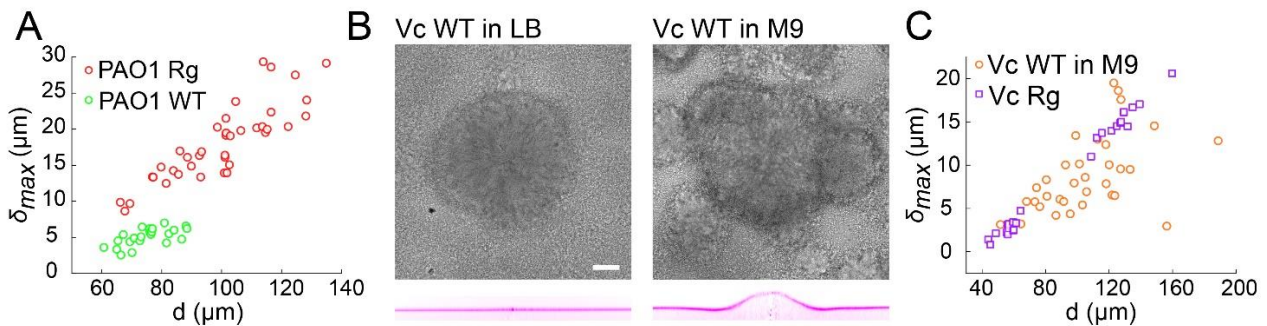


Figure 2.3: Wild-type and rugose biofilms deform soft-substrates.

(A) Biofilm diameter-dependence of maximum deformation for rugose and smooth variants of *P. aeruginosa*. (B) Smooth variant of *V. cholerae* A1552 deforms hydrogels when growing in M9 medium, but not in LB. (C) Biofilm diameter-dependence of maximum deformation for rugose and smooth variants of *V. cholerae*. Data points correspond to biofilms grown in two microfluidic chambers for PAO1 Rg, PAO1 WT and Vc WT and to biofilms grown in one microfluidic chamber for Vc Rg. $E = 38$ kPa. Scale bars: 20 μm .

2.3.5 EPS composition drives biofilm and substrate deformations

We then wondered how matrix composition and associated changes in mechanical properties of biofilms influence substrate deformations. To investigate their contributions, we used *V. cholerae*

EPS matrix mutants with altered biofilm structure and mechanical properties. The *V. cholerae* matrix is mainly composed of a polysaccharide (*vps*) and proteins including Rbma, an extracellular component which specifically strengthens cell-cell cohesion and stiffens the matrix (98, 159). We confirmed that *vpsL* deletion mutants couldn't form biofilms (Supplementary Figure 2.4). More surprisingly, we found that biofilms of *rbmA* deletion mutants were unable to deform the hydrogel substrate, indicating that cell-cell cohesion is an essential ingredient in force generation (Figure 2.4A). Complementation of *rbmA* restored the ability to deform (Supplementary Figure 2.4B). In *P. aeruginosa*, the polysaccharides Pel and Psl, and the protein CdrA play partially redundant functions in maintaining elastic properties of the biofilm (103, 104, 109). In a similar manner, we found that the deformations generated by *P. aeruginosa pel*, *psl* and *cdrA* mutants were lower compared to *Rg*, but were not abolished (Figure 2.4B-C). The largest drop in deformation occurred in the *pel* mutant. This further demonstrates that mechanical cohesion provided by the EPS matrix plays a key role in surface deformation.

We then probed the function of adhesion of the biofilm with the surface by visualizing the deformations generated by a *V.cholerae* *bap1* deletion mutant. Bap1 is specifically secreted at the biofilm-substrate interface to maintain proper surface attachment (159). The *bap1* mutant formed biofilms that did not deform the surface. However, it produced slightly bent biofilms delaminated from the substrate creating a gap between the biofilm and the hydrogel, indicating that it may have buckled (Figure 2.4A). Complementation of *bap1* restored the ability to deform the hydrogel (Supplementary Figure 2.4C). Our observations of delamination of the *bap1* mutant show that adhesion transmits mechanical stress generated by buckling from the biofilm to the substrate. Due to the redundant functions of its EPS components, we could not produce *P. aeruginosa* mutants with altered surface adhesion properties. However, *P. aeruginosa* biofilms growing on hydrogels with large Young's modulus delaminated (Supplementary Figure 2.5). This observation highlights that the transition between deformation and delamination depends on the relative contribution of adhesion strength and substrate elasticity. In summary, cell-cell mechanical cohesion is essential in generating the

internal stress that promotes biofilm buckling, while cell-substrate adhesion transmits this stress to the underlying substrate (Figure 2.4D).

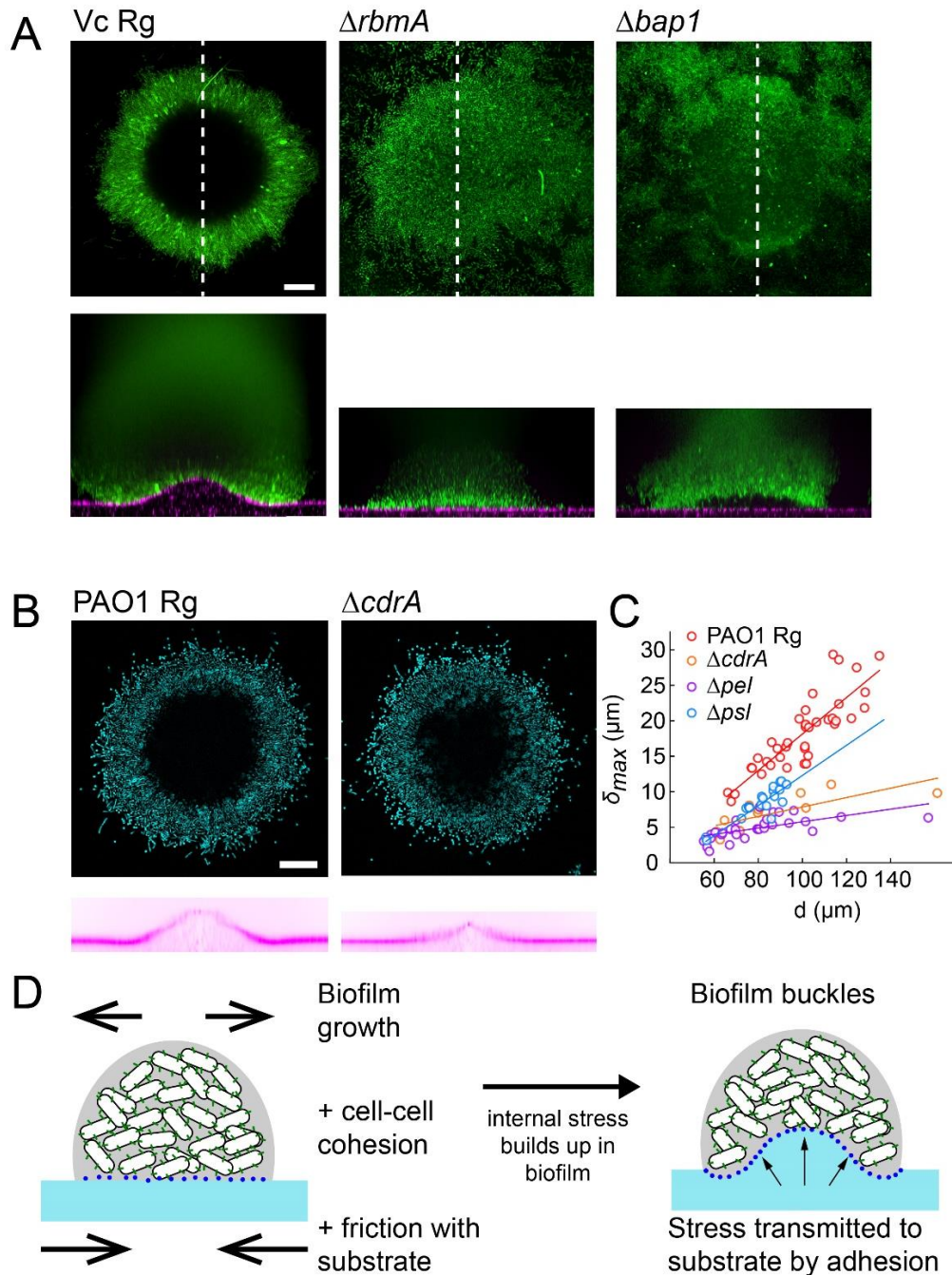


Figure 2.4: EPS composition drives biofilm and substrate deformations.

(A) Deformations of hydrogel substrates by *V. cholerae* Rg, *rbmA*⁻ and *bap1*⁻ biofilms. Biofilms formed by *rbmA*⁻ and *bap1*⁻ fail to deform the substrate. *bap1*⁻ biofilms delaminate from the hydrogel surface. (B) Comparison of hydrogel deformations by *P. aeruginosa* Rg and *cdrA*⁻ biofilms. (C) Dependence of maximum deformations on *P. aeruginosa* Rg, *cdrA*⁻, *pel*⁻ and *psI*⁻ biofilm diameter. All matrix mutants tend to generate weaker deformations compared to Rg. Data points correspond to different biofilms grown in two microfluidic chambers. (D) A model for the mechanism of biofilm deformation of soft substrates. Buildup of mechanical stress in the biofilm induces buckling. Adhesion between the biofilm and the surface transmits buckling-generated stress to the hydrogel, inducing deformations. $E = 38$ kPa. Scale bars: 20 μm .

2.3.6 Biofilms generate large traction forces

Biofilms thus deform soft materials by coupling growth-induced buckling and adhesion to their substrate. Could the mechanical stress generated on the substrate also impact various types of biological surfaces? To first explore this possibility, we quantified the forces exerted by the biofilm on hydrogel films. We used our particle tracking data to perform traction force microscopy (TFM), thereby computing the stress field and surface forces applied by the biofilm on the hydrogel. Traction forces were surprisingly large, reaching 100 kPa at the biofilm center after 12 h of growth (Figure 2.5A). We note that the magnitude of the stress is relatively large, reaching a value close to the typical turgor pressure which in essence drives biofilms growth and stretching (162). In comparison, epithelial cell-cell junctions break when experiencing a few kPa (163). Therefore, we anticipate that biofilms produce sufficient force to mechanically deform and potentially dismantle epithelia.

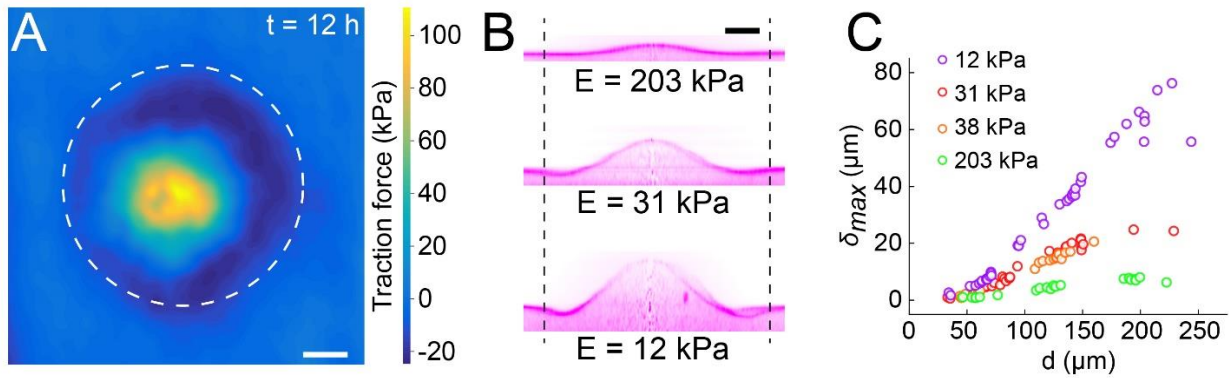


Figure 2.5: Biofilms generate large traction forces.

(A) Traction force microscopy measurements at the hydrogel-biofilm interface. The dashed line shows the edge of the biofilm. Traction force is largest at the biofilm center, reaching 100 kPa. (B) Deformation profiles generated by *V. cholerae* Rg biofilms of equal diameters on three hydrogels with different stiffness. (C) Biofilm diameter-dependence of maximum deformation for four different hydrogel composition representing a typical range of tissue stiffnesses. The softest hydrogel can deform up to 80 μm for a biofilm diameter of 220 μm. Data points correspond to different biofilms grown in one microfluidic chamber. Scale bar: 20 μm.

Given the large forces generated by biofilms on hydrogel substrates, we wondered to which extent they could deform biomaterials of different stiffnesses as defined by their Young's modulus. To test this, we reproduced the mechanical properties of various tissue types by tuning the stiffness of the PEG hydrogel films between $E = 10$ kPa and $E = 200$ kPa (164, 165). The stiffest hydrogels only slightly deformed (Figure 2.5B, $\delta_{max} = 5$ μm for $E = 203$ kPa). In contrast, biofilms growing on

the softest hydrogels displayed large deformations ($\delta_{max} = 27 \mu\text{m}$ for $E = 12 \text{ kPa}$). The rate of increase of deformations was inversely correlated with stiffness, resulting in differences in δ_{max} between colonies of identical diameter growing on substrates with distinct stiffnesses (Figure 2.5C). For each stiffness, the deformation amplitude δ_{max} and the width λ increased linearly with biofilm diameter (Fig. 2.5C and Supplementary Figure 2.6). Rescaling δ_{max} with the biofilm diameter highlights a power-law relationship between deformation and substrate stiffness (Supplementary Figure 2.7).

2.3.7 Biofilms deform and disrupt epithelial cell monolayers

Given the ability of biofilms to generate large forces and to deform materials across a wide stiffness range, we wondered whether they could disrupt soft epithelium-like tissues. To test how biofilms can mechanically perturb host tissue during colonization, we engineered epithelial cell monolayers at the surface of a soft extracellular matrix (ECM). This system replicates the mechanical properties of host epithelia including tissue stiffness and adhesion to underlying ECM. As a result, it constitutes a more realistic host-like environment compared to cell monolayers grown on plastic or glass. We thus engineered epithelial monolayers of enterocyte-like CMT-93 cells on a soft extracellular matrix composed of Matrigel and collagen (Figure 2.6A). This produced soft and tight ECM-adherent epithelia. We seeded the surface of these epithelia with *V. cholerae* *Rg*. We note that the *Rg* strain has reduced virulence compared to WT *V. cholerae* due to its constitutively high levels of cyclic-di-GMP which decrease the expression of virulence factors (166). *V. cholerae* biofilms formed at the epithelial surface within 20 h (Figure 2.6B). Overall, biofilms perturbed the shape of the epithelium. Under biofilms, the cell monolayer detached from its ECM substrate and was often bent as did synthetic hydrogel films (Figure 2.6B-ii). More surprisingly, we observed that CMT-93 cell monolayers lost cohesion and single cells were engulfed by the biofilm. This allowed the biofilm to breach the epithelium and reach the ECM. There, biofilms deformed the ECM substrate, turning the initially flat surface into a dome-like shape as our synthetic hydrogels did (Figure 2.6B-iv). These disruptions did not depend on cell type and species as *V. cholerae* could also damage and bend

monolayers of MDCK cells which have strong cell-cell junctions (Figure 2.6C) (167) and human intestinal epithelial cells Caco-2 (Supplementary Figure 2.8).

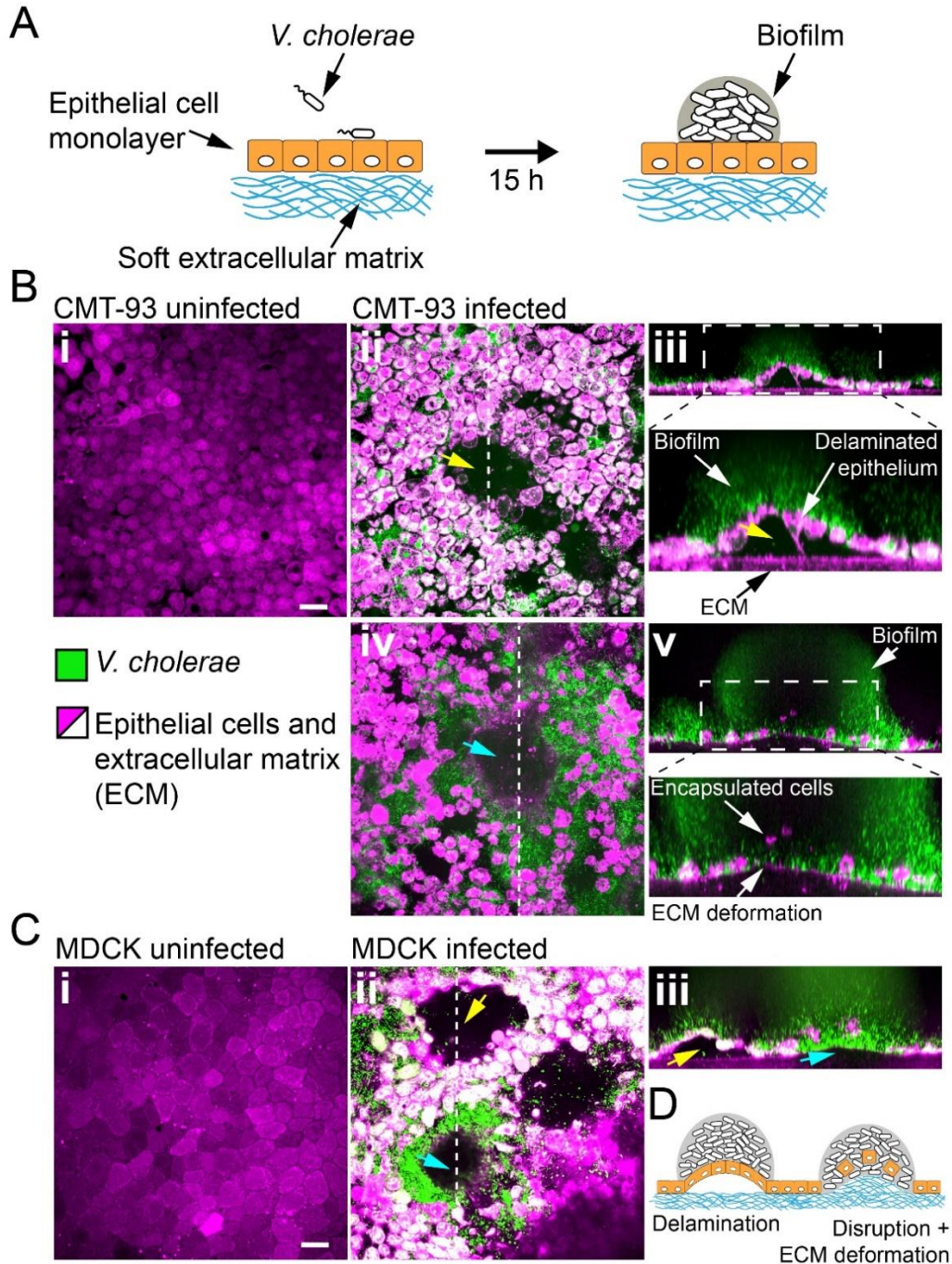


Figure 2.6: Biofilms deform and disrupt epithelial cell monolayer.

(A) CMT-93 and MDCK cells grow at the surface of a soft ECM into a tight monolayer on which we seed a liquid inoculum of *V. cholerae* Rg. (B) Confocal images of uninfected (i) and infected (ii-v) monolayers of CMT-93 cells. Yellow arrow indicates gaps in the epithelial monolayer (ii and iii), blue arrow shows deformed ECM (iv). (C) Confocal images of uninfected (i) and infected (ii-iii) monolayers of MDCK cells, also showing delamination and rupture as illustrated in (D). Scale bars: 20 μ m.

How do these perturbations compromise the barrier function of the epithelium? We further characterized the integrity of cell monolayers near biofilms by measuring permeability and viability. We assessed cell viability using Calcein-AM which only generates a fluorescent signal in live cells. We essentially observed that cells engulfed in the biofilms were dead (Supplementary Figure 2.9). In contrast, the viability of the cells around the biofilm base was not compromised. We then measured epithelial permeability using FITC – Dextran probes. Dextran could diffuse across infected monolayers into the ECM, in contrast with uninfected conditions (Supplementary Figure 2.10 i-ii). In infected monolayers, we could detect fluorescence in the epithelial opening created by the biofilm and between cells as a result of damaged epithelial cell-cell junctions in the vicinity of the biofilm (Supplementary Figure 2.10 iii-v). Our observations suggest that biofilms apply mechanical forces on host tissue which perturb the morphology, integrity and viability of epithelia, as well as its underlying ECM.

2.4 Discussion

We demonstrated that biofilms can deform the surface of soft materials they grow on. We observed that both *V. cholerae* and *P. aeruginosa* generate these deformations, suggesting that it is a feature of biofilm growth and is not species-dependent. We identified key physical and biological components that enable these deformations. In particular, our measurements of hydrogel deformations provide evidence consistent with a mechanism where the biofilm buckles as it grows. This mechanism is reminiscent of Euler buckling where the internal compressive stress in a beam triggers an instability that induces transverse deformations. In our case, we found that the onset of the buckling instability depends on growth under mechanical constraint which generates a buildup of compressive stress. The EPS matrix is a major contributor of the buildup of internal stresses. Indeed, when we compared the rugose variants (matrix overproducer) with the smooth WT strains of *V. cholerae*, we observed a decrease or a complete loss of deformation when grown in LB. In fact, *V. cholerae* does not robustly form biofilms in LB, likely due to poor matrix secretion, making it an unpopular growth medium for flow cell biofilms. In contrast, WT *V. cholera* biofilms growing in M9 generated deformations comparable to the ones caused by the rugose variant, suggesting an

important link with matrix production. The larger variability in deformation amplitudes in WT compared to *Rg* likely originates from heterogeneity in biofilm matrix secretion and regulation.

In-plane hydrogel strain measurements indicate a friction between the surface and the expanding biofilm, which promotes buildup of internal stress. Also, the fact that biofilms of the *V. cholerae* *rbmA* and *P. aeruginosa* EPS genes deletion mutants have reduced or abolished ability to buckle or to deform the surface indicates that cell-cell cohesion in the biofilm may also participate in mechanical constraint. Without cell-cell cohesion and matrix elastic property, the viscous biofilm would flow, dissipating mechanical stress and eluding the elastic instability.

These two contributions, biofilm-surface friction and matrix elasticity, induce a buildup of compressive stress within the biofilm, ultimately causing buckling. Biofilm adhesion transmits buckling-induced stresses to the substrate, generating deformations. While a full description of the physical deformation mechanism is a complex problem involving biofilm and substrate mechanics, we can already highlight important features from our observations. First, the facts that the onset of deformation occurs at a finite critical biofilm diameter and that the width of the deformation λ scales linearly with this diameter are consistent with an Euler-type buckling instability (168). Also, the slight negative deformations (recess) observed near the edge of larger biofilms is reminiscent of higher order buckling modes. Then, the power-law relationship between deformation and substrate stiffness is qualitatively consistent with the theory of buckling of plates coupled to an elastic foundation (169). The delamination of *V. cholerae* mutants and *P. aeruginosa* on stiff substrates highlight the importance of the balance between adhesion and substrate elasticity in force transmission (131). At the time of delamination, elastic deformation and adhesion energies balance. Thus, biofilm delamination could help estimate the adhesive strengths of specific matrix components. Overall, biofilms mechanically shape their environment via a buckling-adhesion mechanism, reminiscent of the buckling and wrinkling of plates and films on elastic foundations (169). A comprehensive understanding of force generation in biofilms and of substrate response will require further development of mechanical models along with measurements of biofilm internal stresses.

Internal stress generated by bacterial expansion under physical constraints influences the morphologies of colony biofilms, forming wrinkles, folds and blisters. The shapes of these colonies are also caused by a buckling/wrinkling-like instability which depends on the mechanical properties of the matrix. These mechanically-generated shapes have been observed in *V. cholerae*, *P. aeruginosa*, *B. subtilis* and *E. coli* and have been instrumental as an obvious phenotype to identify components and regulators of the biofilm matrix and to characterize the mechanics driving multicellular growth (111, 136, 160, 170, 171). However, the impact of these macroscale morphological changes and internal mechanics on the physiology of resident microbes have yet to be identified. Immersed, micrometer scale biofilms that are commonly found in natural microbial niches also undergo architectural transitions due to the emergence of internal mechanical stress. Cell-cell cohesion and cell-substrate adhesion can favor the alignment of single cells within the multicellular structure during biofilm growth. For example, a buckling instability causes *V. cholerae* cell verticalization in the initial step of biofilm formation, in a mechanism that depends on friction of single cells with their glass substrate, generating compressive mechanical stress (120). Single cells in *E. coli* microcolonies reorient through a similar mechanism (117). The physiological functions of these cellular rearrangements have however not yet been identified. The buckling-adhesion model we here propose is consistent with the mechanics of immersed and colony biofilms. Our observations suggest that internal mechanical stress can have a function in the interaction between the biofilm and its surrounding environment, influence the morphology and mechanics of its material substrate. This may result in fouling of abiotic surfaces, in damaging competing biofilms or even host tissues.

Despite being widespread in the environments of microbes, the influence of substrate rigidity is often overlooked in studies of surface attachment and biofilm formation (29, 30, 35). Using a materials approach aimed at reproducing a host-like environment, we found that substrate mechanical properties have a strong impact on biofilm development. Biofilm-induced deformations are particularly relevant when considering their growth at the surface of soft biological tissues. We demonstrated that biofilms generate large forces, and that these forces can be transmitted to underlying epithelia. In response, we observed that epithelial monolayers delaminate from their ECM

and subsequently bend. The biofilm-generated forces also disrupt epithelial monolayers. Consistent with this, traction force microscopy measurements show that biofilms can generate 100 kPa surface stress, which is larger than the strength of epithelial cell-cell junctions that typically rupture under the kPa stress range (167). Thus, the biofilm opened cell-cell junctions increasing epithelial permeability. Biofilms caused epithelial cell death when removed from the monolayer. These observations suggest that mechanical forces generated by biofilms can impact epithelial integrity, in addition to other well-known chemical factors such as toxins (172). We note that a more realistic epithelium would be protected by a layer of mucus of very low elasticity, which could also be strongly deformed by biofilms. Pathogen like *V. cholerae* can however swim through the mucus layer to reach the epithelium surface (173).

In summary, our visualizations in tissue-engineered epithelia and on hydrogel films suggest that biofilms could mechanically damage host tissues when growing *in vivo*. Consistent with this hypothesis, biofilms can cause tissue lesions. For example, the urine of vaginosis patients contains desquamated epithelial cells covered with biofilms (174, 175). Commensal biofilms form scabs at the epithelial surface of honeybee's gut, triggering immune responses (176). Epithelial integrity is also compromised in intestinal diseases such as inflammatory bowel disease in a process that highly depends on the composition of the microbiota (172, 177–179). Finally, hyper-biofilm forming clinical variants of *P. aeruginosa* cause significant damage to the surrounding host tissue despite its reduced virulence (161).

Most studies of biofilm formation have so far focused on their internal organization and mechanics, and on the genetic regulation of matrix production. How biofilms physically interact with their natural environments has been however vastly unexplored, but could vastly contribute to a holistic understanding of host-microbe interactions. Mechanical interactions between bacterial collectives and their host may thus represent an overlooked contributor of infections, colonization and dysbiosis. Non-pathogenic biofilm-forming species, including commensals, could thus very well induce epithelial damage and in fact contribute to chronic inflammation.

2.5 Acknowledgements

We would like to thank Fitnat Yildiz, Matt Parsek, Melanie Blokesch, Bonnie Bassler and Knut Drescher for strains and plasmids, and Carey Nadell, John Kolinski and Pedro Reis for discussions. This work was supported by the Swiss National Science Foundation Projects Grant 31003A_169377, the Gabriella Giorgi-Cavaglieri Foundation, the Gebert R f Stiftung and the Fondation Beytout.

2.6 Methods

2.6.1 Cell culture

CMT-93, Caco-2 and MDCK cells were maintained in T25 tissue culture flasks (Falcon) with DMEM medium (Gibco) supplemented with 10% fetal bovine serum at 37°C in a CO₂ incubator. Cell lines are frequently screened for mycoplasma and were authenticated by STR profiling.

2.6.2 Cell culture on collagen/Matrigel gels

To resemble the extracellular matrix natural niche, we cultured epithelial cells at the surface of collagen and Matrigel based hydrogels. Hydrogel solutions were prepared on ice to avoid premature gelation by mixing 750 µl of neutralized collagen with 250 µl of growth-factor reduced Matrigel matrix (Corning, 356231). The neutralized collagen was obtained by mixing 800 µl of native type I collagen isolated from the bovine dermis (5mg/ml, Cosmo Bio Co., Ltd.) with 10 µl of NaHCO₃ (1 M), 100 µl of DMEM-FBS and 100 µl of DMEM 10X. We then spread 100 µl of the hydrogel solution in glass bottom dishes (P35G-1.5-20-C, MatTek), which were kept on ice. Excess solution was removed from the sides of the well to avoid the formation of a meniscus. To promote collagen adhesion, the wells were previously functionalized with a 2% polyethyleneimine solution (Sigma-Aldrich) for 10 min and a 0.4% glutaraldehyde solution (Electron Microscopy Science) for 30 min. We finally placed the coated dishes at 37°C in a CO₂ incubator for 20 minutes to allow gelation.

MDCK, CMT-93 and Caco-2 cells were detached from the flask using trypsin (Sigma-Aldrich). We seeded the cells at a concentration of 1000 cells/mm² on top of the gels. We let the cells adhere for 1 day and then we filled the dishes with 2 ml of culture medium. The medium was changed every 2 days.

2.6.3 Bacterial strains and culture conditions

A list of the strains and plasmids is provided in Table 2.2. All strains were grown in LB medium at 37°C. Only Vc Rg Δ rbmA pBADrbmA and Vc Rg Δ bap1 pBADbap1, were grown in LB containing 0.5 wt% arabinose and respectively gentamicin and ampicilin before inoculation in the microfluidic channels.

Deletion of the *V. cholerae* genes *rbmA*, *bap1* and *vpsL* were generated by mating a parental A1552 *V. cholerae* strain, rugose variant, with *E. coli* S17 strains harboring the deletion constructs according to previously published protocols (180). The *rbmA* complementation strain was generated by tri-parental mating using *E. coli* S17 harbouring an arabinose-inducible *rbmA* gene and a helper strain. The *bap1* complementation strain was generated by electroporation of an arabinose-inducible plasmid containing the coding region of *bap1* inside the deletion mutant.

P. aeruginosa strains (PAO1 parental strain) are all constitutively expressing GFP (attTn7::miniTn7T2.1-Gm-GW::PA1/04/03::GFP).

2.6.4 Infection of tissue-engineered epithelia by *Vibrio cholerae*

V. cholerae was grown in LB medium at 37°C to mid-exponential phase (OD 0.3-0.6). Bacteria were washed 3 times by centrifugation and resuspension in Dulbecco's phosphate-buffered saline (D-PBS). The cultures were then diluted to an optical density of 10^{-7} and filtered (5.00 μ m-pore size filters, Millex) to ensure the removal of large bacterial clumps, thereby isolating planktonic cells. This ensured that biofilms growing on epithelia formed from single cells. We loaded 200 μ L of diluted culture on top of mammalian cells that were cultured for 1 to 7 days post-confluence on collagen/Matrigel gels. Bacteria were allowed to adhere to the surface for 20 minutes, after which cells were rinsed two times with D-PBS.

Biofilm were grown under flow after seeding of Vc Rg on top of CMT-93 cells, while they were grown in stationary conditions for MDCK and Caco-2 cells. For the implementation of the flow on top of CMT-93 cells, we prepared a circular slab of PDMS with the same dimensions as the dish. We punched 1mm inlet and outlet ports in this PDMS slab. We then glued it to the rim of the dish, where

no cells are present. We then connected the inlet port to a disposable syringe (BD Plastipak) filled with culture medium using a 1.09 mm outer diameter polyethylene tube (Instech) and a 27G blunt needle (Instech). The syringes were mounted onto a syringe pump (KD Scientific) positioned inside a CO₂ incubator at 37°C. The volume flow rate was set to 50 $\mu\text{L}\cdot\text{min}^{-1}$. For stationary biofilm growth on top of MDCK cells, the glass bottom dishes were filled with 2 mL of culture medium and were incubated at 37°C in a CO₂ incubator.

2.6.5 Fabrication of PEG hydrogels and mechanical characterization

To generate PEG hydrogels films we prepared solutions of M9 minimal medium containing poly(ethylene glycol) diacrylate (PEGDA) as the precursor and lithium phenyl-2,4,6-trimethylbenzoylphosphinate (LAP, Tokio Chemical Industries) as the photoinitiator. Molecular weight and concentration of PEGDA were tuned to obtain hydrogels with different stiffnesses (Table 2.1), while the concentration of LAP is kept constant at 2 mM.

To incorporate fluorescent microparticles into the PEG hydrogels, we modified the original solution by substituting 2 μL (for a solution with a final volume of 100 μL) of M9 medium with 2 μL of red fluorescent particles solution (ThermoFischer, FluoSpheres, Carboxylate-modified Microspheres, 0.1 μm diameter, 2% solids, F8887).

To prepare the samples for mechanical characterization, we filled PDMS wells (5 mm diameter, 4 mm height) with the hydrogel solution. We covered the wells with a coverslip and we let them polymerize in a UV transilluminator (Bio-Rad Universal Hood II) for 5 minutes. The resulting hydrogel cylinders were immersed in M9 overnight and tested with a rheometer (TA instruments) in compression mode, at a deformation rate of 10 $\mu\text{m}/\text{s}$. Beforehand, the diameter of the cylinders was measured with a digital caliper, while the height of the cylinder was defined as the gap distance at which the force starts differing from zero. The elastic modulus corresponds to the slope of the linear fit of the stress-strain curves in the range of 15% strain. The final modulus is the average modulus of 3 replicates.

2.6.6 Fabrication of thin PEG hydrogel layers and implementation with PDMS microfluidic chip

We fabricated microfluidic chips following standard soft lithography techniques. More specifically, we designed 2 cm-long, 2 mm-wide channels in Autodesk AutoCAD and printed them on a soft plastic photomask. We then coated silicon wafers with photoresist (SU8 2150, Microchem), with a thickness of 350 μm . The wafer was exposed to UV light through the mask and developed in PGMEA (Sigma-Aldrich) in order to produce a mold. PDMS (Sylgard 184, Dow Corning) was subsequently casted on the mold and cured at 70 °C overnight. After cutting out the chips, we punched 1 mm inlet and outlet ports. We finally punched a 3 mm hole right downstream of the inlet port. This hole, after being covered with a PDMS piece, acts as a bubble trap.

To obtain thin and flat hydrogel layers, a drop of about 80 μL of the hydrogel solution was sandwiched between two coverslips and incubated in the UV transilluminator for 5 minutes to allow gelation. The bottom coverslip (25x60 mm Menzel Gläser) was cleaned with isopropanol and MilliQ water, while the upper one (22x40 mm Marienfeld) was functionalized with 3-(Trimethoxysilyl)propyl methacrylate (Sigma-Aldrich) following the standard procedure. In short, cleaned coverslips were immersed in a 200 mL solution of ethanol containing 1 mL of the reagent and 6ml of dilute acetic acid (1:10 glacial acetic acid:water) for 5 minutes. They were subsequently rinsed in ethanol and dried. This functionalization enables the covalent linkage of the hydrogel to the coverslip.

Right after polymerization, the coverslips were separated using a scalpel and thus exposing the hydrogel film surface. We then positioned the PDMS microfluidic chip on top of the hydrogel film. This results in a reversible, but sufficiently strong bond between the hydrogel and the PDMS, allowing us to use the chips under flow without leakage for several days. The assembled chips were filled with M9 to maintain the hydrogel hydrated.

2.6.7 Biofilm growth in microfluidic chambers

All *V. cholerae* and *P. aeruginosa* strains were grown in LB medium, unless specified, at 37°C until mid-exponential phase (OD 0.3-0.6). The cultures were diluted to an optical density of 10^{-3} and

subsequently filtered (5.00 μm -pore size filters, Millex) to ensure the removal of large bacterial clumps. We then loaded 6.5 μL of the diluted bacterial culture in the channels, from the outlet port. We let them adhere for 20 minutes before starting the flow. We connected the inlet port to a disposable syringe (BD Plastipak) filled with the medium and mounted onto a syringe pump (KD Scientific), using a 1.09 mm outer diameter polyethylene tube (Instech) and a 27G needle (Instech). The volume flow rate was 10 $\mu\text{L}\cdot\text{min}^{-1}$, which corresponds to a mean flow speed of about 0.25 $\text{mm}\cdot\text{s}^{-1}$ inside the channels. The biofilms were grown at 25°C in LB, unless specified. For Vc Rg ΔrbmA pBADrbmA, both liquid cultures and biofilms were grown in LB containing 30 $\mu\text{g}/\text{ml}$ of gentamicin and 0.5 wt% arabinose. For Vc Rg Δbap1 pBADbap1, both liquid cultures and biofilms were grown in LB containing 100 $\mu\text{g}/\text{ml}$ of ampicillin and 0.5 wt% arabinose. For *V. cholerae* N16961 and C6706 we loaded the bacterial cultures at an optical density of 0.5 and we let them adhere for 1 hour before starting the flow at a volume flow rate of 2 $\mu\text{L}\cdot\text{min}^{-1}$. Unless specified the medium used was LB. For some conditions we used M9 minimal medium supplemented with 2mM MgSO_4 , 100 μM CaCl_2 , 0.5% glucose, MEM Vitamins, and 15 mM triethanolamine (pH 7.1).

2.6.8 Staining procedures

Mammalian cells were incubated for 20 minutes in a 10 μM solution of CellTracker Orange CMRA (Invitrogen, C34551) and washed with DPBS before seeding the bacteria. For standard visualization of biofilm grown on top of epithelial monolayers, since *V. cholerae* strains were not constitutively fluorescent, samples were incubated for 20 minutes with a 10 μM solution of SYTO9 (Invitrogen, S34854) and washed with DPBS before visualization. This results in double staining of epithelial cells. For the visualization of live and dead cells in infected monolayers we instead incubated the samples for 20 minutes in a solution containing 5 $\mu\text{g}/\text{ml}$ Hoechst (Thermo Fischer Scientific, 62249) and 5 μM Calcein-AM (Sigma Aldrich, 17783). For the visualization of epithelial cells monolayers permeability, we added 1 ml of a 2 μM solution of fluorescein isothiocyanate-dextran (Sigma Aldrich, 46944) on top of the cells and imaged after 30 minutes.

V. cholerae biofilms grown in microfluidic channels were incubated for 20 minutes with a 10 μ M solution of SYTO9 (Invitrogen, S34854) and washed with M9 minimal medium before visualization.

2.6.9 Visualization

For all visualizations, we used an Nikon Eclipse Ti2-E inverted microscope coupled with a Yokogawa CSU W2 confocal spinning disk unit and equipped with a Prime 95B sCMOS camera (Photometrics). For low magnification images, we used a 20x water immersion objective with N.A. of 0.95, while for all the others we used a 60x water immersion objective with a N.A. of 1.20. We used Imaris (Bitplane) for three-dimensional rendering of z-stack pictures and Fiji for the display of all the other images.

To obtain the deformation profiles, z-stacks of the hydrogel containing fluorescent microparticles were performed every 0.5 μ m, while a brightfield image of the base of the biofilm was taken to allow measurement of the diameter of the biofilm. For the visualization of the full biofilm, z-stacks of the samples were taken every 2-3 μ m. For timelapse experiments, biofilms were imaged as soon as the flow was started, while for all the other experiments biofilms were imaged between 10 and 48 h post-seeding.

2.6.10 Image analysis and computation of deformation profiles

Starting from confocal imaging pictures of the microparticle-containing hydrogel, we aimed at identifying the gel surface and extracting quantitative information about its deformation induced by the biofilms. In most cases, we used an automated data analysis pipeline as described below. To get an average profile of the deformation caused by the biofilms, we performed a radial reslice in Fiji over 180 degrees around the center of the deformation (one degree per slice). We then performed an average intensity projection of the obtained stack. To calculate the diameter of the biofilm, we averaged 4 measurements of the biofilm diameter taken at different angles. The resliced images were then imported in Matlab R2017a (Mathworks) as two-dimensional (x-y) matrices of intensities. In these images, the surface was consistently brighter than the rest of the gel. Therefore, we identified the surface profile as the pixels having the maximal intensity in each column of the matrix.

Note that the bottom of the gel sometimes also comprised bright pixels that introduced noise in the profile. To reduce this problem, we thus excluded 20 rows at the bottom of each image ($\sim 3.7 \mu\text{m}$). We then calculated the baseline position of our gel – namely, the height of the non-deformed portion of the gel. In our pictures, this corresponds to the height at the left and right extremities of the profile. Therefore, we defined the baseline as the average of the first 50 and last 50 pixels of the profile ($\sim 9 \mu\text{m}$ on each side of the profile). We then offset the whole picture so that the baseline position corresponded to $y = 0$. We undersampled the extracted surface profiles to further reduce noise, by keeping only the maximal y value over windows of 40 pixels. Finally, we fitted a smoothing spline to the undersampled profile using the built-in *fit* function in Matlab, with a smoothing parameter value of 0.9999.

To quantify the deformation that biofilms induced on the hydrogel, we measured the amplitude (δ_{max}) of the deformed peak and its full width at half maximum (λ). First, we evaluated the fitted profile described above at a range of points spanning the whole width of the picture and spaced by $0.0005 \mu\text{m}$. We identified the maximal value of the profile at these points, which corresponds to the amplitude of the peak δ_{max} (with respect to the baseline, which is defined as $y = 0$). We then split the profile in two: one part on the left of the maximum, and one part on its right. On each side, we found the point on the profile whose y value was the closest to $0.5 \cdot \delta_{max}$ using the Matlab function *knnsearch*. We then calculated the distance between their respective x values, which corresponds to the λ of the deformed peak. Our data analysis program also included a quality control feature, which prompted the user to accept or reject the computed parameters. When imaging quality was insufficient to ensure proper quantification with our automated pipeline, we measured the deformation manually in Fiji. Graphs were plotted with OriginPro.

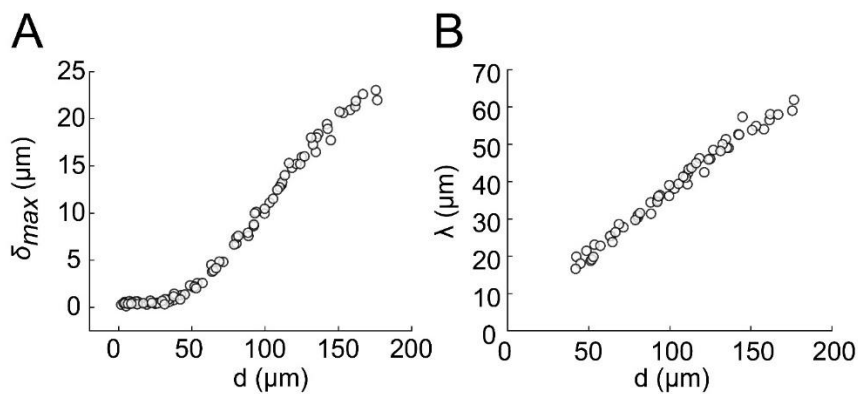
2.6.11 Digital volume correlation and traction force microscopy

We performed particle tracking to measure local deformations and ultimately compute stress and traction forces within hydrogels as biofilms grew. To do this, we performed timelapse visualizations of the hydrogel during the formation of a biofilm at high spatial resolution with a 60X, NA 0.95 water

immersion objective. We thus generated $200\ \mu\text{m} \times 200\ \mu\text{m} \times 25\ \mu\text{m}$ (50 stacks of 1200×1200 pixels) volumes at 14 different time points. These images were subsequently registered to eliminate drift using the Correct 3D Drift function in Fiji. To compute local material deformations which we anticipated to generate large strains, we used an iterative Digital Volume Correlation (DVC) scheme (158). These were performed with $128 \times 128 \times 64$ voxel size in cumulative mode, meaning deformations are calculated by iterations between each time point over the whole 4D timelapse, rather than directly from the reference initial image. The DVC code computes material deformation fields in 3D which we subsequently use as input for the associated large deformation traction force microscopy (TFM) algorithm (158). The TFM calculates stress and strain fields given the material's Young modulus ($E = 38\ \text{kPa}$ in our case) and Poisson ratio (0.459 taken from measurements for polyacrylamide (181)) to ultimately generate a traction force map at the hydrogel surface.

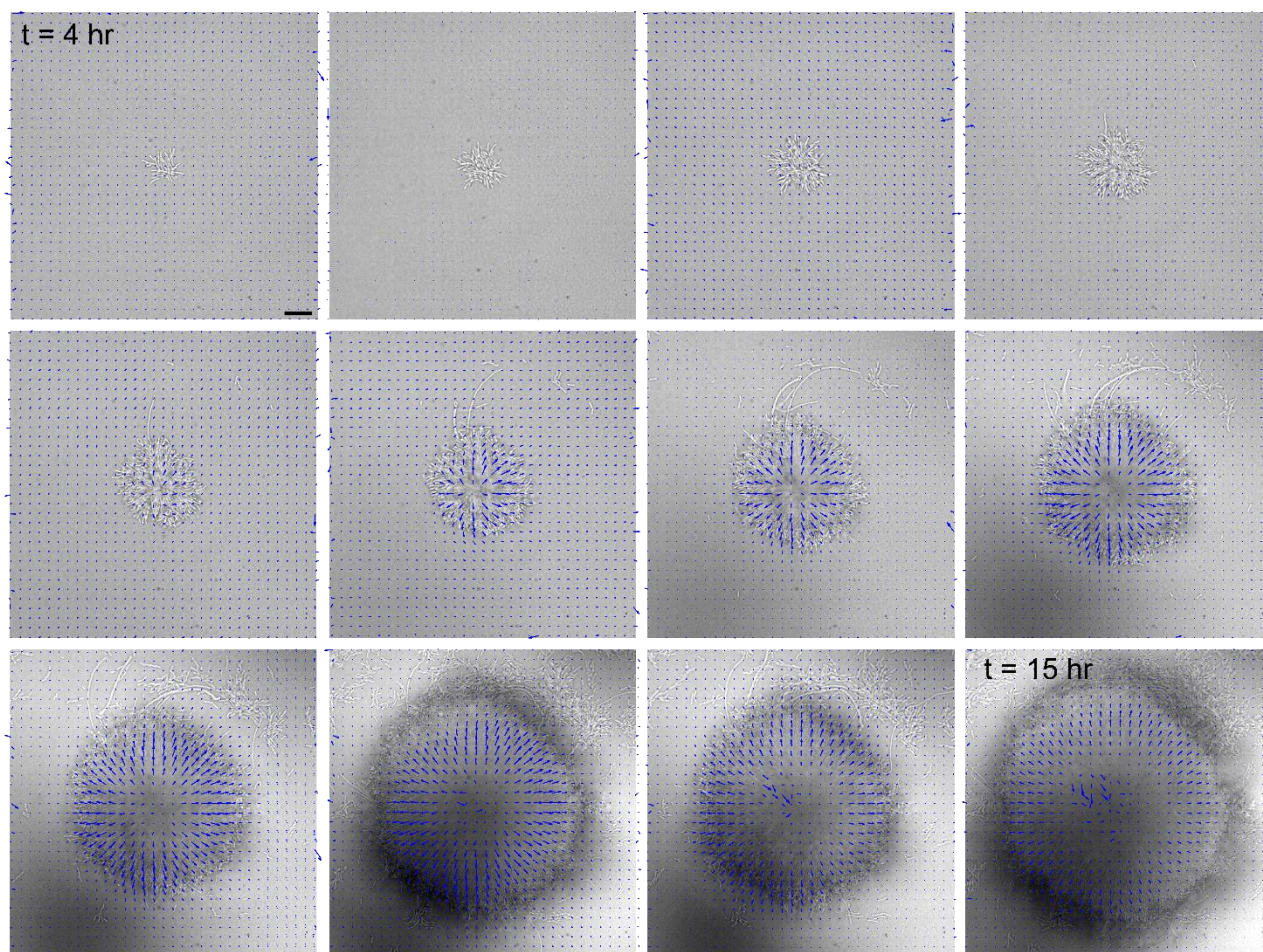
2.7 Supplementary information

2.7.1 Supplementary figures



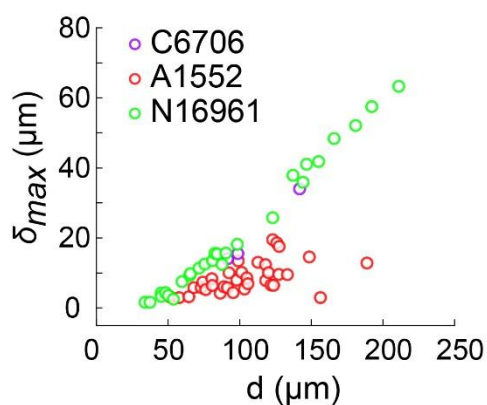
Supplementary Figure 2.1: Biofilm diameter-dependence of δ_{max} and λ .

Both δ_{max} and λ linearly scale with the diameter d of the biofilm.



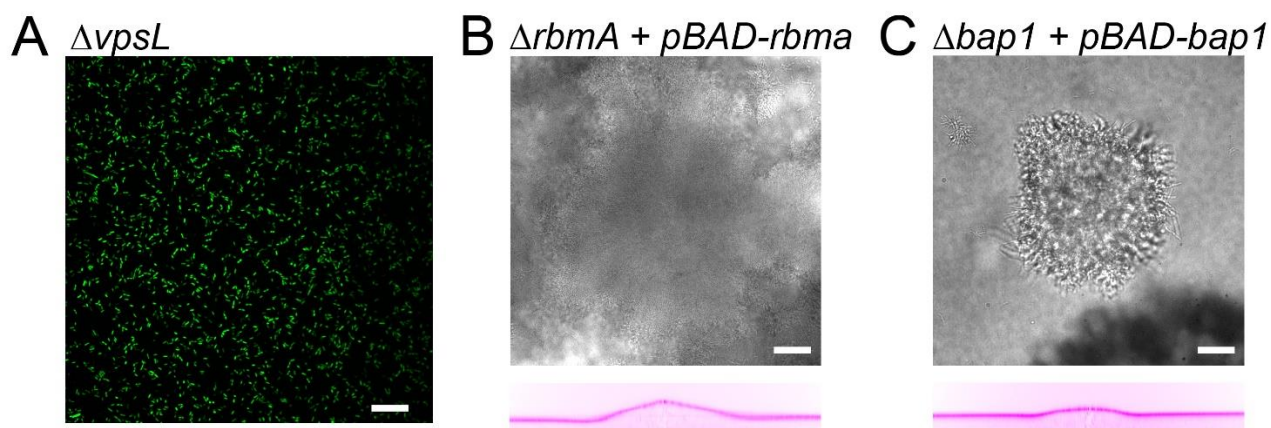
Supplementary Figure 2.2: Hydrogel deformation field computed at different growth stages, superimposed with a brightfield image of the biofilm.

The force field at each timestep is normalized by its maximum displacement, thereby showing relative deformations. Scale bar: 20 μm .



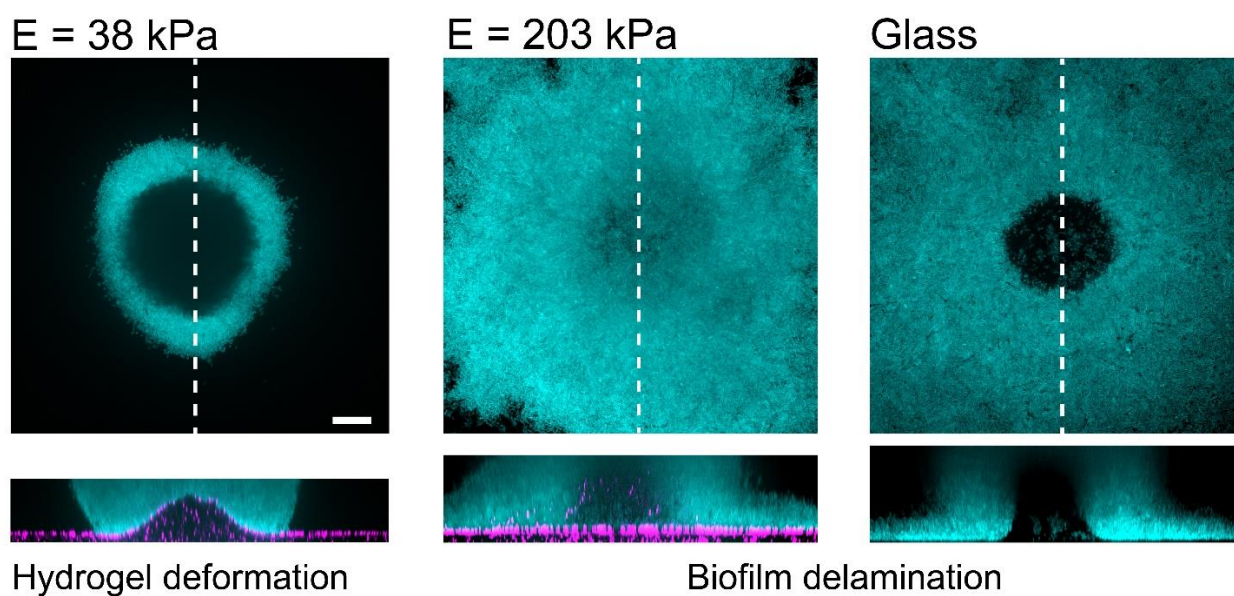
Supplementary Figure 2.3: Biofilm diameter-dependence of maximum deformation for the smooth variant of different *V. cholerae* strains grown in M9.

Data points correspond to different biofilms grown in two microfluidic chambers for A1552 and to biofilms grown in one microfluidic chamber for C6706 and N16961.



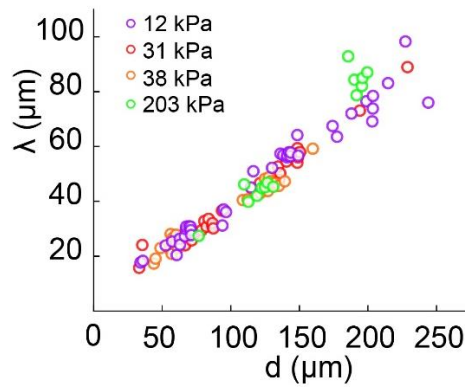
Supplementary Figure 2.4: Deformation behaviour for *vpsL* deletion mutant and complementation strains.

(A) *VpsL* deletion mutant can not form biofilms. Complementation of (B) *V. cholerae rbmA* and (C) *bap1* deletion mutants (brightfield, top) restore the ability of the biofilm to deform the hydrogel (reslice, bottom). $E = 38$ kPa. Scale bars: 20 μm .



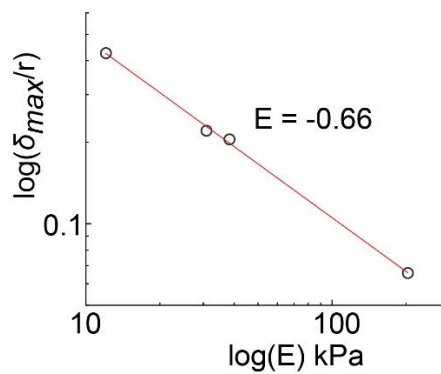
Supplementary Figure 2.5: *P. aeruginosa* biofilms on substrates with different stiffness.

Increasing hydrogel stiffness to 200 kPa induces delamination of biofilms, as observed on glass. Scale bars: 20 μm .



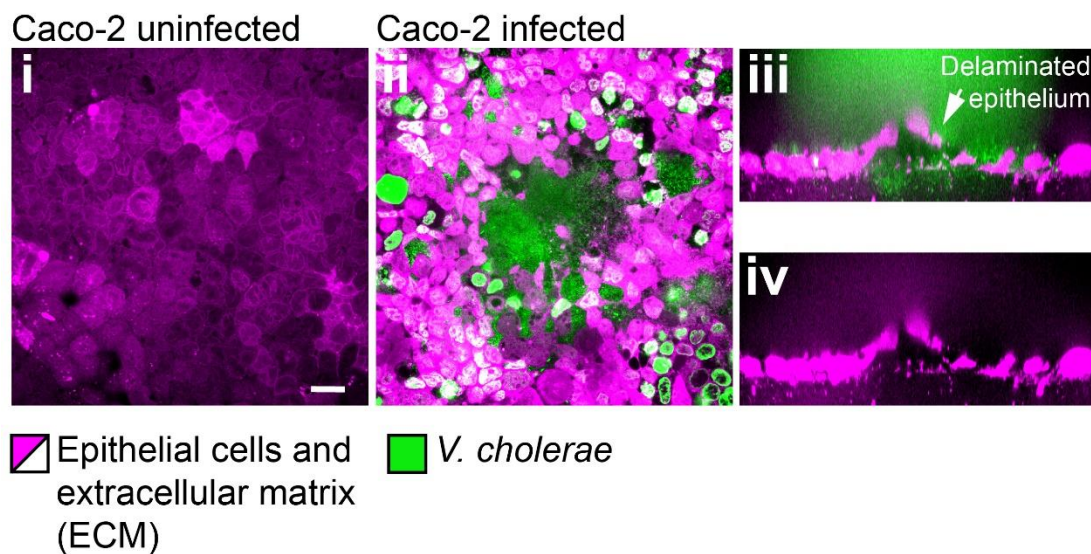
Supplementary Figure 2.6: Biofilm diameter-dependence of λ for substrates with different moduli.

λ scales linearly and it is not substrate-stiffness dependent.



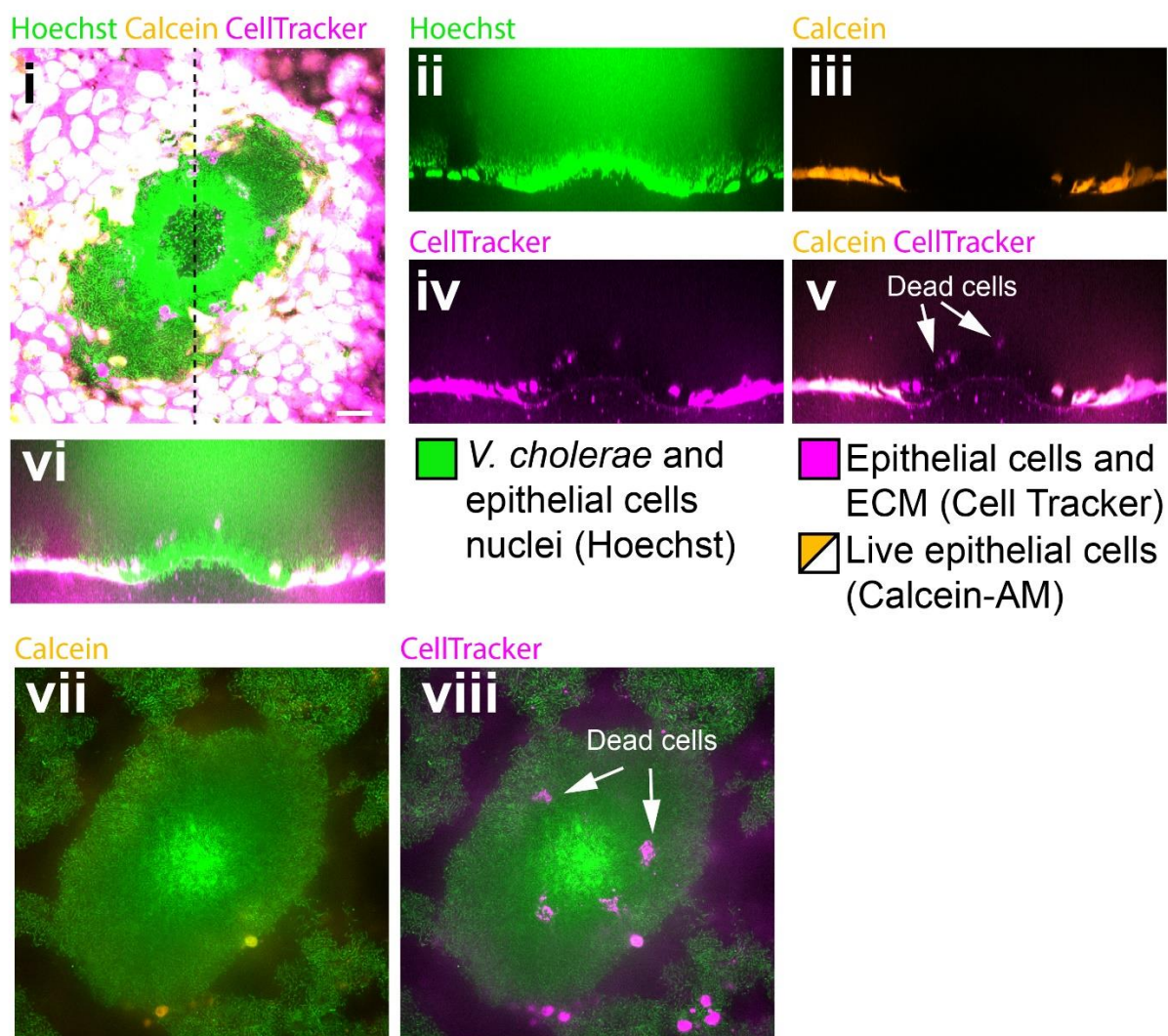
Supplementary Figure 2.7: Power-law relationship between deformation δ_{max} and substrate moduli (E).

Values for δ_{max}/r were extrapolated from linear regression of the data points in Figure 2.5C for $r = 50 \mu\text{m}$ ($d = 100 \mu\text{m}$).



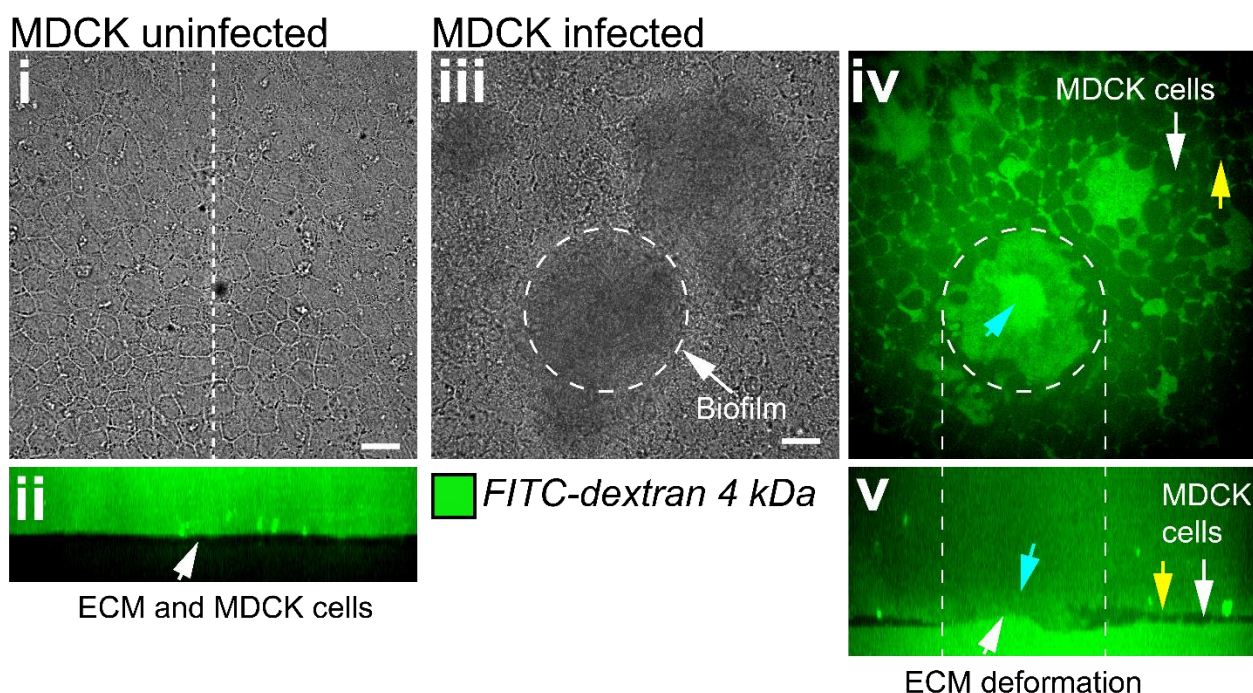
Supplementary Figure 2.8: Confocal images of uninfected (i) and infected (ii-iv) monolayers of Caco-2 cells.

Scale bars: $20 \mu\text{m}$.



Supplementary Figure 2.9: Biofilms perturb the viability of MDCK cell monolayers.

(i) Confocal in plane visualization of a Vc Rg biofilm growing on top of an MDCK cell monolayer stained with CellTracker, Hoechst and Calcein-AM. Cross section visualization of the infected MDCK monolayer stained with Hoechst (ii), Calcein-AM (iii), Cell Tracker (iv) and merged visualizations (v, vi). (vii, viii) Confocal in plane visualization of the biofilm on a focal plane above (i). Scale bars: 20 μ m.



Supplementary Figure 2.10: Biofilms increase the permeability of MDCK cell monolayers.

(i) Bright-field in plane image of an uninfected MDCK cell monolayer grown at the surface of a soft ECM. (ii) Confocal cross-section shows that uninfected monolayers are impermeable to FITC labeled Dextran. (iii) Bright-field in plane visualization of an MDCK cell monolayer infected with Vc Rg. The dashed line shows the approximate edge of the biofilm. Confocal in plane (iv) and cross section (v) visualization of FITC labeled Dextran permeability through the damaged epithelium. Blue arrows show Dextran permeability through the biofilm in direct contact with the ECM, yellow arrows indicate Dextran permeability through epithelial cells junctions. Scale bars: 20 μm .

2.7.2 Movies

Movies are located at the following link: <https://doi.org/10.7554/eLife.56533>

Movie 2.1

Timelapse visualization of *V. cholerae* Rg biofilm growth (brightfield) and corresponding hydrogel deformation ($E = 38 \text{ kPa}$) in the xy and xz planes. Scale bar 20 μm .

2.7.3 Tables

Numerical values for all figures and figure supplements are located at the following links:

Figure 2.2, Supplementary Figure 2.1: <https://cdn.elifesciences.org/articles/56533/elife-56533-fig3-data1-v2.xlsx>

Figure 2.3, Supplementary Figure 2.3: <https://cdn.elifesciences.org/articles/56533/elifesciences-56533-fig3-data1-v2.xlsx>

Figure 2.4: <https://cdn.elifesciences.org/articles/56533/elifesciences-56533-fig4-data1-v2.xlsx>

Figure 2.5, Supplementary Figure 2.6, Supplementary Figure 2.7:

<https://cdn.elifesciences.org/articles/56533/elifesciences-56533-fig5-data1-v2.xlsx>

Table 2.1: Molecular weight and concentrations of the precursors used for the generation of the hydrogels and resulting elastic modulus

PEGDA precursor	Concentration wt/vol	Modulus kPa
PEGDA MW 10000 (Biochempeg)	10%	12.1 ± 0.8
PEGDA MW 6000 (Biochempeg)	10%	38.3 ± 1.0
PEGDA MW 3400 (Biochempeg)	10%	30.9 ± 2.0
PEGDA MW 700 (Sigma-Aldrich)	15%	203.3 ± 13.7

Table 2.2: Key Resources Table. Bacterial strains, cell lines, plasmids, chemicals, others

Reagent type (species) or resource	Designation	Source or reference	Additional information
strain, strain background (<i>V. cholerae</i> A1552)	Vc Rg	(160)	rugose variant
strain, strain background (<i>V. cholerae</i> A1552)	Vc WT	(160)	smooth wild type variant
strain, strain background (<i>V. cholerae</i> A1552)	Vc Rg $\Delta vpsL$	This study	in frame deletion of <i>vpsL</i> in rugose background obtained by matings of Vc Rg with S17 harboring deletion plasmid pFY_922
strain, strain background (<i>V. cholerae</i> A1552)	Vc Rg $\Delta rbmA$	This study	in frame deletion of <i>rbmA</i> in rugose background obtained by matings of Vc Rg with S17 harboring deletion plasmid pFY_113
strain, strain background (<i>V. cholerae</i> A1552)	Vc Rg $\Delta bap1$	This study	in frame deletion of <i>bap1</i> in rugose background obtained by matings of Vc Rg with S17 harboring deletion plasmid pFY_330
strain, strain background (<i>V. cholerae</i> A1552)	Vc Rg $\Delta rbmA$ pBAD $rbmA$	This study	Vc Rg $\Delta rbmA$ harboring the plasmid pNUT1236

strain, strain background (<i>V. cholerae</i> A1552)	Vc Rg $\Delta bap1$ pBAD bap1	This study	Vc Rg $\Delta bap1$ harboring the plasmid pBAD/Myc-His B
strain, strain background (<i>V. cholerae</i> N16961)	N16961	(118)	smooth wild type variant
strain, strain background (<i>V. cholerae</i> C6706)	C6706	(182)	smooth wild type variant
strain, strain background (<i>P. aeruginosa</i>)	PAO1 WT	(183)	
strain, strain background (<i>P. aeruginosa</i>)	PAO1 Rg	(184)	in frame deletions of <i>wspF</i>
strain, strain background (<i>P. aeruginosa</i>)	PAO1 Rg Δpel	(184)	in frame deletions of <i>wspF</i> , <i>pelA</i> genes
strain, strain background (<i>P. aeruginosa</i>)	PAO1 Rg Δpsi	(184)	in frame deletions of <i>wspF</i> , <i>psiBCD</i> genes
strain, strain background (<i>P. aeruginosa</i>)	PAO1 Rg $\Delta cdrA$	(185)	in frame deletions of <i>wspF</i> , <i>cdrA</i> genes
cell line (<i>Homo sapiens</i>)	Caco-2 HTB-37 RRID: CVCL_0025	ATCC	
cell line (<i>Canis</i>)	MDCK 84121903-1VL RRID: CVCL_0422	Sigma Aldrich	
cell line (<i>Mus musculus</i>)	CMT-93 CCL-223 RRID: CVCL_1986	ATCC	
recombinant DNA reagent	pFY_113 (plasmid)	(96)	plasmid for generation of in-frame <i>rbmA</i> deletion mutants
recombinant DNA reagent	pFY_330 (plasmid)	(96)	plasmid for generation of in-frame <i>bap1</i> deletion mutants
recombinant DNA reagent	pFY_922 (plasmid)	(186)	plasmid for generation of in-frame <i>vpsL</i> deletion mutants
recombinant DNA reagent	pNUT1236 (plasmid)	(115)	arabinose inducible plasmid containing the coding region of <i>rbmA</i>

recombinant DNA reagent	pBAD/Myc-His B (plasmid)	(187)	arabinose inducible plasmid containing the coding region of <i>bap1</i>
chemical compound, drug	lithium phenyl-2,4,6-trimethylbenzoylphosphinate (LAP)	Tokio Chemical Industries	
chemical compound, drug	PEGDA (MW 3400, 6000, 10000)	Biochempeg	
chemical compound, drug	PEGDA (MW 700)	Sigma-Aldrich	
software	Fiji	Fiji	
software	OriginPro	OriginLab Corporation	
software	MATLAB	Mathworks	
software	Imaris	Bitplane	
algorithm	3D TFM	(158)	
other	SYTO9 stain S34854	Invitrogen	10 μ M
other	CellTracker Orange CMRA stain C34551	Invitrogen	10 μ M
other	Hoechst stain 62249	Thermo Fischer Scientific	5 μ g/ml
other	Calcein-AM stain 17783	Sigma Aldrich	5 μ M

Chapter 3. Mechanical control of biofilm architectures promotes *Pseudomonas aeruginosa* antibiotic tolerance

This chapter has been adapted from the preprint (188):

<https://www.biorxiv.org/content/10.1101/2022.02.16.480709v1>

Authors:

Alice Cont, Joseph Vermeil, Alexandre Persat*

Affiliations:

Institute of Bioengineering and Global Health Institute, EPFL, Lausanne, Switzerland

*Corresponding author: alexandre.persat@epfl.ch

Keywords:

Biofilms, Mechanobiology, Type IV Pili, Twitching Motility

My contributions: Design of the experiments, data acquisition and data analysis.

3.1 Abstract

In the wild, bacteria are most frequently found in the form of multicellular structures called biofilms. Biofilms grow at the surface of abiotic and living materials with wide-ranging mechanical properties. The opportunistic pathogen *Pseudomonas aeruginosa* forms biofilms on indwelling medical device and on soft tissues including burn wounds and the airway mucosa. Despite the critical role of substrates in the foundation of biofilms, we still lack a clear understanding of how material mechanics regulate their architecture and the physiology of resident bacteria. Here, we demonstrate that mechanical properties of hydrogel material substrates define *P. aeruginosa* biofilm architecture. We show that hydrogel mesh size regulates twitching motility, a surface exploration mechanism priming

biofilms, ultimately controlling the organization of single cells in the multicellular community. The resulting architectural transitions increase *P. aeruginosa*'s tolerance to colistin, a last resort antibiotic. In addition, mechanical regulation of twitching motility impacts *P. aeruginosa* clonal lineages, so that biofilms are more mixed on relatively denser materials. Our results thereby establish material properties as a factor that dramatically impacts biofilm architecture, antibiotic efficacy and evolution of the resident population.

3.2 Introduction

Bacteria preferentially colonize surface environments as multicellular communities called biofilms (1). Biofilms form when bacteria attach to surfaces and subsequently divide while embedding themselves in a self-secreted matrix (2, 153). Cells residing in biofilms have selective advantages compared to their planktonic counterpart. For example, the matrix mechanical properties not only provide cohesion but also physically protects cells against physical and predatory challenges such as flow and grazing (2). The biofilm lifestyle also confers protection against chemical stressors such as antimicrobials (154). As a result, biofilm-dwelling bacterial populations are overall more tolerant to antibiotic treatment. The resilience of biofilms against antibiotic treatment has both biological and physical causes (6, 154). Biofilm residents undergo metabolic adaptation that decreases their drug sensitivity. On the physical side, the presence of the matrix and the three-dimensional cellular arrangement within a biofilm can reduce the penetration of molecular compounds to its core (6, 154). As a result, biofilm architecture can critically regulate bacterial tolerance to antibiotic treatment.

Due to their resilience, biofilms are a common cause of chronic, persistent infections (155, 156). Biofilms of the opportunistic pathogen *Pseudomonas aeruginosa* frequently cause burn wound infections and chronic airway infections, particularly in cystic fibrosis patients. To form biofilms, *P. aeruginosa* explores surfaces using surface-specific twitching motility powered by type IV pili (59). During this process, single cells aggregate and initiate a collective growth phase that results in biofilm maturation. *P. aeruginosa* biofilms frequently grow in contact with soft host tissue including cells, extracellular matrices such as mucus (6). The mechanical properties of these materials are quite different from the ones *P. aeruginosa* encounters in traditional biofilm assays in the lab, which

employ much stiffer materials including glass and hard plastics. As a result, our knowledge of biofilm formation on realistic soft substrates remains limited.

Mechanics plays an important role during the development of a biofilm (5, 22). When cells grow to form a biofilm, they exert forces on their elastic matrix which ultimately generate internal mechanical stresses. The buildup of internal stress has an impact on biofilm morphogenesis, causing instabilities such as buckling or wrinkling (132). When growing on soft surfaces, these instabilities cause material substrates to deform, be it hydrogels or host epithelial tissue (152). Material surface physicochemical properties such as topography, chemistry, charge, hydrophobicity have an effect on the adhesion of single bacteria (18–21, 74, 75). However, despite host-associated biofilms ubiquitously forming on soft surfaces of various rigidities, the mechanisms by which mechanical properties of a substrate impacts the structure and organization of a biofilm have been neglected. Explorations of bacterial physiology on PDMS and hydrogels indicate that material mechanics may mediate biofilm formation (29, 30, 35). Despite the conclusions being contrasting across materials, this suggests that substrate rigidity could play a role in bacterial physiology and biofilm formation.

Given the importance of surface sensing in *P. aeruginosa* in twitching motility (63) and in the onset of biofilm formation (52), we hypothesized that the mechanical properties of material substrates influence the process of biofilm formation. We tested this hypothesis by employing synthetic hydrogels with finely tunable mechanical properties. We found that substrate material properties have a profound impact on biofilm architecture. We could attribute these differences to initial the exploratory phase: *P. aeruginosa*'s surface motility differs between materials of different mesh sizes but whose stiffness and chemistry is identical. As a result, biofilm populations on denser hydrogels form shallower biofilms that are more sensitive to the last resort antibiotic colistin. In addition, mechanical regulation of twitching motility impacts the spatial organization of different bacterial lineages, which has a potential impact on social interactions in heterogenous biofilms.

3.3 Results

3.3.1 *P. aeruginosa* biofilm architecture depends on substrate mechanics

To investigate the link between substrate mechanics and *P. aeruginosa* biofilm formation, we exploited poly(ethylene glycol) diacrylate (PEGDA) hydrogels. These synthetic polymeric networks are optically clear, biocompatible, have homogeneous mechanical properties and are relatively soft thereby matching properties of living tissues (8). Moreover, PEGDA hydrogels are mechanically tunable so that their elastic moduli can be readily manipulated by controlling cross-linking (165). To investigate the contributions of material properties on biofilm formation, we screened an assortment of PEGDA hydrogels cross-linked from prepolymer of different chain length (700 Da to 6000 Da) and concentrations (10% wt/vol to 30% wt). We generated thin hydrogels films (~50 μm) at the bottom surface of microfluidic channels. These hydrogels were sufficiently thin to accommodate high resolution confocal imaging. We seeded constitutively fluorescent *P. aeruginosa* strains at the surface of hydrogels and subsequently initiated biofilm growth under flow (Figure 3.1A).

P. aeruginosa successfully colonized the surface of all hydrogels by forming biofilms. We however observed differences in colonization patterns across conditions (Figure 3.1B, Supplementary figure 3.1). On hydrogels with relatively long and dilute PEG, *P. aeruginosa* predominantly formed well-defined isolated biofilms (Figure 3.1Bi, Supplementary figure 3.1i). These biofilms grew into tall structures with large height-to-width aspect ratio. In comparison, *P. aeruginosa* populations appeared to colonize more uniformly the surface of hydrogels as molecular weight decreased (Figure 3.1Bi-iii) or PEGDA concentration increased (Figure 3.1Biii-iv, Supplementary Figure 3.1iii-iii). These biofilms were shallower, only slightly extending in the depth of the channel, normal to the surface. In the most extreme case of a 20% PEGDA at 700 Da, *P. aeruginosa* colonized the surface almost as a monolayer, making it difficult to distinguish biofilm colonies. In other words, decreasing the polymer chain length and increasing concentration promotes the transition from compact dome-shaped structures with near unity aspect ratio, to flat and spread out biofilms with relatively lower aspect ratio (Figure 3.1C).

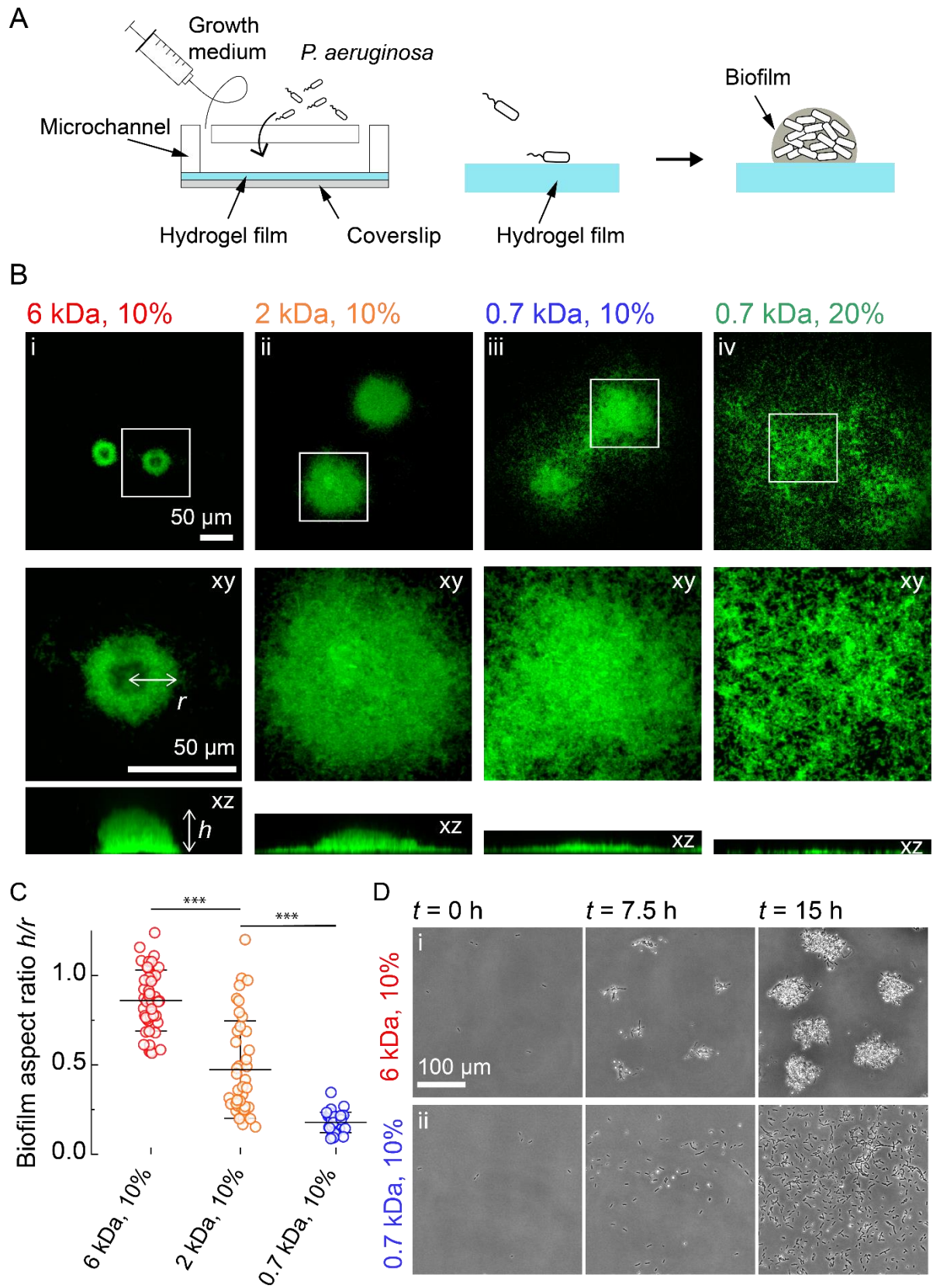


Figure 3.1: Hydrogel elastic substrates regulate *P. aeruginosa* biofilm architecture.

(A) Illustration of experimental setup where we generate thin PEG hydrogel films at the bottom surface of microchannels. These devices allow us to study biofilm formation on soft materials at high resolution. (B) In-plane

and cross-sectional confocal visualizations show different architectures of *P. aeruginosa* biofilms grown on hydrogels with different chain length (molecular weight, MW) and concentration of PEGDA precursors. For (i) MW = 6000 Da, 10% wt/vol, (ii) MW = 2000 Da, 10% wt/vol, (iii) MW = 700 Da, 10% wt/vol, (iv) MW = 700 Da, 20% wt. **(C)** Quantification of biofilm height (h) and radius (r) on different hydrogels shows an increase in aspect ratio h/r with increasing chain length. Each circle corresponds to one colony, black bars represent mean and standard deviation across all values. Colonies were selected from stacks acquired for 3 biological replicates. Statistics: one-way ANOVA for each gel, followed by a post-hoc Tukey test if the null hypothesis was rejected. Differences between the gels were statistically significant ($p < 0.001$). Numerical values can be found in Table 3.2. **(D)** Timelapse visualization indicates that hydrogels modulate *P. aeruginosa* biofilm architecture by regulating initial steps of biogenesis. (i) Biofilms form by division and local attachment in the vicinity of founder cells on long chain PEGDA hydrogels. (ii) Single cells explore the surface of short chain PEGDA hydrogels to form biofilms by aggregation.

The stiffness of substrate materials can influence *P. aeruginosa* adhesion (35). We therefore anticipated that a mechanism associated with bacterial attachment and material rigidity could regulate biofilm biogenesis. We were however surprised that biofilms adopted strikingly different architectures on PEGDA hydrogels with nearly identical Young's moduli (Figure 3.1B, Table 3.1). We therefore subsequently investigated the mechanisms by which material properties regulate biofilm architecture. Timelapse visualizations revealed noticeable differences between materials at the early stages of biofilm formation. Microcolonies rapidly appeared in the first few hours of growth on PEGDA hydrogels with high molecular weight (Figure 3.1Di, movie 1). On shorter chain PEGDA, we observed most *P. aeruginosa* cells exploring the surface as they grew and divided, leading to a more uniform distribution on the surface (Figure 3.1Dii, movie 1). While this mechanism tends to decrease local cell density near founder cells, it still promotes bacterial aggregation on longer timescale, allowing the development of multicellular structures. These visualizations suggest that distinct hydrogels control biofilm architecture by regulating initial surface exploration. We therefore investigated how material properties could impact surface motility.

3.3.2 Mechanical modulation of twitching motility

To nucleate biofilms, *P. aeruginosa* first attaches to and navigates on surfaces using twitching motility, which ultimately promotes aggregation (73). Long and thin retractile protein filaments called type IV pili (T4P) power twitching motility. T4P propel single cells forward by successively extending, attaching to the surface and retracting (60). How substrate mechanical properties regulate twitching motility remains unclear, but theory predicts cells move more efficiently on stiffer materials (91). Driven by our observations of early biofilm formation, we hypothesized that material properties

regulate twitching motility, thereby leading to the different biofilm architectures. Consistent with this scenario, we found that a $\Delta pilTU$ deletion mutant which lacks type IV pili retraction machinery formed biofilms on shorter chain PEGDA gels that resemble the ones formed by WT cells on long PEGDA gels (movie 2). To further explore this hypothesis, we performed extensive measurements of *P. aeruginosa* twitching at the single cell level on different PEGDA hydrogels. We recorded the trajectories of hundreds of cells per condition, and computed mean speed for each cell along their track (Figure 3.2 A-C, movie 3). Single *P. aeruginosa* cells barely migrated on PEGDA hydrogels that favored the formation of defined dome-like biofilms (Figure 3.2 Ai and C). In contrast, cells were much more motile on hydrogels that favored the formation of biofilm monolayers (Figure 3.2 Aii and C). Thus, the final architecture of a biofilm reflects the motility patterns observed on the distinct hydrogels. On substrates inhibiting motility, *P. aeruginosa* cells divide and accumulate near the initial founder cells, forming tightly packed dome-shaped biofilms. On substrates promoting motility, cells disperse on the surface as they divide, thereby limiting accumulation near founder cells but promoting surface occupation.

How does the material substrate modulate twitching motility? Consistent with our initial qualitative observations of biofilm architecture (Figure 3.1B), we only found a slight correlation between PEGDA Young's modulus and twitching speed (Figure 3.2Di). At equal polymer chain length, increasing stiffness with larger precursor concentration sped up twitching. However, this trend failed across gels with same concentration but different chain lengths: we measured a 3-fold change in twitching speed on hydrogels of nearly identical moduli (Figure 3.2Dii). We therefore wondered how bacteria could perceive these materials at their scale. Given the importance of cell and T4P attachment in twitching motility, we reasoned that hydrogel surface density and topology may affect *P. aeruginosa*'s motility. To estimate substrate density at the surface, we measured the mesh size of the hydrogel films using equilibrium swelling theory. Twitching speeds showed a stronger, negative correlation with mesh size across concentrations and chain lengths (Figure 3.2E). This revealed that hydrogel mesh size has an impact on twitching motility of single *P. aeruginosa* cells. Mesh may affect motility by affecting cell body adhesion or efficiency of T4P force generation.

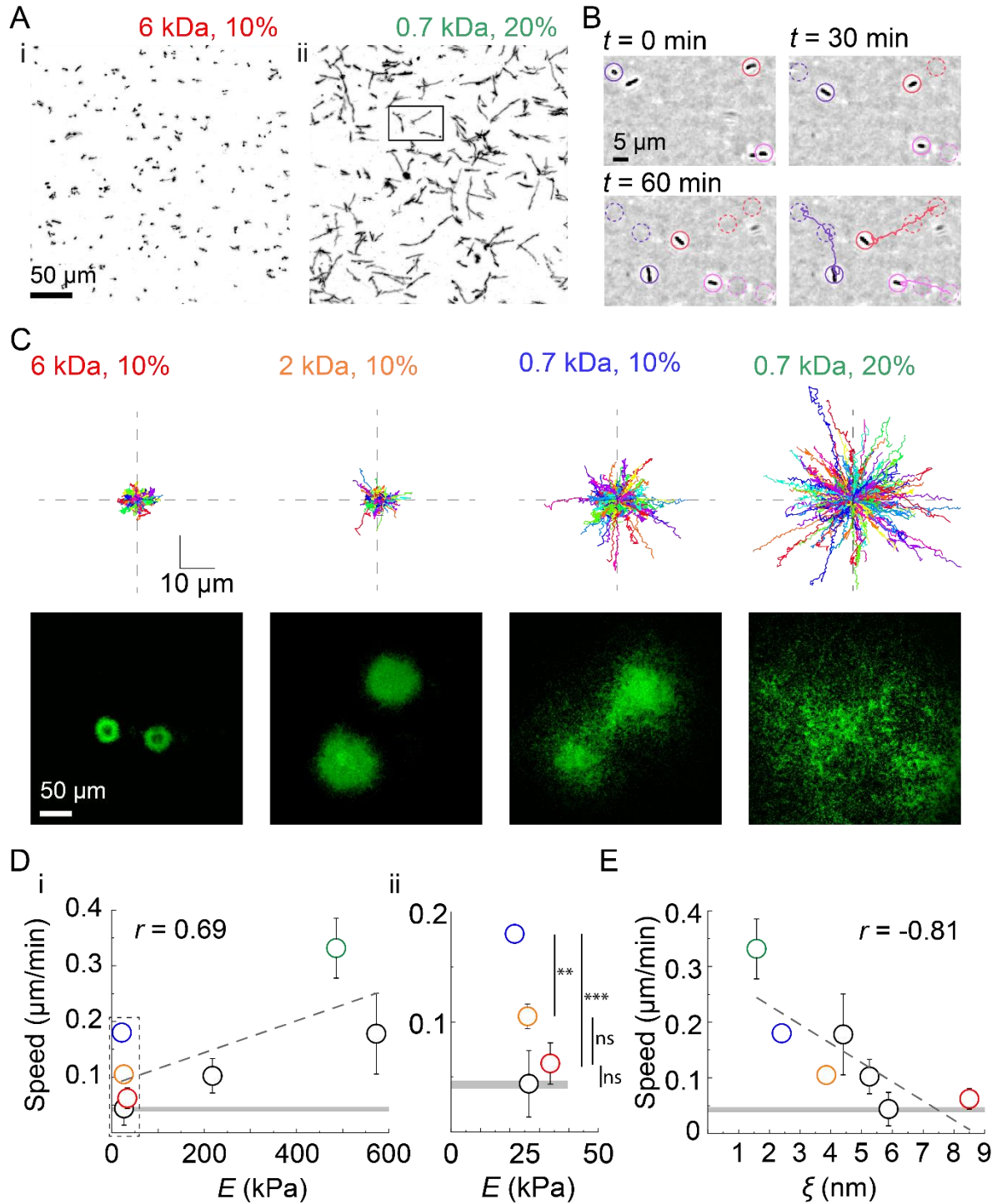


Figure 3.2: Hydrogel mesh size modulates biofilm architecture by regulating twitching motility.

(A) Cumulative surface coverage of bacterial trajectories during the first hour of contact with the indicated PEGDA gel. Black signal corresponds to bacterial, white corresponds to unexplored surface. (B) Timelapse visualization of *P. aeruginosa* twitching on the surface of PEGDA 700 Da at 20%, and respective trajectories (from selection in Figure 3.2Aii). (C) Trajectories of 300 randomly selected cells (one replicate for illustrative purposes) on four different hydrogels and resulting biofilm morphology after 40 h of growth (reshow of Figure 3.1). All trajectories start from the center of the graph. (D) Hydrogel mechanical property impact twitching speed. i) Population mean twitching speed increases with Young's modulus, but with limited correlation (Pearson correlation coefficient $r = 0.69$). ii) Closeup of twitching speed as a function of modulus at low stiffness. Despite modulus being nearly identical on the four gels,

we found large differences in twitching speeds. **(E)** Twitching speed decreases with increasing hydrogel mesh size, with relatively stronger correlation (Pearson correlation coefficient $r = -0.81$). For **(D, E)** dashed lines indicate the linear fit of the data. Circles represent the mean across 3 biological replicates and black bars represent standard deviation (SD). The horizontal grey line represents the mean speed across 3 biological replicates for a T4P retraction-deficient mutant ($\Delta fliC\Delta pilTU$), and the thickness of the line corresponds to the SD. Colored circles correspond to the gels 6 kDa, 10% (red), 0.7, 10% (blue) and 0.7 kDa, 20% (green). Black circles represent the speed values for the gels 3.4 kDa, 10% ($E = 27$ kPa, $\xi = 5.9$ nm), 6 kDa, 20% ($E = 265$ kPa, $\xi = 5.3$ nm), 6 kDa, 20% ($E = 470$ kPa, $\xi = 4.4$ nm). Visualizations of biofilms grown on these gels are in **S1**. For **D(i)** we performed a one-way ANOVA statistical test for gels with similar moduli, followed by a post-hoc Tukey test. For 6 kDa, 10% and 3.4 kDa, 10% we could not resolve statistically significant differences in twitching speed compared to a T4P retraction-deficient mutant ($\Delta fliC\Delta pilTU$, grey line). Differences between 6 kDa, 10% and 0.7 kDa, 10% ($p < 0.001$) and between 2kDa, 10% and 0.7 kDa, 10% ($p < 0.01$) are statistically significant. Numerical values can be found in Table 3.3.

Substrates stiffness had been shown to impact bacterial adhesion (35). We therefore verified whether *P. aeruginosa* initial cells density was different between gels. We however could not distinguish any difference in initial bacterial density across conditions, ruling out the possibility that initial adhesion causes the different biofilm morphologies (Supplementary figure 3.2A). We then explored the possibility that differences in adhesion strength of the cell body might explain changes in twitching speed. To test this hypothesis, we applied hydrodynamic forces on hydrogel-associated *P. aeruginosa* $\Delta fliC\Delta pilA$. We measured bacterial detachment at 0.2 Pa and 2 Pa mean shear stress. We found that the strength of adhesion of bacterial cell bodies is indistinguishable between the three hydrogels (Supplementary figure 3.2Bi). There was also no difference in bacterial adhesion strength in $\Delta fliC$ on the different hydrogel compositions (Supplementary figure 3.2Bii). The surface motility of WT also increased as a function of mesh size, demonstrating that the flagellum does not play a role in mechanical control of twitching (Supplementary figure 3.3).

As EPS production participates in initial *P. aeruginosa* surface exploration by chemically patterning the surface to generate trails (73), we also tested mutants that cannot produce Psl or Pel polysaccharides. ΔpsI mutant could not adhere to the gel surfaces so that we could not quantify twitching. The Δpel mutant could however attach and twitch. The twitching speed of single Δpel mutant cells increases with decreasing mesh size, as does WT (Supplementary figure 3.4). These results show that Psl is necessary at least for attachment to the soft surface, but Pel is not required. In addition, we explored the alternative hypothesis that material stiffness could differentially stimulate mechanosensing that transcriptionally regulates adhesion and motility. For example, c-di-GMP

levels increase on surface over the timescale of hours to regulate the production of EPS matrix (52). In addition, material stiffness regulates cyclic AMP (cAMP) levels upon surface contact via T4P (189). To test the contributions of mechanosensing in early surface exploration, we measured changes in intracellular levels of cAMP and c-di-GMP using the fluorescent transcriptoinal reporters for *PaQa-yfp* and *P_{cdra}-gfp* respectively. We could not detect any difference in intensity of these reporters across gel compositions on the timescale of our twitching experiments, ruling out the mechanosensing hypothesis (Supplementary figure 3.5).

As a result, we propose a model where the likelihood of T4P attachment depends on mesh size, rather than the strength of cell body adhesion or the activation of mechanosensory systems. The differences in T4P attachment ultimately controls the rate of productive T4P retractions. Consistent with this model, twitching speeds increase on hydrogels with mesh sizes below 5 nm, a dimension that corresponds to the diameter of the T4P fiber (190). Overall, our results suggest that T4P attachment to the hydrogel substrate with larger mesh sizes is less frequent, limiting the efficiency of force transmission during retraction.

3.3.3 Substrate mechanics impact antibiotic tolerance of biofilms

The biofilm lifestyle is a major contributor of human chronic infections due to its resilience against antibiotic treatments (6, 155, 191). Chronically infected patients are subject to lifelong *P. aeruginosa* infection even under strong antibiotic therapy, which favours the emergence of antibiotic resistant mutants. Multiple bacterial physiological factors improve tolerance to antibiotics. In biofilms, matrix impermeability, metabolic state of residents and increased cell density all contribute to protecting single bacteria from antibiotic stress (6, 155, 191). We however know very little about how environmental factors influence the sensitivity of *P. aeruginosa* to antibiotics by regulating biofilm formation. In light of the distinct biofilm architectures observed on PEGDA hydrogels, we hypothesized that antibiotic efficacy could differ as a result of material properties. We thus tested the efficacy of colistin, a last resort antibiotic against *P. aeruginosa* infections.

We grew biofilms on the different hydrogels for 46 h and subsequently challenged them with colistin for 1 h. To test antibiotic efficacy, we measured the volume of live biomass after treatment. After 1 h of colistin treatment, 50% of the population was killed for biofilms growing on smaller mesh size hydrogels (Figure 3.3A). This proportion was reduced to 40% on intermediate hydrogels, and went as low as 20% on the lowest mesh-size hydrogels, highlighting a strong decrease in drug efficacy.

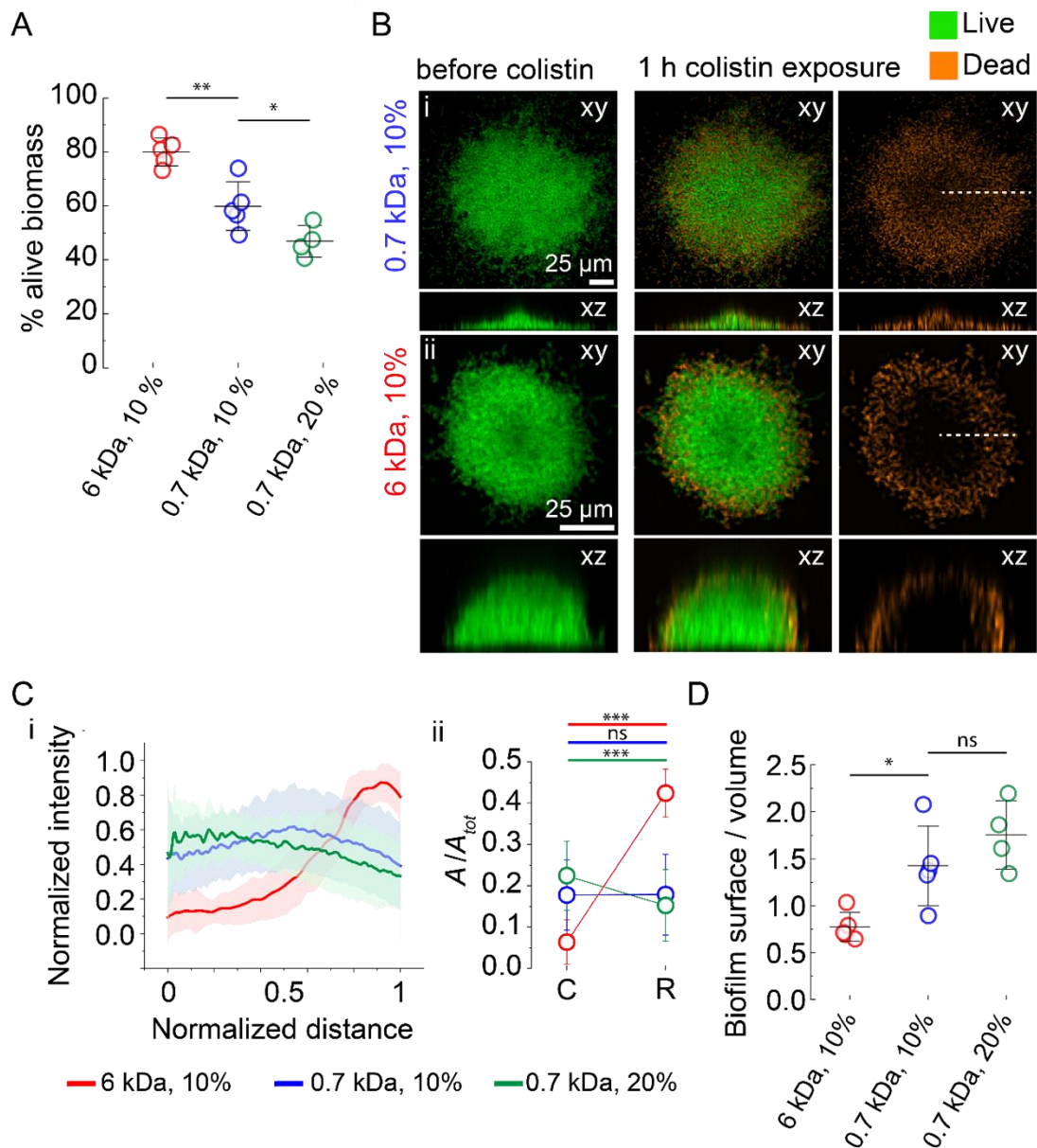


Figure 3.3: Mechanical control of biofilm architecture promotes *P. aeruginosa*'s tolerance to antibiotics.

(A) Quantification of live biomass after a 1 h colistin treatment, relative to the total biomass before antibiotic exposure. Biofilms grown on hydrogels with larger mesh size are more tolerant to colistin. (B) In-plane and cross-sectional confocal visualizations shows differences in colistin killing patterns. (C) (i) Dead stain fluorescence intensity

profiles computed along a biofilm radius (dashed lines in Figure 3.3B) highlight a more uniform distribution of dead cells in biofilms grown on hydrogels with smaller mesh size. Distance is normalized to each biofilm radius. Lines represent the average across around 30 single colonies selected from stacks acquired for 3 biological replicates, and shaded area correspond to the standard deviation. ii) Integrated normalized area under the curves in the biofilm core (C, between 0 and 0.2 distance unit) and the biofilm rim (R, between 0.8 and 1 distance unit). Circles represent the integrated normalized area and error bars the SD from the curve in shown in panel i. **(D)** Biofilm surface-to-volume ratios grown on different gels. Lower surface to volume ratio decreases overall exposure of single cells to antibiotics, which represses bacterial killing and increases tolerance to colistin. For **(A, D)** Circles represent the mean value for each chip (4-5 chips distributed across 3 biological replicates), black bars represent mean and error bars the SD across these values. Statistics in **A** and **B**: one-way ANOVA for each gel, followed by a post-hoc Tukey test if the null hypothesis was rejected. In (A) differences between 6 kDa, 10% and 0.7 kDa, 10% ($p < 0.01$) and between 0.7 kDa, 10% and 0.7 kDa, 20% ($p < 0.05$) are statistically significant. In (B) the difference between 6kDa, 10% and 0.7 kDa, 10% ($p < 0.05$) is statistically significant. Statistics in (C-ii): paired samples Student t-test (***) correspond to $p < 0.001$). Numerical values can be found in Table 3.4.

High resolution confocal images of biofilms stained with propidium iodide to highlight cell death revealed distinct spatial patterns of colistin killing (Figure 3.3B). On small pore size gels, bacteria were killed uniformly, irrespective of their position in the biofilm. In contrast, biofilms grown on larger mesh size hydrogels showed heterogeneity in cell death. Intensity profiles of biofilms stained with propidium iodide show that on these gels, bacteria at the outer edge of colonies (rim, R) were mostly dead, while cells at the core (C) of biofilms remained largely unaffected by colistin treatment (Figure 3.3C). Given the spatial pattern of killing, we reasoned that such differences were due to colistin transport into the biofilm. We therefore computed the surface to volume ratio in each architecture. Defined biofilms growing on more porous gels have lower surface to volume ratio than less porous gels (Figure 3.3D). Biofilms of low surface-to-volume ratio growing on large mesh size gels are densest (Supplementary figure 3.6). Thus, cells at the biofilm core are protected by the ones at the rim. In contrast, flat biofilms that have high surface-to-volume ratio are less dense, thereby exposing single cells to the external fluidic environment. Thus, biofilms growing on more porous gels are more tolerant due to longer diffusion times towards the biofilm core. Treatment on the less porous gels is more efficient as single cells are further exposed to the surrounding fluid.

3.3.4 Material mechanics mediate biofilm heterogeneity

Initial patterns of surface colonization are crucial to the architecture of biofilms. These patterns can also control the foundations of bacterial lineages, thereby influencing the interactions between different bacterial strains colonizing the surface evolution of microbial interaction traits. The mechanisms by which environmental conditions, such as fluid flow, and microbial response to these

factors influence the spatial architecture of polymicrobial communities, however, are still unclear. Single cell movements modulate the spatial organization of heterogeneous biofilms, ultimately governing how different clones or species compete or cooperate (93, 192). In flow, swimming motility tends to disperse *Caulobacter crescentus* biofilm lineages by spreading out the progeny of founder cells (149). This in turn affects the mixing of different clones coming from distinct founder cells. By analogy, we reasoned that twitching patterns observed on the different materials may affect the clonal organization by affecting lineage structure. We therefore explored the relationship between hydrogel mechanical properties and the mixing of heterogeneous biofilms. We grew biofilms from mixtures of two wild-type *P. aeruginosa* strains that each constitutively expressed the fluorescent proteins mScarlet and mNeonGreen (Figure 3.4A). On large mesh size hydrogels that inhibited motility, biofilms formed into separate, isolated clusters (Figure 3.4Ai). Finding *P. aeruginosa* cells of one color within a biofilm of the other was rare. mScarlet- and mNeonGreen-expressing cells were only found in close proximity when biofilms of distinct clones grew sufficiently to touch each other. Clonal lineages became however less segregated as hydrogel mesh size decreased, permitting twitching-dependent dispersion. On intermediate mesh size gels, while biofilms grew into defined colonies, there was a clear mixing between clones (Figure 3.4Aii, Supplementary figure 3.7i). Finally, on the hydrogels with smallest mesh size, clones were well mixed (Figure 3.4Aiii, Supplementary figure 3.7ii). For each hydrogel condition, we computed the mean first nearest neighbor distance between the mNeonGreen and mScarlet clones (Figure 3.4B). This distance decreased from 20 μm on large mesh size hydrogels (a length-scale corresponding to the typical radius of a biofilm) to 3 μm on the lowest mesh size hydrogel (corresponding to the size of a *P. aeruginosa* cell). Altogether, we showed that substrate material can have a strong influence on the distribution of genetically distinct bacterial population on the surface. The material-dependent mixing is of key importance in the fitness of each clone and the evolution of traits that mediate interactions.

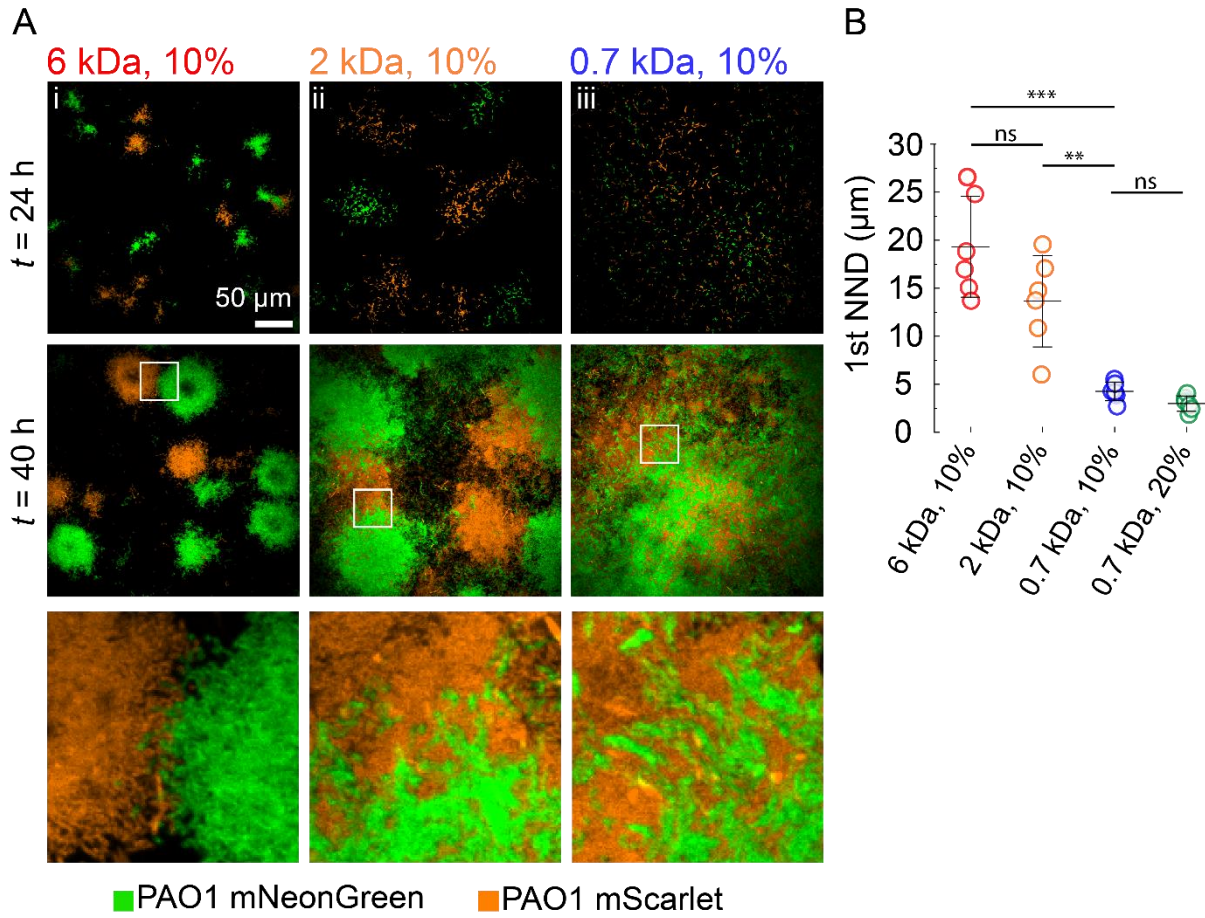


Figure 3.4: Hydrogel substrates regulate the spatial organization of heterogeneous *P. aeruginosa* biofilms.

We grew biofilms from a mixture of *P. aeruginosa* clones constitutively expressing mScarlet (orange) or mNeonGreen (green). **(A)** In-plane confocal visualization at 24 h and 40 h of heterogeneous biofilms on hydrogels with identical modulus but different mesh sizes. Larger mesh size promotes the growth of segregated biofilm clusters. In contrast, hydrogels with smaller mesh sizes promotes clonal mixing due to increased surface exploration. The bottom row shows close up views from the regions indicated by white frames. **(B)** Quantification of the mean first nearest neighbor distance (1st NND) between the mNeonGreen and mScarlet clones. Bacteria forming biofilms on small mesh size hydrogels are more prone to encounters with different clones, forcing them to compete. Circles represent the mean value for each chip (2 chips for each biological triplicate, 6 in total), black bars represent their mean and error bars their SD. Statistics: one-way ANOVA for each gel, followed by a post-hoc Tukey test if the null hypothesis was rejected. Differences between 6 kDa, 10% and 0.7 kDa, 10% ($p < 0.001$) and between 2kDa, 10% and 0.7 kDa, 10% ($p < 0.01$) are statistically significant. Numerical values in Table 3.5.

3.4 Discussion

Although mechanics play a role in *P. aeruginosa* surface adaptation, how these communities colonize physically-realistic environments has been overlooked (156). In particular, we know little

about how mechanical signals regulate biofilm formation and how biofilms form on soft tissue-like materials (5). Here, by investigating the regulation of biofilm architecture at the surface of defined and tunable hydrogels, we found that material properties can determine biofilm architecture by regulating T4P-dependent twitching motility of single *P. aeruginosa* cells.

Theory predicts that twitching migration speed increases with the rigidity of continuous materials in regimes where adhesion of the cell body is weak compared to T4P (91, 193). On hydrogels, we observe that twitching speed rather depends on cross-linking density than on Young's modulus. The discrepancy between theory and experiments points out to the way bacteria perceive their mechanical environments. On hydrogels, pore size could be sufficiently large so that T4P attaches with lower frequency or strength. As such, *P. aeruginosa* does not experience a continuous material. Consistent with this model, we found that cells start moving on hydrogels with a mesh size below 5 nm, a value that corresponds to the width of the pilus (190). In summary, we propose a model where twitching speed is determined by the probability of T4P to attach to the material surface. Thus, fewer binding events would limit the frequency of productive T4P retractions. We also measured that increasing the stiffness of the hydrogels by modulating the concentration of the precursors promotes twitching motility. These results are consistent with recent studies of *P. aeruginosa* on polyacrylamide gels (193). By extension, mechanics could regulate the architecture and antibiotic tolerance of biofilms of other piliated species. Looking further, mechanisms involving fimbriae, flagella or other protein receptors in the initial steps of biofilm formation may be affected by material density.

Our work provides a perspective on how bacteria touch and perceive solid materials. Force transmission and successful motility depends on T4P and cell body attachment. In this process, cells may in concert engage mechanosensory systems, such as the ones regulating the production of second messenger molecules. For example, surface contact promotes the production of cyclic-di-GMP, a known regulator of biofilm formation (52). Also, T4P couple with a chemotaxis-like system called Chp to guide twitching motility and upregulate virulence factors upon surface association (50, 63). The mechanical properties of materials substrate, more specifically substrate stiffness, can

differentially stimulate c-di-GMP levels on longer timescales of biofilm formation (37, 57). In addition, a combination of theory and experiments suggests that substrate stiffness regulates cAMP levels upon surface contact in a T4P-dependent manner (189). However, we found that cAMP and c-di-GMP levels are identical across conditions during the timescale of our twitching experiments. Therefore, *P. aeruginosa* does not need to engage transcriptional mechanoregulation of twitching motility to generate biofilms with distinct morphologies we observed. To fully comprehend how bacteria mechanically experience solid materials, it will be critical to address the fundamental principles of force transmission between bacteria and surfaces, identifying the mechanical regimes where these forces actively signal to dedicated sensory systems.

By influencing the foundations of nascent microcolonies, material properties regulate biofilm morphogenesis. On hydrogels with smaller mesh size, shallow biofilms have a larger surface to volume ratio, improving molecular diffusion throughout the population. Biofilms that adopt a characteristic dome architecture have decreased surface-to-volume ratio. As a result, the bacterial population at the rim of the biofilm effectively protects the core population from antibiotics, which is consequently largely unaffected by the treatment. This could in turn also favor the rise of antibiotic resistant mutants on a longer timescale (6, 194). Such mechanical regulation of tolerance adds to the many chemical and biological facets regulating sensitivity to antimicrobials (6, 154). Our observations has therefore the potential to guide the design of antifouling materials for biomedical applications.

P. aeruginosa encounters materials of distinct or heterogeneous mesh sizes as it colonizes extracellular matrices in burn wounds or mucus with altered viscoelasticity in cystic fibrosis patients. Our system may capture architectural transitions found in these different natural environments. The impact of material properties on the spatial organization of heterogeneous biofilms shows that mechanics could also play a role in social interactions between different species, influencing the relative fitness of bacteria of distinct backgrounds on an evolutionary timescale. We expect biofilm clones forming on materials with smaller mesh size would enter in competitive interactions, for example through contact-dependent toxin injections or through mechanisms like 'surface blanketing'.

At the same time, mixing of different populations might favour reciprocal benefits and cooperation through sharing of metabolic byproducts and degrading enzymes. Conversely, bigger mesh size could favour a positive interactions coexistence within genotypes. Further efforts to understand how biofilms form in realistic physical contexts will reveal the relative contributions of mechanics in biofilm biogenesis, evolution and how they contribute to infection dynamics.

3.5 Acknowledgements

We would like to thank Rok Simic and Nicholas Spencer for performing nanoindentation measurements and for helpful discussions. We are grateful for the financial support provided by the by the Swiss National Science Foundation through the Projects grant number 310030_189084 and the Human Frontier Science Program grant number RGY0077/2020.

3.6 Methods

3.6.1 PEG hydrogels fabrication

Solutions

To generate PEG hydrogels we prepared solutions of poly(ethylene glycol) diacrylate (PEGDA) as the precursor and lithium phenyl-2,4,6- trimethylbenzoylphosphinate (LAP, Tokio Chemical Industries) as the photoinitiator in M9 minimal medium (no calcium or magnesium). Different molecular weights (6000 Da, 3400 Da, 2000 Da, 700 Da) and concentrations (10 wt/vol%, 20 wt%, 30 wt%) of PEGDA were used for the formation of the hydrogels (see Table 3.1 for details), while the concentration of LAP was kept constant at 2 mM.

Hydrogel preparation for mechanical characterization

To measure bulk moduli and mesh sizes of PEGDA hydrogels, we prepared samples by filling cylindrical molds made of PDMS (5 mm diameter, 4 mm height) with the precursor solutions. The molds were covered with a coverslip and hydrogels were formed by irradiating the samples in a UV transilluminator (Bio-Rad Universal Hood II) for 5 min.

Hydrogel thin film preparation in microfluidic channels

To obtain thin and flat hydrogel layers, a prepolymer solution was sandwiched between two coverslips. One of the coverslip (25 × 60 mm Menzel Gläser) was cleaned with isopropanol and MilliQ water. The other coverslip (22 × 40 mm Marienfeld) was functionalized with 3-(Trimethoxysilyl)propyl methacrylate (Sigma-Aldrich) to covalently link the hydrogel to the coverslip: we immersed the coverslips for 10 minutes in a solution composed of 1 mL of 3-(Trimethoxysilyl)propyl methacrylate and 6 ml of diluted acetic acid (1:10 glacial acetic acid:water) in 200 mL of ethanol solution 70%. These were subsequently rinsed in ethanol and dried. We then deposited a 30 μ L droplet of prepolymer solution on the first coverslip and sandwiched it with the second. The assembly was then placed under the UV transilluminator for 5 min to allow cross-linking. Right after polymerization, the coverslips were separated using a scalpel thereby exposing the hydrogel film surface.

3.6.2 PEG hydrogels characterization

Bulk modulus

The hydrogel cylinders resulting from the polymerization in the PDMS molds were immersed in M9 overnight and tested with a rheometer (TA instruments) in compression mode, at a deformation rate of 20 μ m/s. Beforehand, the diameter of the cylinders was measured with a digital caliper, while the height of the cylinder was defined as the gap distance at which the force increases. The elastic modulus corresponds to the slope of the linear fit of the stress-strain curves in the range of 15% strain. The final Young's modulus is the average modulus of three replicates.

Nanoindentation

The hydrogel coated coverslips were immersed in M9 medium right after polymerization. Nanoindentation experiments were performed using an atomic force microscope (AFM, MFP-3D™, Asylum Research, Santa Barbara, USA). The indentation probe was prepared by attaching a silica microsphere (Kromasil, Nouryon - Separation Products, Bohus, Sweden) with a radius of $R = 11 \mu$ m

to the end of a tipless cantilever (NSC-36, Mikromash, Bulgaria) with the help of a 2-component epoxy glue (UHU GmbH, Germany). The effective spring constant was calculated as $k = k_0(L_0/L)^3 = 10.01 \text{ N/m}$, where k_0 is the spring constant of the bare cantilever, and L_0 and L are the distances from the base of the cantilever to its tip and to the microsphere, respectively (195). The spring constant of the bare cantilever k_0 was determined according to the Sader method before attaching the microsphere (196). After installing the probe, the laser path was adjusted to center the laser beam on the photodiode and maximize the intensity. The system was then calibrated by pressing the probe against a silicon wafer in water. The force was determined as $F = k x$, and the indentation depth was thus calculated as $d = Z - x$, where Z is the vertical piezo displacement and x is the cantilever displacement. The contact with the gel in liquid was determined at the point where the force signal began to deviate more than 2σ from the zero-force line, with σ being the standard deviation of the signal noise ($\sim 20\text{-}30 \text{ pN}$). The approach and retraction speeds were set to $1 \mu\text{m/s}$. The measurements were performed at $25 \text{ }^\circ\text{C} \pm 1 \text{ }^\circ\text{C}$. Forty force curves were obtained at different locations of a sample. Elastic moduli were extracted by fitting the Hertzian model to the indentation parts of the measured curves, which showed no adhesion upon the approach (197). For the curves that showed a snap-in during the approach, the JKR model was used (198).

Mesh size

Mesh size was estimated from the equilibrium swelling theory using protocols previously described (165, 199–202). For each hydrogel cylinder we determined the volume and the mass in the relaxed (r), swollen (s) and dry (d) states. We measured the volume of the cylinder right after polymerization (V_r) and after immersion in M9 for 24 h (V_s) with a caliper. We then washed the swollen hydrogels in deionized water to remove salts and we dried them overnight in the oven at 80°C . We then measured the mass of the dry network (M_d) and calculated V_d as M_d/ρ_{PEG} , with ρ_{PEG} taken to be 1.18 g/mL . We then calculated the average molecular weight between cross-links, M_c using eq. 1:

$$\frac{1}{\overline{M}_c} = \frac{2}{\overline{M}_n} - \frac{\left(\frac{\bar{v}}{V_1}\right) [\ln(1 - v_{2,s}) + v_{2,s} + \chi v_{2,s}^2]}{v_{2,r} \left[\left(\frac{v_{2,s}}{v_{2,r}}\right)^{\frac{1}{3}} - \frac{1}{2} \left(\frac{v_{2,s}}{v_{2,r}}\right) \right]} \quad \text{eq. 1}$$

where \bar{v} is the specific volume of the polymer (taken to be 0.93 mL/g for PEG), V_1 is the molar volume of water (18 mL/mol), χ is the polymer–solvent interaction parameter (taken to be 0.426 for PEG in water), \overline{M}_n is the average molecular weight of the polymer before cross-linking and $v_{2,r}$ and $v_{2,s}$ are the polymer volume fractions:

$$v_{2,r} = \frac{V_d}{V_r} \quad v_{2,s} = \frac{V_d}{V_s}$$

We finally obtained the mesh size ξ with eq.2:

$$\xi = v_{2,s}^{-1/3} l \sqrt{\frac{2C_n \overline{M}_c}{M_r}} \quad \text{eq. 2}$$

Where l is the bond length along the polymer backbone (0.15 nm), C_n is the Flory characteristic ratio (4 for PEG) and M_r is the molecular weight of the repeat unit (44 g/mol).

3.6.3 Assembly of hydrogel-coated coverslips with microfluidic chips

We fabricated microfluidic chips following standard soft lithography techniques. For biofilm experiments we designed 2 cm-long, 2 mm-wide channels in Autodesk AutoCAD and printed them on a soft plastic photomask. We then coated silicon wafers with the photoresist (SU8 2150, Microchem), with a thickness of 350 μm . The wafer was exposed to UV light through the mask and developed in PGMEA (Sigma-Aldrich) in order to produce a mold. PDMS (Sylgard 184, Dow Corning) was subsequently casted on the mold and cured at 80°C overnight. After cutting out the chips, we punched 1 mm inlet and outlet ports. We finally punched a 3 mm hole right downstream of the inlet port. This hole, after being covered with a PDMS piece, acts as a bubble trap. To fabricate channels for the twitching experiments, we followed a similar procedure, but we used a different photoresist

(SU8 2025 Microchem) and we adjusted the dimensions of the channel to be 500 μm wide and 100 μm high.

The final assembled chips were obtained by placing the PDMS chips on top of the hydrogel-coated coverslips right after polymerization. This results in a reversible, but sufficiently strong bond between the hydrogel and the PDMS, allowing us to use the chips under flow without leakage for several days. The channels of the chips were filled with M9 medium to keep the hydrogel hydrated for at least 12 hours before being used.

3.6.4 Bacterial strains

Strains used in this work are listed in Table 3.9. All strains were grown in LB medium at 37°C. Overnight bacterial cultures were diluted 1:1000 in fresh LB and grown until mid-exponential phase (optical density at 600 nm: 0.3 to 0.6).

3.6.5 Single cell twitching and adhesion

Overnight bacterial cultures of PAO1 $\Delta flic$, PAO1 $\Delta flic \Delta pilTU$, PAO1, PAO1 Δpel and PAO1 Δpsi were diluted 1:1000 in fresh LB and grown until mid-exponential phase (OD 0.4–0.6). Bacterial cultures were diluted to reach an optical density of 0.4 for PAO1 $\Delta flic$ and PAO1, and 0.1 for PAO1 $\Delta flic \Delta pilTU$. For PAO1 Δpel and PAO1 Δpsi 200 μL of bacterial cultures at OD 0.5 were centrifuged at 6000 rpm and resuspended in 50 μL of LB to increase the number of adhering cells. We then loaded 10 μL of the bacterial culture in the small microfluidic chips (500 μm wide and 100 μm deep) assembled with either hydrogel-coated coverslips or with glass coverslips. We let the bacteria adhere for 30 minutes. We connected the inlet port to a disposable syringe (BD Plastipak) filled with the medium and mounted onto a syringe pump (KD Scientific), using a 1.09 mm outer diameter polyethylene tube (Instech) and a 27G needle (Instech). For twitching experiments, we used a flow of 60 $\mu\text{L}\cdot\text{h}^{-1}$ for 5 minutes in order to remove bacteria that did not adhere to the hydrogel surface. We then switched to a flow of 30 $\mu\text{L}\cdot\text{h}^{-1}$ before starting image acquisition. Images were taken every 30 s for 1 h.

For adhesion experiments 200 μL of bacterial cultures of PAO1 $\Delta flic \Delta pilA$ and PAO1 $\Delta flic$ at OD 0.5 were centrifuged at 6000 rpm and resuspended in 50 μL of LB. We load 10 μL of the bacterial suspension in small microfluidic chips that were hold together with a custom-built clamp to avoid delamination of the chip from the gel under large flow rate. We connected the inlet port as described above and we let the cells adhere for 30 min. We used a flow of 60 $\mu\text{L}\cdot\text{h}^{-1}$ for 5 min in order to remove bacteria that did not adhere to the hydrogel surface. Images were then taken every 10 s for 6 min in the center of the channel with a flow of 60 $\mu\text{L}\cdot\text{h}^{-1}$ for the first 2 min, 600 $\mu\text{L}\cdot\text{h}^{-1}$ for the next 2 and 6000 $\mu\text{L}\cdot\text{h}^{-1}$ for the final 2 min.

We aquired images on a Nikon TiE widefield microscope equipped with a Hamamatsu ORCA Flash 4 camera. Images were acquired in phase contrast with a 20x Plan APO NA 0.75 objective.

3.6.6 Biofilm formation

Overnight bacterial cultures of PAO1 were diluted 1:1000 in fresh LB and grown until mid-exponential phase. Bacterial cultures were diluted to reach an optical density of 0.05. We then loaded 6.5 μL of the diluted bacterial culture in the big channels (2 mm wide and 350 μm high), from the outlet port. It is important that injected cells do not reach the well of the bubble trap. We let the cells adhere for 30 min before starting the flow. The biofilms were grown at 25°C at a flow rate of 10 $\mu\text{L}\cdot\text{min}^{-1}$. For timelapse visualizations of early-stage biofilm formation, we acquired images every 15 min for 15 h in phase contrast with a 40x Plan APO NA 0.9 objective. For the visualization of biofilms, we used a Nikon Eclipse Ti2-E inverted microscope coupled with a Yokogawa CSU W2 confocal spinning disk unit and equipped with a Prime 95B sCMOS camera (Photometrics). We used a 20x water immersion objective with N.A. of 0.95 and z-stacks of the biofilms were taken every 2 μm .

3.6.7 Quantification of cAMP and c-di-GMP during surface growth

To quantify intracellular levels of cAMP, we used the PaQa-YFP reporter system as previously described (50). To quantify intracellular levels of c-di-GMP, we used the P_{cdrA} -GFP reporter system (184). Single colonies of PAO1 containing PaQa-YFP or P_{cdrA} -GFP reporter plasmids were grown overnight respectively in LB-carbenicillin and LB-gentamicin. The cultures were then diluted 1:1000

in fresh antibiotic-free LB and grown until OD 0.5. We then loaded 10 μL of the bacterial culture in the small microfluidic chips and we let the bacteria adhere for 25 minutes. We then washed the channels for 5 minutes and acquired images in the appropriate fluorescent channels at 30 min and 90 min. Image acquisition was done with the confocal spinning disk microscope equipped with a 100x oil immersion objective (N.A. of 1.45) as described above.

3.6.8 Image processing and analysis

Snapshot images and movies were generated with Fiji. Images were processed with macros in Fiji and data were analyzed in Python 3 and OriginPro.

Single cell twitching

When necessary, drift was corrected using the Correct 3D Drift plugin. Cells were segmented and then tracked using a Trackmate script that tracks spots based on a result table that contains the position of each cell's center of mass in the movie. Subsequent analysis of cell trajectories was done with a custom Python script. Only tracks with a duration above 10 min were considered. Cell speed was calculated as the net displacement (distance between the last and the first spot of the track) divided by the track duration. An average speed was calculated for each replicate based on at least 50 tracks and displayed values are the average among three replicates and the corresponding standard deviation.

Single cell adhesion

Only a portion of the stack with a width equal to half of the channel width taken in the center was considered. Cells were segmented and tracked as above. Only cells attached to the surface from time 0 were considered. We defined the shear stress at the wall of the channel as $\sigma_s = 6Q\mu/wh^2$, where Q is the volumetric flow, μ the viscosity of the fluid and w and h the width and the height of the channel respectively. The initial cell number is defined as the number of cells that stays attached for at least 90 s under a shear stress of 0.02 Pa ($Q = 60 \mu\text{L}\cdot\text{h}^{-1}$). The percentage of cells that stays attached to the surface under a shear stress of 0.2 and 2 Pa is defined as the number of cells

attached to the surface just before the next increase of shear stress normalized by the initial cell number.

cAMP and c-di-GMP quantification

Images were background-subtracted. Cells were then segmented and the corresponding mean PaQa-YFP to mKate2 fluorescent intensity ratios or mean cdrA-GFP intensity were computed. For each biological replicate at least 50 cells were analyzed. The displayed values correspond to the average intensity ratios or intensities for each biological replicate.

Biofilm morphology

Biofilms were imaged after 40 h of growth in proximity to the channel inlet. For each condition we imaged 6 chips (2 chips for each biological replicate) and around 30 single colonies were selected and segmented. The radius of the colony is defined as the radius of a circle with an area equal to the substrate area covered by the biofilm. The height of the colony is defined as the maximum height of the orthogonal projection at the center of the colony (found by fitting a circle to the area covered by the biofilm). The displayed height to radius ratio corresponds to all measured colonies.

Biofilm spatial organization

For mixing experiments, PAO1 mNeonGreen and PAO1 mScarlet were mixed at a 1:1 ratio before inoculation in the channels. Biofilms were imaged after 40 h of growth at the beginning of the channel. For each condition we imaged 6 chips (2 chips for each biological replicate) and for each chip we acquired around 10 stacks. To correct for the slide tilting we performed a maximum intensity projection of the first 3 slices for each stack. Images were then segmented for the 2 fluorescent channels. To quantify the 1st nearest neighbor distance (1st NND) we selected 100 random pixels in the segmented mNeonGreen picture for each stack. We then calculated the distance between the selected pixels and their nearest neighbor pixels in the corresponding segmented mScarlet picture. This way we obtained an average 1st NND for each stack. For each chip the highest 1st NND value

was filtered out and a mean value of the remaining stacks was calculated. The displayed 1st NND corresponds to the average 1st NND for each chip.

Antibiotic treatment of biofilms

Biofilms of PAO1 GFP were imaged after 46 h (time 0) of growth at the beginning of the channel. For each condition we imaged 4-5 chips (distributed among 3 biological replicates) and for each chip we acquired 6 stacks. We then switched the medium from LB to LB containing the antibiotic colistin (5 µg/mL, Acros organics) and the dye Propidium Iodide (5 µM, Cayman chemical) for staining of dead cells. Biofilms were imaged every hour in the same positions set at time 0. Stacks acquired at time 0 and after antibiotic treatment were concatenated and the drift was corrected.

To quantify the effect of the antibiotic on the biofilms we measured the volume of live biomass (expressing GFP). Stacks were segmented and the biofilm volume at different times was quantified with the plugin 3D Objects counter and normalized by the value at time 0. We then obtained an average value for each chip. Biofilm volume and surface at time 0 were quantified with the plugin 3D Objects counter. The substrate area covered by the biofilm was measured after performing a maximum intensity projection of the segmented stack. The exposed surface was calculated as the difference between the total surface and the substrate area covered by the biofilm. Exposed surface to volume ratio was calculated for each stack and we obtained an average value for each chip.

To quantify cell death induced by colistin, we selected around 30 - 40 single colonies from stacks acquired after 1 h of antibiotic treatment. Images in the green channel were segmented and used to define the core (C) and the rim (R) of the colony by fitting a circle to the area covered by the biofilm. We then performed a radial reslice over 360 degrees in the red channel (dead biofilm) by rotating a line with a length equal to R around one of its ends placed in C. We performed an average intensity projection of the resulting stack and measured the intensity profile along a line of length equal to R drawn slightly above the plane of contact between the biofilm and the substrate. The intensity of the curves was normalized by the highest value, while the distance was normalized by R. We then averaged the curves and calculated the standard deviation for each condition. We then

performed integration of the curve between 0 and 0.2 (C) and between 0.8 and 1 (R) and we normalized the results by the total area under the curve.

Biofilm surface density

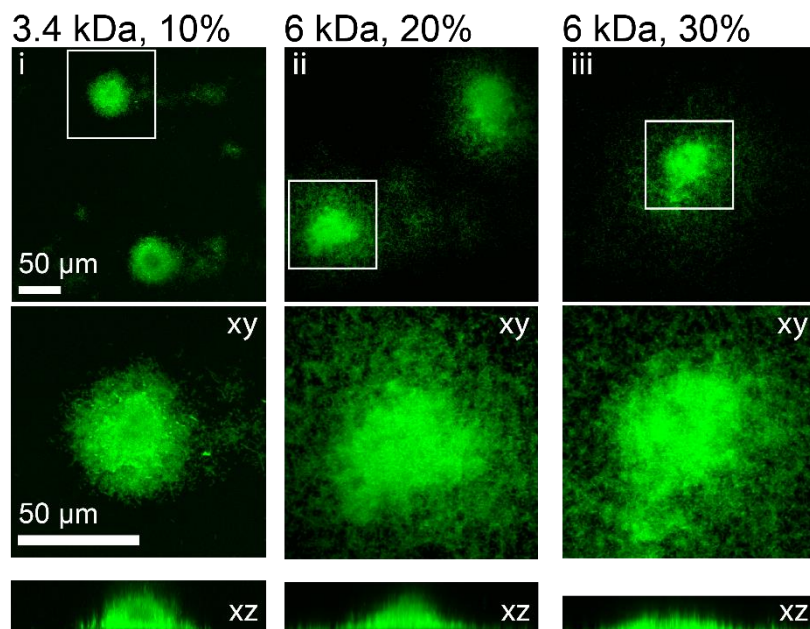
To quantify the density of the biofilm, we selected about 40 colonies from stacks acquired before antibiotic treatment (same colonies used for the quantification of colistin induced death). Images in the green channels were segmented and used to define the center of the colony by fitting a circle to the area covered by the biofilm. We then defined the dimension of the biofilm to be the radius of a circle that contains 90% of the total colony surface area. For each colony we then defined a grid with the dimension of the fitting circle and made of 20x20 μm squares. For each square in the grid we quantified the area fraction occupied by the biofilm on the surface. We defined the biofilm surface density as the proportion of occupied surface for each colony by averaging the values across the grid. Distributions of biofilm surface density for each gel were obtained by plotting the area fraction of all the corresponding squares.

Statistics

All statistical tests were run in OriginPro. For one-way ANOVA statistics, if the null hypothesis was rejected, we followed up with a post-hoc Tukey test.

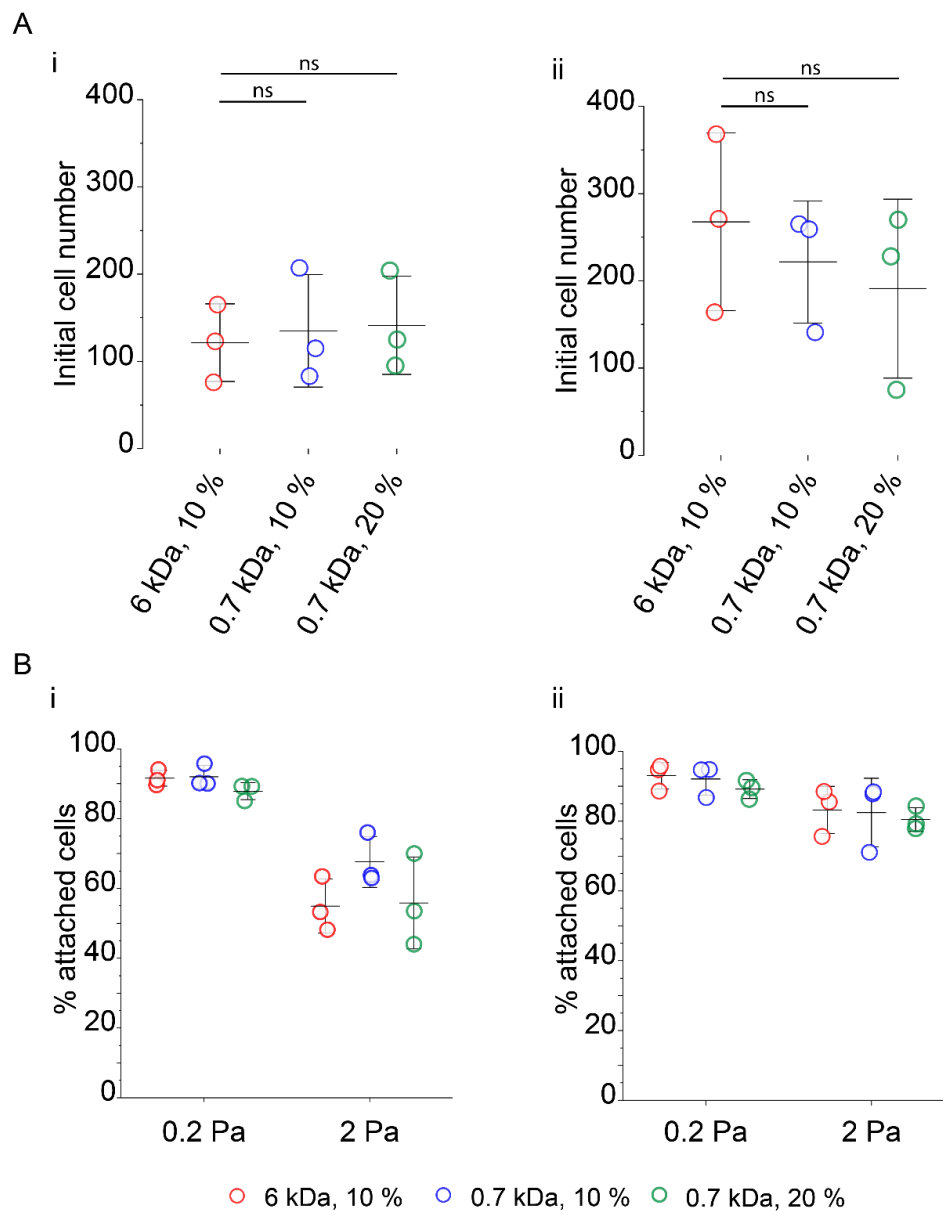
3.7 Supplementary information

3.7.1 Supplementary Figures



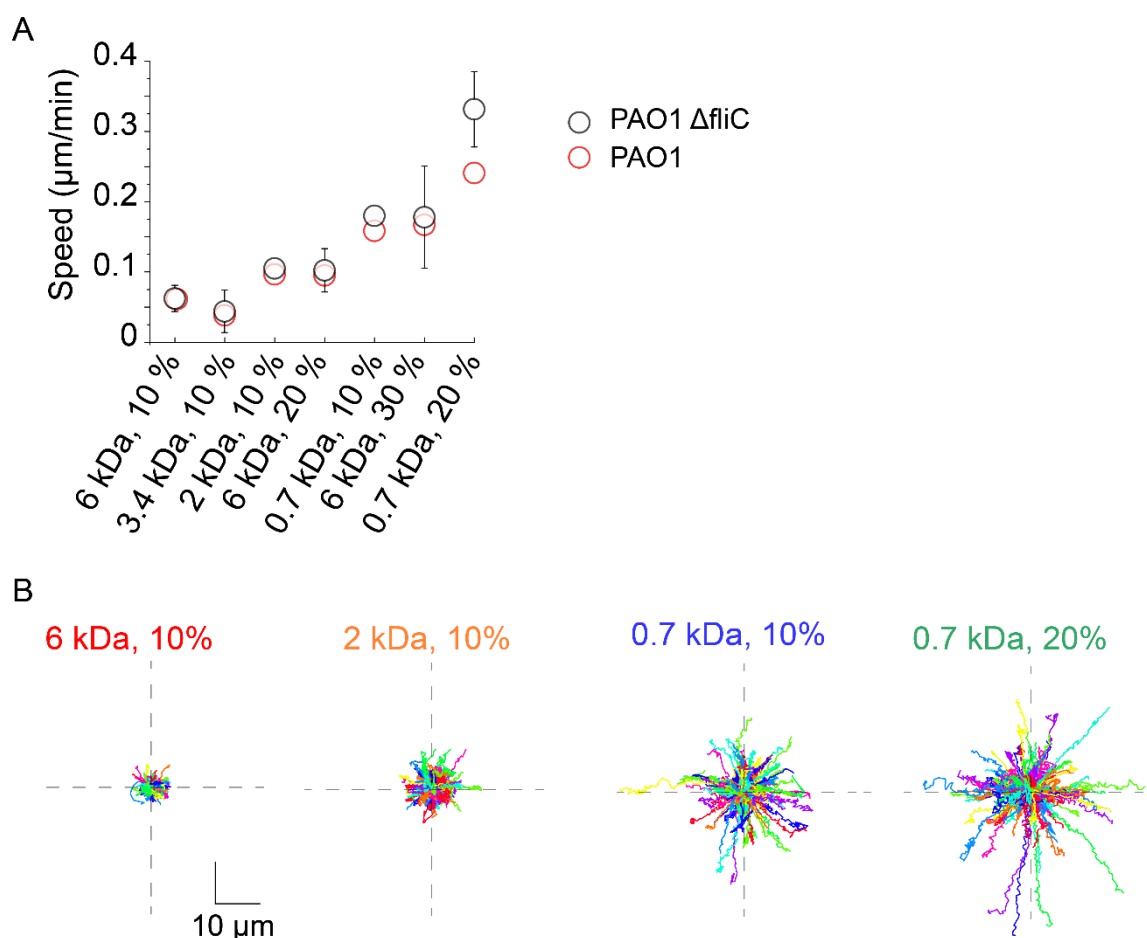
Supplementary Figure 3.1: Hydrogel substrates regulate *P. aeruginosa* biofilm architecture.

In-plane and cross-sectional confocal visualizations show different architectures of *P. aeruginosa* biofilms grown on hydrogels with different MW and concentration of PEGDA precursors. For (i) MW = 3400 Da, 10% wt/vol, (ii) MW = 6000 Da, 20% wt, (iii) MW = 6000 Da, 30% wt.



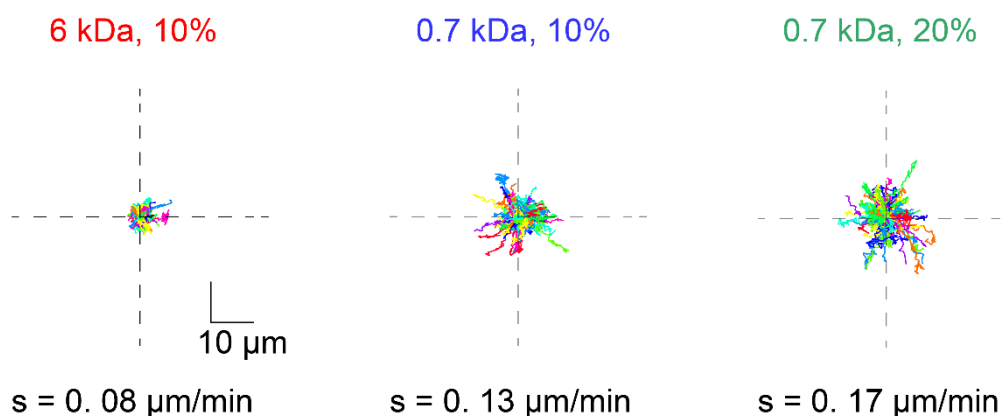
Supplementary Figure 3.2: *P. aeruginosa* initial attachment and adhesion strength are independent of hydrogel mesh size.

(A) Quantification of the number of *P. aeruginosa* attached to hydrogels before twitching and biofilm experiments for (i) $\Delta fliC$ and (ii) pilus-deficient mutant $\Delta fliC\Delta pilA$. There is no detectable difference in bacterial attachment between gel compositions. (B) Percentage of cells that remain attached after applying a shear stress of 0.2 or 2 Pa for a (i) T4P-deficient mutant $\Delta fliC\Delta pilA$ and (ii) $\Delta fliC$. Cells are uniformly removed by the flow, independently of hydrogel mesh size. Circles represent biological replicates and black bars represent mean and SD of displayed values. Statistics: in both A and B one-way ANOVA statistical test did not reject the null hypothesis, the means are therefore not significantly different. Numerical values can be found in Table 3.6.



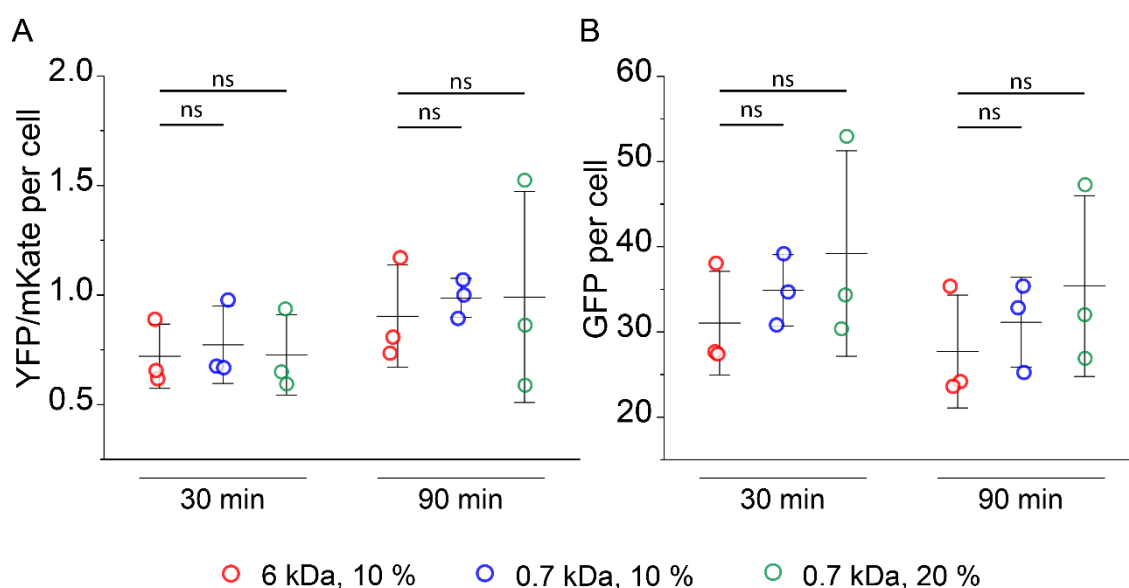
Supplementary Figure 3.3: Flagella are not affecting the mechanoregulation of twitching motility.

(A) Comparison of twitching speed on the different gel compositions for WT PAO1 and PAO1 ΔfliC . Black circles represent the mean across 3 biological replicates and black bars represent standard deviation (SD). Red circles represent one biological replicate. (B) Trajectories of 300 randomly selected PAO1 cells on four different hydrogels.



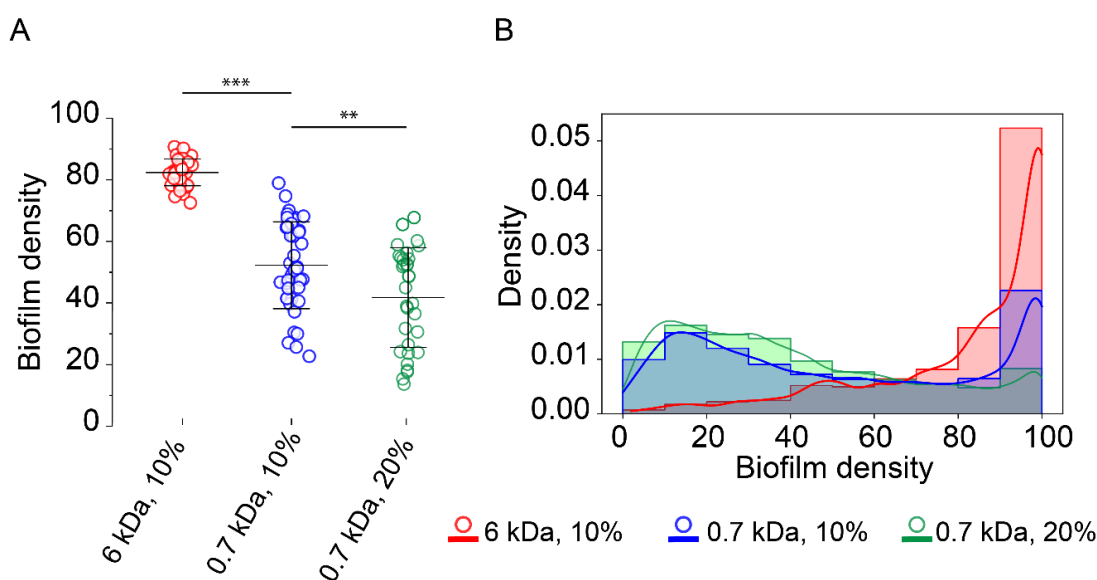
Supplementary Figure 3.4: Twitching motility of the mutant Δpel is sensitive to the mechanical properties of the gels.

Trajectories of 200 randomly selected PAO1 Δpel cells on 3 different hydrogels. Twitching speed values for one replicate are indicated underneath.



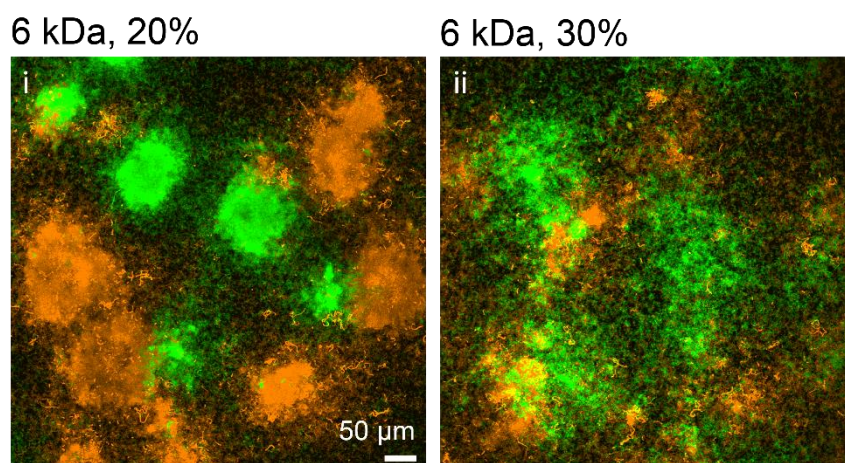
Supplementary Figure 3.5: *P. aeruginosa* does not increase intracellular levels of cAMP and c-di-GMP on hydrogels of different compositions during early times of surface colonization.

(A) cAMP levels measured by PaQa-YFP reporter fluorescence. (B) c-di-GMP levels measured by cdrA-GFP reporter fluorescence. Cells were imaged after 30 and 90 minutes of contact with the surface. Circles represent biological replicates and black bars represent mean and SD of displayed values. Statistics: one-way ANOVA statistical test did not reject the null hypothesis, the means are therefore not significantly different. Numerical values in Table 3.7.



Supplementary Figure 3.6: Hydrogel mechanical properties impact cell density of biofilms.

(A) Biofilms are more dense on hydrogels with larger mesh size. The biofilm density is defined as the percentage of occupied area within each colony. Each circle corresponds to one colony, black bars represent mean and standard deviation across all values. Colonies were selected from stacks acquired for 3 biological replicates. Statistics: one-way ANOVA for each gel, followed by a post-hoc Tukey test if the null hypothesis was rejected. Differences between 6 kDa, 10% and 0.7 kDa, 10% ($p < 0.001$) and between 0.7 kDa, 10% and 0.7 kDa, 20% ($p < 0.01$) are significant. (B) Frequency distribution of biofilm surface density on the different gels. On gels with smaller mesh size the frequency of high surface density areas decreases while the frequency of lower surface density areas increases. Lines represent the kernel density estimate (KDE) of the distributions. Numerical values in Table 3.8.



Supplementary Figure 3.7: Hydrogel substrates regulate the spatial organization of heterogeneous *P. aeruginosa* biofilms.

In-plane confocal visualization at 40 h of heterogeneous biofilms on hydrogels with different mesh sizes and modulus. Biofilms appear more mixed on hydrogels with smaller mesh size and bigger modulus. For 6 kDa, 20% $E = 265$ kPa and $\xi = 5.3$ nm, for 6 kDa, 20% $E = 470$ kPa and $\xi = 4.4$ nm. The biofilm mixing is qualitatively similar to the one on hydrogels with comparable twitching speed (6kDa, 20 % with 2kDa, 10% and 6kDa, 30% with 0.7 kDa, 10%).

3.7.2 Movies

Movies are located at the following link:

<https://www.dropbox.com/sh/4kzej3em9seuwe7/AABLYrixlrntfYm6JNNs-7xVa?dl=0>

Movie 3.1

Timelapse visualization of *P. aeruginosa* biofilm formation on PEGDA hydrogels with similar modulus (6 kDa, 10% w/v on the left, 0.7 kDa, 10% w/v on the right). Time is in h:min.

Movie 3.2

Timelapse visualization of *P. aeruginosa* biofilm formation on PEGDA hydrogels with similar modulus (6 kDa, 10% w/v on the left, 0.7 kDa, 10% w/v in the center and on the right). PAO1 in the left and central panel, PAO1 Δ pilTU in the right one. Time is in h:min.

Movie 3.3

Timelapse visualization of *P. aeruginosa* cells twitching on PEGDA hydrogels (6 kDa, 10% w/v on the left, 0.7 kDa, 20% w/w on the right).

3.7.3 Tables

Table 3.1: Summary of mechanical properties of PEGDA hydrogels

PEGDA precursor	Concentration (% w/v or % w/w)	Young's modulus (bulk) \pm SD (kPa)	Young's modulus (AFM) \pm SD (kPa)	Mesh size \pm SD (nm)
PEGDA MW 6000 (Biochempeg)	10% w/v	38.0 \pm 13.9	33.7 \pm 0.8	8.50 \pm 1.20
PEGDA MW 6000 (Biochempeg)	20% w/w	265.0 \pm 0.3	218 \pm 6	5.26 \pm 0.25
PEGDA MW 6000 (Biochempeg)	30% w/w	470 \pm 28	573 \pm 27	4.40 \pm 0.14
PEGDA MW 3400 (Biochempeg)	10% w/v	26.9 \pm 1.1	26.4 \pm 0.6	5.88 \pm 0.06
PEGDA MW 2000 (Biochempeg)	10% w/v	37.6 \pm 2.1	26 \pm 0.6	3.85 \pm 0.17
PEGDA MW 700 (Sigma-Aldrich)	10% w/v	48.0 \pm 1.3	21.6 \pm 0.6	2.40 \pm 0.05
PEGDA MW 700 (Sigma-Aldrich)	20% w/w	750 \pm 57	486 \pm 14	1.59 \pm 0.03

Table 3.2: Numerical values of biofilm aspect ratio h/r from Figure 3.1C

PEGDA precursor	Concentration (% w/v or % w/w)	h/r \pm SD
PEGDA MW 6000	10% w/v	0.86 \pm 0.17
PEGDA MW 2000	10% w/v	0.47 \pm 0.27
PEGDA MW 700	10% w/v	0.18 \pm 0.06

Table 3.3: Numerical values of twitching speed from Figure 3.2D-E

PEGDA precursor	Concentration (% w/v or % w/w)	Young's modulus (AFM) \pm SD (kPa)	Mesh size \pm SD (nm)	Twitching speed \pm SD (μ m/min)
PEGDA MW 6000	10% w/v	33.7 \pm 0.8	8.50 \pm 1.20	0.06 \pm 0.02
PEGDA MW 6000	20% w/w	218 \pm 6	5.26 \pm 0.25	0.10 \pm 0.03
PEGDA MW 6000	30% w/w	573 \pm 27	4.40 \pm 0.14	0.18 \pm 0.07
PEGDA MW 3400	10% w/v	26.4 \pm 0.6	5.88 \pm 0.06	0.04 \pm 0.03
PEGDA MW 2000	10% w/v	26 \pm 0.6	3.85 \pm 0.17	0.11 \pm 0.01
PEGDA MW 700	10% w/v	21.6 \pm 0.6	2.40 \pm 0.05	0.18 \pm 0.01
PEGDA MW 700	20% w/w	486 \pm 14	1.59 \pm 0.03	0.33 \pm 0.05
Δ pilTU on glass				0.041 \pm 0.004

Table 3.4: Numerical values of alive biomass and biofilm surface to volume ratio from Figure 3.3(A, D)

PEGDA precursor	Concentration (% w/v or % w/w)	alive biomass \pm SD (%)	Biofilm surface/volume \pm SD (1/ μ m)
PEGDA MW 6000	10% w/v	80 \pm 5	0.78 \pm 0.15
PEGDA MW 700	10% w/v	60 \pm 9	1.43 \pm 0.42
PEGDA MW 700	20% w/w	47 \pm 6	1.75 \pm 0.36

Table 3.5: Numerical values of 1st NND from Figure 3.4B

PEGDA precursor	Concentration (% w/v or % w/w)	1st NND \pm SD (μ m)
PEGDA MW 6000	10% w/v	19.3 \pm 5.3
PEGDA MW 2000	10% w/v	13.7 \pm 4.8
PEGDA MW 700	10% w/v	4.3 \pm 1.0
PEGDA MW 700	20% w/w	3.0 \pm 0.8

Table 3.6: Numerical values of initial cell number and attached cells under a shear stress of 0.2 and 2 Pa from Supplementary Figure 3.2

PEGDA precursor	Concentration (% w/v or % w/w)	Strain	Initial cell number \pm SD	Attached cells at $\sigma_s = 0.2$ Pa \pm SD (%)	Attached cells at $\sigma_s = 2$ Pa \pm SD (%)
PEGDA MW 6000	10% w/v	Δ fliC Δ pilA	267 \pm 102	92 \pm 2	55 \pm 8
PEGDA MW 700	10% w/v	Δ fliC Δ pilA	221 \pm 70	92 \pm 3	68 \pm 7
PEGDA MW 700	20% w/w	Δ fliC Δ pilA	191 \pm 103	88 \pm 2	56 \pm 13
PEGDA MW 6000	10% w/v	Δ fliC	121 \pm 44	93 \pm 4	83 \pm 7
PEGDA MW 700	10% w/v	Δ fliC	135 \pm 64	92 \pm 5	82 \pm 10
PEGDA MW 700	20% w/w	Δ fliC	141 \pm 56	89 \pm 3	80 \pm 3

Table 3.7: Numerical values of YFP/mKate and GFP per cell from Supplementary Figure 3.5

PEGDA precursor	Concentration (% w/v or % w/w)	YFP/mKate (time 0) \pm SD	YFP/mKate (time 1) \pm SD	GFP (time 0) \pm SD (A.U.)	GFP (time 1) \pm SD (A.U.)
PEGDA MW 6000	10% w/v	0.72 \pm 0.15	0.90 \pm 0.23	31.04 \pm 6.07	27.71 \pm 6.62
PEGDA MW 700	10% w/v	0.77 \pm 0.18	0.99 \pm 0.09	34.88 \pm 4.18	31.14 \pm 5.27

PEGDA MW 700	20% w/w	0.73 ± 0.18	0.10 ± 0.48	39.21 ± 12.06	35.39 ± 10.60
--------------	---------	-----------------	-----------------	-------------------	-------------------

Table 3.8: Numerical values of biofilm density from Supplementary Figure 3.6

PEGDA precursor	Concentration (% w/v or % w/w)	Biofilm density \pm SD
PEGDA MW 6000	10% w/v	82.4 ± 4.3
PEGDA MW 700	10% w/v	52.3 ± 14.1
PEGDA MW 700	20% w/w	41.8 ± 16.2

Table 3.9: List of bacterial strains

Name	Description	Origin/reference
PAO1		(203)
PAO1 $\Delta fliC$	in-frame deletion of PA1092	(204)
PAO1 $\Delta fliC \Delta pilA$	in-frame deletion of PA1092 and PA4525	(204)
PAO1 $\Delta fliC \Delta pilTU$	in-frame deletion of PA1092, PA0395 and PA0396	(204)
PAO1 mNeonGreen	PAO1 constitutively expressing mNeonGreen (attTn7::miniTn7T-Gm-ptet::mNeonGreen)	
PAO1 mScarlet	PAO1 constitutively expressing mScarlet (attTn7::miniTn7T-Gm-ptet::mScarlet)	
PAO1 GFP	PAO1 constitutively expressing GFP (attTn7::miniTn7T2.1-Gm-GW::PA1/04/03::GFP)	
PAO1 $\Delta pilTU$	in-frame deletion of PA0395 and PA0396	(204)
PAO1 $\Delta psiI$	in frame deletion of psiBCD genes	(205)
PAO1 $\Delta pelI$	in frame deletion of pelA genes	(111)
PAO1 PaQa-YFP mKate	PAO1 containing the PaQa reporter plasmid	(50)
PAO1 P _{cdrA} -GFP	PAO1 containing the cdrA reporter plasmid	(184)

Chapter 4. Conclusion

In this thesis I investigated the growth of immersed biofilms on soft hydrogels. The use of synthetic PEGDA gels combined with microfluidics allowed to reproduce key mechanical cues experienced by bacterial cells growing inside human hosts, including fluid flow and the presence of a soft elastic substrate. This platform allowed dynamic visualization at high resolution and magnification of both multicellular and single cell phenotypes such as adhesion, surface motility, gene expression and biofilm expansion. In this work, the flow was simply used to provide a constant and homogeneous influx of nutrients. However, given the abundant literature describing the effect of fluid shear on biofilm formation, we can envision that the simultaneous modulation of both flow and substrate mechanical properties can impact biofilm morphogenesis.

In chapter 2 we demonstrated that biofilms of the pathogens *V. cholerae* and *P. aeruginosa* can deform the soft substrates they grow on. We showed that this behavior is caused by the fact that the biofilm growth is constrained by its adhesion to the non-growing hydrogel substrate: the strain mismatch between the two layers causes the build-up of internal stresses and eventually leads to a buckling instability when a certain threshold is reached. We demonstrated that the material and mechanical properties of the biofilms, defined by the composition and the amount of EPS, are the major contributors for the generation of internal compressive stresses and their transmission to the underlying substrate. Finally, we showed that biofilms can generate forces large enough to bend and damage epithelial cell monolayers.

The fact that substrate deformation was observed for two different species, suggests that this might be a widespread phenomenon. For example, immersed biofilms of *Burkholderia thailandensis* form dome structures when grown on glass, in a mechanism that is dependent on matrix production (206). These structures resemble the ones formed by *P. aeruginosa* in our system and could therefore be associated to a buckling-delamination mechanism. Hence, we can expect that as long as the minimal requirements for the buckling and its transmission to the underlying substrate are met, any bacterial species, pathogenic or not, has the potential to disrupt human tissues. In addition,

the damage could involve even soft abiotic materials, such as soft tissue implants or wound dressings (6, 207–210). Our observations offer a proof of concept for growth-induced material deformations and tissue damage. However, future work should try to elucidate the role played by this phenotype *in vivo*.

Compressive stresses play important functions in the biofilm morphogenesis. The results of the forces generated by expanding biofilms are indeed visible both at the macroscopic level, as in the formation of wrinkles in colonies grown on agar and in confined pellicles, and at the microscopic level, in the orientation and arrangement of single cells. It has been proposed that the formation of wrinkles and channels could enhance the uptake of oxygen and nutrients (135–137). In addition, it has been hypothesized that growing cells could generate a force strong enough to make eukaryotic cells burst from the inside (123, 211). I demonstrated that growth-induced instabilities and forces can directly damage host tissues. In addition, to the best of my knowledge, this is the first time that global mechanical instabilities have been observed in immersed biofilms, or, at least, that they have been recognized as such. This system offers the unique opportunity to dynamically and simultaneously visualize global biofilm mechanical behaviors, such as force generation, wrinkling and delamination, and single cell behaviors such as orientation, growth, matrix production and gene expression. As biofilms are very dynamic structures in space and time, we could use this technique to understand the connection between the macroscopic and the microscopic phenotypes at different stages in their development. How does the remodeling of the matrix (its degradation or a change in its composition) and its localization affect the generation of forces? How does the loss of biofilm mass (at the periphery during erosion, or in the center because of dispersion) influence the substrate deformation? How does growth speed or the mismatch in growth between different metabolic active subpopulations impact the build-up of internal stresses? How does the cell orientation impact the circumferential and the radial stresses and therefore the overall instability pattern? Combining TFM with matrix staining and single cell measurements to develop mechanical models could help answer those questions. In situ characterization of the biofilm mechanical properties, by using techniques

such as microrheology or nanoindentation, could additionally help in gaining a comprehensive understanding of biofilm morphomechanics.

Biofilm-dwelling bacteria, as well as bacteria engulfed by host cells or located inside tissues and secretions, experience compressive forces. Could cells sense and respond to these forces? It has been shown, for example, that *E. coli* grown in confined chambers responds to self-generated compressive forces by increasing matrix production (122). Could compression more generally mediate biofilm formation, dispersion or matrix remodeling? To test whether cells respond to compressive forces, one could grow biofilms within synthetic hydrogels, instead of on top of them. ‘Click chemistry’ is more suitable for cell encapsulation as it offers the advantage of fast, mild and orthogonal reactions compared to the photoinitiated chain polymerization used in my thesis (212). Preliminary results showed that different bacterial species, namely *V. cholerae*, *P. aeruginosa* and *E. coli*, could grow inside hydrogels obtained via thiol-ene photoclickchemistry, proving the cytocompatibility of this method (Figure 4.1). RNA sequencing of cells embedded in hydrogels of different stiffness would reveal which genes are upregulated under stronger compression. The generation of reporter fusion to those genes could also be a way to visualize the stress distribution inside the biofilm.

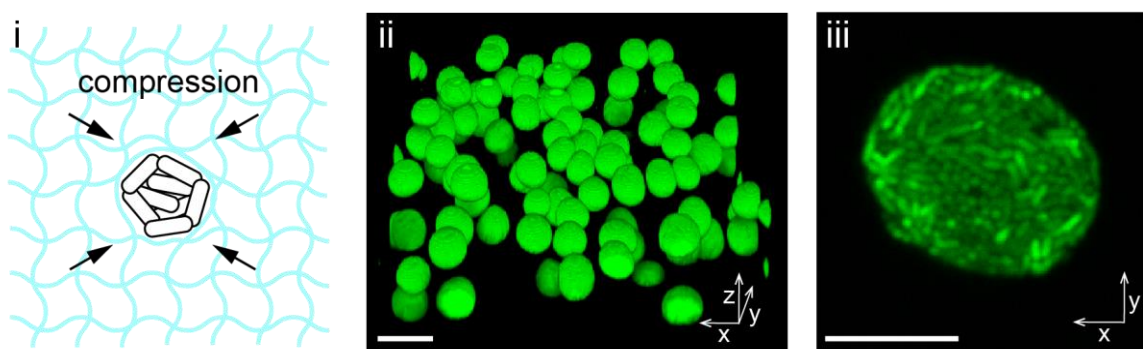


Figure 4.1 Bacterial clusters growing inside PEG hydrogels formed via thiol-ene photoclickchemistry.

(i) Schematic illustration of bacterial clusters growing under compression inside a hydrogel. (ii) 3D reconstruction of clusters of *V. cholerae* and (iii) in-plane view of a cluster of *P. aeruginosa*. Clusters were grown for 16 hr at 37°C inside a gel with $E \sim 1$ kPa. Scale bars: 50 μm for (ii) and 10 μm for (iii). Courtesy of Sourabh Monnappa.

In chapter 3, we showed that the mechanical properties of the substrate can influence twitching motility in *P. aeruginosa*. We found that increasing the substrate modulus by changing the concentration of precursors, boosts surface motility. However, the same trend was observed for hydrogels which display similar modulus, but that are synthesized with precursors of different molecular weight. We showed that cell speed is modulated by the mesh size of the gels, rather than by the elastic modulus, according to a mechanism where the efficiency of cell displacement is dependent on the ‘stickiness’ of the pili to the substrate. The regulation of single-cell twitching behavior impacts the architecture of the biofilm later on. Decreasing the hydrogel mesh size promotes the transition from compact dome-shaped biofilms to flat and dispersed ones, eventually influencing their tolerance to antibiotics and the spatial arrangement of different lineages.

For this study, only the pathogen *P. aeruginosa* was used. A natural follow up would be to investigate the behavior of other twitching species, such as *Neisseria gonorrhoeae*, *Myxococcus xanthus* or *Acinetobacter baumannii*. In addition, to test the generality of mesh-size dependent twitching and biofilm morphogenesis, other materials should be tested. Our results are consistent with studies of bacterial twitching on nanopillared surfaces, where the speed increases with increasing pillar packing density, and therefore higher availability of pili attachment sites (80). It has to be noted that soft materials consist in general of polymeric networks, and therefore present mesh-like surface topographies (18). Elastomers and hydrogels are widely employed in biomedical applications, for example in the production of contact lenses, drug delivery systems, wound dressing and breast implants or as scaffolds for tissue engineering (207–209). All these medical implants are at high risk of biofilm infections. Our results could therefore be relevant for the development of new antifouling strategies.

Our results show that twitching and biofilm morphology are stronger correlated to the mesh size of the substrate, than its modulus. However, we cannot say that the elastic modulus of the substrate does not modulate bacterial behavior. Indeed, in our data we can observe a steeper increase in twitching speed for gels that present both an increase of modulus and a decrease in mesh size, compared to gels where only the mesh size gets smaller. Future work should try to

investigate biofilm morphogenesis on hydrogels with different moduli but comparable mesh size. Even though molecular weight, concentration, mesh size and modulus are strictly related, some studies showed that this is possible. For example, in polyacrylamide gels, an increase in the concentration of crosslinker increases the hydrogel stiffness without significantly perturbing the mesh size (150), while the addition of 4-arm PEG cross-linker allows independent tuning of mesh size and modulus in PEG gels (213).

We showed that mechanosensing is not responsible for the differences in biofilm morphogenesis, as the levels of cAMP and c-di-GMP were comparable across conditions. In addition, differences in cell motility are observed very soon after attachment. We therefore attribute the observed variation in bacterial phenotypes to a purely physical principle. However, it is possible that differences in biofilm structure can modulate cell-cell interactions and gene expression later on. In addition, other mechanosensitive machineries might be activated upon surface attachment. RNA sequencing of cells attached to gels with different mesh sizes and/or moduli can be used to characterize the contribution of mechanics in gene regulation. We also showed that differences in cell body adhesion cannot explain the observed twitching behavior. However, despite the hypothesis that mesh size could control the probability of pili adhesion and adhesion strength, we lack a direct confirmation. The use of techniques like TFM and AFM combined with fluorescent labeling of pili will help in the validation of this theory (56, 214).

Biological tissues are very heterogeneous materials. The tissue bulk modulus results from the mechanical properties of the singular components and their interaction. Cells have a modulus that goes from 0.1 to 10 kPa and have membranes that are fluid in the horizontal plane. ECM, on the other end is composed of fibrillary protein of different thicknesses with moduli above 1 MPa which are embedded in soft matrix of water and biomolecules (7, 114, 215, 216). Bacteria will then experience different elasticities, viscosities and mesh sizes at different locations and at different scales. Therefore, while global biofilm mechanical instabilities might be less sensitive to heterogeneity in the tissues, we cannot say the same thing for phenotypes such as adhesion, motility and surface sensing. In order to really understand how bacteria mechanically interact with their

substrate it is therefore important to control what the bacteria actually experience at different scales, from its nanometer sized appendages, to single cell and biofilm clusters.

Altogether, we showed that the mechanical properties of a substrate can influence biofilm morphogenesis which affects tolerance to antibiotics. Reciprocally, biofilm formation can mechanically impact the substrates, potentially damaging host tissue. Overall, by showing how mechanics can contribute to the development and evolution of the biofilm, as well as to the dynamics of an infection, these results reveal the importance of studying biofilm formation in realistic physical conditions.

References

1. H. C. Flemming, *et al.*, Biofilms: An emergent form of bacterial life. *Nat. Rev. Microbiol.* **14**, 563–575 (2016).
2. H. C. Flemming, J. Wingender, The biofilm matrix. *Nat. Rev. Microbiol.* **8**, 623–633 (2010).
3. L. Hall-Stoodley, J. W. Costerton, P. Stoodley, Bacterial biofilms: from the Natural environment to infectious diseases. *Nat. Rev. Microbiol.* **2**, 95–108 (2004).
4. H. C. Flemming, S. Wuertz, Bacteria and archaea on Earth and their abundance in biofilms. *Nat. Rev. Microbiol.* **17**, 247–260 (2019).
5. Y. F. Dufrêne, A. Persat, Mechanomicrobiology: how bacteria sense and respond to forces. *Nat. Rev. Microbiol.*, 1–14 (2020).
6. O. Ciofu, C. Moser, P. Ø. Jensen, N. Høiby, Tolerance and resistance of microbial biofilms. *Nat. Rev. Microbiol.*, 1–15 (2022).
7. C. F. Guimarães, L. Gasperini, A. P. Marques, R. L. Reis, The stiffness of living tissues and its implications for tissue engineering. *Nat. Rev. Mater.* **5**, 351–370 (2020).
8. C. A. DeForest, K. S. Anseth, Advances in Bioactive Hydrogels to Probe and Direct Cell Fate. *Annu. Rev. Chem. Biomol. Eng.* **3**, 421–444 (2012).
9. B. Ladoux, R. Mège, V I Mechanobiology of collective cell behaviours. *Nat. Publ. Gr.* **18**, 743–757 (2017).
10. K. Uto, J. H. Tsui, C. A. DeForest, D.-H. Kim, Dynamically Tunable Cell Culture Platforms for Tissue Engineering and Mechanobiology. *Prog. Polym. Sci.* **65**, 53–82 (2016).
11. C. Yang, *et al.*, Spatially patterned matrix elasticity directs stem cell fate. *Proc. Natl. Acad. Sci.* **113**, E4439–E4445 (2016).
12. M. A. Wozniak, C. S. Chen, Mechanotransduction in development: a growing role for contractility. *Nat. Rev. Mol. Cell Biol.* **10**, 34–43 (2009).
13. P. K. Chaudhuri, B. C. Low, C. T. Lim, Mechanobiology of Tumor Growth. *Chem. Rev.* **118**, 6499–6515 (2018).
14. K. Sauer, *et al.*, The biofilm life cycle: expanding the conceptual model of biofilm formation. *Nat. Rev. Microbiol.*, 1–13 (2022).
15. S. Zheng, *et al.*, Implication of Surface Properties, Bacterial Motility, and Hydrodynamic Conditions on Bacterial Surface Sensing and Their Initial Adhesion. *Front. Bioeng. Biotechnol.* **9**, 82 (2021).
16. C. Berne, C. K. Ellison, A. Ducret, Y. V. Brun, Bacterial adhesion at the single-cell level. *Nat. Rev. Microbiol.* **16**, 616–627 (2018).
17. K. Yang, *et al.*, Bacterial anti-adhesion surface design: Surface patterning, roughness and wettability: A review. *J. Mater. Sci. Technol.* **99**, 82–100 (2022).
18. Y. Cheng, G. Feng, C. I. Moraru, Micro-and nanotopography sensitive bacterial attachment mechanisms: A review. *Front. Microbiol.* **10**, 191 (2019).
19. F. Song, H. Koo, D. Ren, Effects of material properties on bacterial adhesion and biofilm

- p>formation.
- J. Dent. Res.*
- 94**
- , 1027–1034 (2015).
20. H. H. Tuson, D. B. Weibel, Bacteria-surface interactions. *Soft Matter* **9**, 4368–4380 (2013).
 21. V. Carniello, B. W. Peterson, H. C. van der Mei, H. J. Busscher, Physico-chemistry from initial bacterial adhesion to surface-programmed biofilm growth. *Adv. Colloid Interface Sci.* **261**, 1–14 (2018).
 22. A. Persat, *et al.*, The mechanical world of bacteria. *Cell* **161**, 988–997 (2015).
 23. W. E. Thomas, L. M. Nilsson, M. Forero, E. V. Sokurenko, V. Vogel, Shear-dependent “stick-and-roll” adhesion of type 1 fimbriated *Escherichia coli*. *Mol. Microbiol.* **53**, 1545–1557 (2004).
 24. S. Lecuyer, *et al.*, Shear stress increases the residence time of adhesion of *Pseudomonas aeruginosa*. *Biophys. J.* **100**, 341–350 (2011).
 25. S. Kreve, A. C. D. Reis, Bacterial adhesion to biomaterials: What regulates this attachment? A review. *Jpn. Dent. Sci. Rev.* **57**, 85–96 (2021).
 26. J. J. Martinez, M. A. Mulvey, J. D. Schilling, J. S. Pinkner, S. J. Hultgren, Type 1 pilus-mediated bacterial invasion of bladder epithelial cells. *EMBO J.* **19**, 2803–2812 (2000).
 27. J. S. Mattick, Type IV Pili and Twitching Motility. *Annu. Rev. Microbiol.* **56**, 289–314 (2002).
 28. S. K. Arora, B. W. Ritchings, E. C. Almira, S. Lory, R. Ramphal, The *Pseudomonas aeruginosa* flagellar cap protein, FliD, is responsible for mucin adhesion. *Infect. Immun.* **66**, 1000–1007 (1998).
 29. J. A. Lichter, *et al.*, Substrata mechanical stiffness can regulate adhesion of viable bacteria. *Biomacromolecules* **9**, 1571–1578 (2008).
 30. K. W. Kolewe, S. R. Peyton, J. D. Schiffman, Fewer Bacteria Adhere to Softer Hydrogels. *ACS Appl. Mater. Interfaces* **7**, 19562–19569 (2015).
 31. N. Saha, C. Monge, V. Dulong, C. Picart, K. Glinel, Influence of polyelectrolyte film stiffness on bacterial growth. *Biomacromolecules* **14**, 520–528 (2013).
 32. D. Keskin, O. Mergel, H. C. Van Der Mei, H. J. Busscher, P. Van Rijn, Inhibiting Bacterial Adhesion by Mechanically Modulated Microgel Coatings. *Biomacromolecules* **20**, 243–253 (2019).
 33. H. H. Tuson, L. D. Renner, D. B. Weibel, Polyacrylamide hydrogels as substrates for studying bacteria. *Chem. Commun.* **48**, 1595–1597 (2012).
 34. Y. Wang, *et al.*, Interactions of *Staphylococcus aureus* with ultrasoft hydrogel biomaterials. *Biomaterials* **95**, 74–85 (2016).
 35. F. Song, D. Ren, Stiffness of cross-linked poly(dimethylsiloxane) affects bacterial adhesion and antibiotic susceptibility of attached cells. *Langmuir* **30**, 10354–10362 (2014).
 36. F. Song, *et al.*, How Bacteria Respond to Material Stiffness during Attachment: A Role of *Escherichia coli* Flagellar Motility. *ACS Appl. Mater. Interfaces* **9**, 22176–22184 (2017).
 37. F. Song, H. Wang, K. Sauer, D. Ren, Cyclic-di-GMP and *oprF* are involved in the response of *Pseudomonas aeruginosa* to substrate material stiffness during attachment on polydimethylsiloxane (PDMS). *Front. Microbiol.* **9**, 1–13 (2018).
 38. S. Siddiqui, A. Chandrasekaran, N. Lin, N. Tufenkji, C. Moraes, Microfluidic shear assay to

- distinguish between bacterial adhesion and attachment strength on stiffness-tunable silicone substrates. *Langmuir* **35**, 8840–8849 (2019).
39. H. Straub, *et al.*, Bacterial Adhesion on Soft Materials: Passive Physicochemical Interactions or Active Bacterial Mechanosensing? *Adv. Healthc. Mater.* **8**, 1801323 (2019).
40. J. D. P. Valentin, *et al.*, Substrate viscosity plays an important role in bacterial adhesion under fluid flow. *J. Colloid Interface Sci.* **552**, 247–257 (2019).
41. F. Pan, *et al.*, A nanolayer coating on polydimethylsiloxane surfaces enables a mechanistic study of bacterial adhesion influenced by material surface physicochemistry. *Mater. Horizons* **7**, 93–103 (2020).
42. K. W. Kolewe, J. Zhu, N. R. Mako, S. S. Nonnenmann, J. D. Schiffman, Bacterial Adhesion Is Affected by the Thickness and Stiffness of Poly(ethylene glycol) Hydrogels. *ACS Appl. Mater. Interfaces*, acsami.7b12145 (2018).
43. K. W. Kolewe, S. Kalasin, M. Shave, J. D. Schiffman, M. M. Santore, Mechanical Properties and Concentrations of Poly(ethylene glycol) in Hydrogels and Brushes Direct the Surface Transport of Staphylococcus aureus. *ACS Appl. Mater. Interfaces* **11**, 320–330 (2019).
44. C. Guégan, *et al.*, Alteration of bacterial adhesion induced by the substrate stiffness. *Colloids Surfaces B Biointerfaces* **114**, 193–200 (2014).
45. Q. Peng, *et al.*, Three-Dimensional Bacterial Motions near a Surface Investigated by Digital Holographic Microscopy: Effect of Surface Stiffness. *Langmuir* **35**, 12257–12263 (2019).
46. A. Persat, Bacterial mechanotransduction. *Curr. Opin. Microbiol.* **36**, 1–6 (2017).
47. K. Otto, T. J. Silhavy, Surface sensing and adhesion of Escherichia coli controlled by the Cpx-signaling pathway. *Proc. Natl. Acad. Sci. U. S. A.* **99**, 2287–2292 (2002).
48. L. Rizzello, *et al.*, Molecular response of Escherichia coli adhering onto nanoscale topography. *Nanoscale Res. Lett.* **7**, 575 (2012).
49. G. Alsharif, *et al.*, Host attachment and fluid shear are integrated into a mechanical signal regulating virulence in *Escherichia coli* O157:H7. *Proc. Natl. Acad. Sci.* **112**, 5503–5508 (2015).
50. A. Persat, Y. F. Inclan, J. N. Engel, H. A. Stone, Z. Gitai, Type IV pili mechanochemically regulate virulence factors in *Pseudomonas aeruginosa*. *Proc. Natl. Acad. Sci.* **112**, 7563–7568 (2015).
51. L. O’Neal, *et al.*, The Wsp system of *Pseudomonas aeruginosa* links surface sensing and cell envelope stress. *Proc. Natl. Acad. Sci. U. S. A.* **119**, e2117633119 (2022).
52. C. R. Armbruster, *et al.*, Heterogeneity in surface sensing suggests a division of labor in pseudomonas aeruginosa populations. *Elife* **8** (2019).
53. C. A. Rodesney, *et al.*, Mechanosensing of shear by *Pseudomonas aeruginosa* leads to increased levels of the cyclic-di-GMP signal initiating biofilm development. *Proc. Natl. Acad. Sci.* **114**, 5906–5911 (2017).
54. C. J. Jones, N. Grotewold, D. J. Wozniak, E. S. Gloag, *Pseudomonas aeruginosa* Initiates a Rapid and Specific Transcriptional Response during Surface Attachment. *J. Bacteriol.* **204** (2022).
55. J. E. Sanfilippo, *et al.*, Microfluidic-based transcriptomics reveal force-independent bacterial

- p>
rheosensing.
- Nat. Microbiol.*
- 4**
- , 1274–1281 (2019).
56. M. D. Koch, M. E. Black, E. Han, J. W. Shaevitz, Z. Gitai, *Pseudomonas aeruginosa* distinguishes surfaces by stiffness using retraction of type IV pili. *Proc. Natl. Acad. Sci. U. S. A.* **119**, e2119434119 (2022).
 57. J. Blacutt, Z. Lan, E. M. Cosgriff-Hernandez, V. D. Gordon, Quantitative confocal microscopy and calibration for measuring differences in cyclic-di-GMP signalling by bacteria on biomedical hydrogels. *R. Soc. Open Sci.* **8**, 201453 (2021).
 58. N. Wadhwa, H. C. Berg, Bacterial motility: machinery and mechanisms. *Nat. Rev. Microbiol.* **20**, 161–173 (2022).
 59. L. L. Burrows, *Pseudomonas aeruginosa* Twitching Motility: Type IV Pili in Action. *Annu. Rev. Microbiol.* **66**, 493–520 (2012).
 60. L. Talà, A. Fineberg, P. Kukura, A. Persat, *Pseudomonas aeruginosa* orchestrates twitching motility by sequential control of type IV pili movements. *Nat. Microbiol.* **4**, 774–780 (2019).
 61. C. K. Ellison, *et al.*, Obstruction of pilus retraction stimulates bacterial surface sensing. *Science* **358**, 535–538 (2017).
 62. J. C. Conrad, *et al.*, Flagella and pili-mediated near-surface single-cell motility mechanisms in *P. aeruginosa*. *Biophys. J.* **100**, 1608–1616 (2011).
 63. M. J. Kühn, *et al.*, Mechanotaxis directs *Pseudomonas aeruginosa* twitching motility. *Proc. Natl. Acad. Sci. U. S. A.* **118** (2021).
 64. C. K. Ellison, *et al.*, Retraction of DNA-bound type IV competence pili initiates DNA uptake during natural transformation in *Vibrio cholerae*. *Nat. Microbiol.* **3**, 773–780 (2018).
 65. L. Craig, M. E. Pique, J. A. Tainer, Type IV pilus structure and bacterial pathogenicity. *Nat. Rev. Microbiol.* **2**, 363–378 (2004).
 66. G. A. O'Toole, R. Kolter, Flagellar and twitching motility are necessary for *Pseudomonas aeruginosa* biofilm development. *Mol. Microbiol.* **30**, 295–304 (1998).
 67. T. J. Kirn, M. J. Lafferty, C. M. P. Sandoe, R. K. Taylor, Delineation of pilin domains required for bacterial association into microcolonies and intestinal colonization by *Vibrio cholerae*. *Mol. Microbiol.* **35**, 896–910 (2000).
 68. Y. Shen, A. Siryaporn, S. Lecuyer, Z. Gitai, H. A. Stone, Flow directs surface-attached bacteria to twitch upstream. *Biophys. J.* **103**, 146–151 (2012).
 69. A. Beaussart, *et al.*, Nanoscale adhesion forces of *Pseudomonas aeruginosa* type IV pili. *ACS Nano* **8**, 10723–10733 (2014).
 70. B. Maier, G. C. L. Wong, How Bacteria Use Type IV Pili Machinery on Surfaces. *Trends Microbiol.* **23**, 775–788 (2015).
 71. Y. Li, *et al.*, Extracellular polysaccharides mediate pilus retraction during social motility of *Myxococcus xanthus*. *Proc. Natl. Acad. Sci. U. S. A.* **100**, 5443–5448 (2003).
 72. J. Ribbe, A. E. Baker, S. Euler, G. A. O'Toole, B. Maier, Role of cyclic di-GMP and exopolysaccharide in type IV pilus dynamics. *J. Bacteriol.* **199** (2017).
 73. K. Zhao, *et al.*, Psl trails guide exploration and microcolony formation in *Pseudomonas aeruginosa* biofilms. *Nature* **497**, 388–391 (2013).

74. R. M. Landry, D. An, J. T. Hupp, P. K. Singh, M. R. Parsek, Mucin-Pseudomonas aeruginosa interactions promote biofilm formation and antibiotic resistance. *Mol. Microbiol.* **59**, 142–151 (2006).
75. O. Rzhepishevskaya, *et al.*, The surface charge of anti-bacterial coatings alters motility and biofilm architecture. *Biomater. Sci.* **1**, 589–602 (2013).
76. A. M. Carabelli, *et al.*, Single-Cell Tracking on Polymer Microarrays Reveals the Impact of Surface Chemistry on Pseudomonas aeruginosa Twitching Speed and Biofilm Development. *ACS Appl. Bio Mater.* **3**, 8471–8480 (2020).
77. C. Meel, N. Kouzel, E. R. Oldewurtel, B. Maier, Three-dimensional obstacles for bacterial surface motility. *Small* **8**, 530–534 (2012).
78. Y. R. Chang, E. R. Weeks, D. Barton, J. Dobnikar, W. A. Ducker, Effect of Topographical Steps on the Surface Motility of the Bacterium Pseudomonas aeruginosa. *ACS Biomater. Sci. Eng.* **5**, 6436–6445 (2019).
79. Y. R. Chang, E. R. Weeks, W. A. Ducker, Surface Topography Hinders Bacterial Surface Motility. *ACS Appl. Mater. Interfaces* **10**, 9225–9234 (2018).
80. R. Rosenzweig, *et al.*, Nanopillared Surfaces Disrupt Pseudomonas aeruginosa Mechanoresponsive Upstream Motility. *ACS Appl. Mater. Interfaces* **11**, 10532–10539 (2019).
81. D. L. Higashi, *et al.*, Influence of type IV pilus retraction on the architecture of the Neisseria gonorrhoeae-infected cell cortex. *Microbiology* **155**, 4084–4092 (2009).
82. I. Alarcon, D. J. Evans, S. M. J. Fleiszig, The role of twitching motility in Pseudomonas aeruginosa exit from and translocation of corneal epithelial cells. *Investig. Ophthalmol. Vis. Sci.* **50**, 2237–2244 (2009).
83. V. Nieto, *et al.*, Type IV pili can mediate bacterial motility within epithelial cells. *MBio* **10** (2019).
84. T. Rossy, *et al.*, Pseudomonas aeruginosa contracts mucus to rapidly form biofilms in tissue-engineered human airways. *bioRxiv*, 2022.05.26.493615 (2022).
85. P. Jung Kang, *et al.*, Identification of Pseudomonas aeruginosa genes required for epithelial cell injury. *Mol. Microbiol.* **24**, 1249–1262 (1997).
86. K. H. Turner, J. Everett, U. Trivedi, K. P. Rumbaugh, M. Whiteley, Requirements for Pseudomonas aeruginosa Acute Burn and Chronic Surgical Wound Infection. *PLoS Genet.* **10**, e1004518 (2014).
87. C. Holz, D. Opitz, J. Mehlich, B. J. Ravoo, B. Maier, Bacterial motility and clustering guided by microcontact printing. *Nano Lett.* **9**, 4553–4557 (2009).
88. R. Zhang, L. Ni, Z. Jin, J. Li, F. Jin, Bacteria slingshot more on soft surfaces. *Nat. Commun.* **5**, 1–6 (2014).
89. F. Jin, J. C. Conrad, M. L. Gibiansky, G. C. L. Wong, Bacteria use type-IV pili to slingshot on surfaces. *Proc. Natl. Acad. Sci. U. S. A.* **108**, 12617–12622 (2011).
90. B. Sabass, H. A. Stone, J. W. Shaevitz, Collective force generation by groups of migrating bacteria. **114**, 1–6 (2017).
91. A. N. Simsek, *et al.*, Substrate-rigidity dependent migration of an idealized twitching bacterium. *Soft Matter* **15**, 6224–6236 (2019).

92. S. G. Ho, L. Bureau, K. John, D. Débarre, S. Lecuyer, Substrate stiffness impacts early biofilm formation by modulating *Pseudomonas aeruginosa* twitching motility. *bioRxiv*, 2022.02.18.480999 (2022).
93. C. D. Nadell, K. Drescher, K. R. Foster, Spatial structure, cooperation and competition in biofilms. *Nat. Rev. Microbiol.* **14**, 589–600 (2016).
94. B. Peterson, *et al.*, Viscoelasticity of biofilms and their recalcitrance to mechanical and chemical challenges (2015) <https://doi.org/10.1093/femsre/fuu008>.
95. T. Shaw, M. Winston, C. J. Rupp, I. Klapper, P. Stoodley, Commonality of elastic relaxation times in biofilms. *Phys. Rev. Lett.* **93**, 098102 (2004).
96. V. Berk, *et al.*, Molecular architecture and assembly principles of *Vibrio cholerae* biofilms. *Science* (80-.). **337**, 236–239 (2012).
97. Z. Jiang, T. Nero, S. Mukherjee, R. Olson, J. Yan, Searching for the Secret of Stickiness: How Biofilms Adhere to Surfaces. *Front. Microbiol.* **12**, 1642 (2021).
98. J. Yan, *et al.*, Bacterial Biofilm Material Properties Enable Removal and Transfer by Capillary Peeling. *Adv. Mater.* **30**, 1804153 (2018).
99. E. C. Hollenbeck, *et al.*, Molecular determinants of mechanical properties of *V. cholerae* biofilms at the air-liquid interface. *Biophys. J.* **107**, 2245–2252 (2014).
100. J. Yan, A. G. Sharo, H. A. Stone, N. S. Wingreen, B. L. Bassler, *Vibrio cholerae* biofilm growth program and architecture revealed by single-cell live imaging. *Proc. Natl. Acad. Sci. U. S. A.* **113**, e5337–e5343 (2016).
101. B. J. Cooley, *et al.*, The extracellular polysaccharide Pel makes the attachment of *P. aeruginosa* to surfaces symmetric and short-ranged. *Soft Matter* **9**, 3871–3876 (2013).
102. L. Ma, *et al.*, Assembly and Development of the *Pseudomonas aeruginosa* Biofilm Matrix. *PLoS Pathog.* **5**, e1000354 (2009).
103. K. M. Colvin, *et al.*, The Pel and Psl polysaccharides provide *Pseudomonas aeruginosa* structural redundancy within the biofilm matrix. *Environ. Microbiol.* **14** (2012).
104. L. K. Jennings, *et al.*, Pel is a cationic exopolysaccharide that cross-links extracellular DNA in the *Pseudomonas aeruginosa* biofilm matrix. *Proc. Natl. Acad. Sci. U. S. A.* **112**, 11353–11358 (2015).
105. C. B. Whitchurch, T. Tolker-nielsen, P. C. Ragas, J. S. Mattick, Extracellular DNA Required for Bacterial Biofilm Formation <https://doi.org/10.1126/science.295.5559.1487>.
106. E. Secchi, *et al.*, The structural role of bacterial eDNA in the formation of biofilm streamers. *Proc. Natl. Acad. Sci. U. S. A.* **119**, e2113723119 (2022).
107. C. Reichhardt, C. Wong, D. P. da Silva, D. J. Wozniak, M. R. Parsek, CDRA interactions within the *pseudomonas aeruginosa* biofilm matrix safeguard it from proteolysis and promote cellular packing. *MBio* **9** (2018).
108. C. Reichhardt, *et al.*, The Versatile *Pseudomonas aeruginosa* Biofilm Matrix Protein CdrA Promotes Aggregation through Different Extracellular Exopolysaccharide Interactions. *J. Bacteriol.* **202** (2020).
109. K. Kovach, *et al.*, Evolutionary adaptations of biofilms infecting cystic fibrosis lungs promote

- p>mechanical toughness by adjusting polysaccharide production.
- npj Biofilms Microbiomes*
- 3**
- , 0–1 (2017).
110. M. U. Rahman, *et al.*, Effect of collagen and EPS components on the viscoelasticity of *Pseudomonas aeruginosa* biofilms. *Soft Matter* **17**, 6225–6237 (2021).
 111. M. Starkey, *et al.*, *Pseudomonas aeruginosa* Rugose small-colony variants have adaptations that likely promote persistence in the cystic fibrosis lung. *J. Bacteriol.* **191**, 3492–3503 (2009).
 112. J. Sneyd, G. Theraula, E. Bonabeau, J.-L. Deneubourg, N. R. Franks, *Self-Organization in Biological Systems* (Princeton University Press, 2001) <https://doi.org/10.1515/9780691212920> (August 24, 2022).
 113. M. Asally, *et al.*, Localized cell death focuses mechanical forces during 3D patterning in a biofilm. *Proc. Natl. Acad. Sci.* **109**, 18891–18896 (2012).
 114. C. Even, *et al.*, Recent advances in studying single bacteria and biofilm mechanics. *Adv. Colloid Interface Sci.* **247**, 573–588 (2017).
 115. R. Hartmann, *et al.*, Emergence of three-dimensional order and structure in growing biofilms. *Nat. Phys.* **15**, 251–256 (2019).
 116. M. A. A. Grant, B. Waław, R. J. Allen, P. Cicuta, The role of mechanical forces in the planar-to-bulk transition in growing *Escherichia coli* microcolonies. *J. R. Soc. Interface* **11**, 20140400 (2014).
 117. M. C. Duvernoy, *et al.*, Asymmetric adhesion of rod-shaped bacteria controls microcolony morphogenesis. *Nat. Commun.* **9**, 25–28 (2018).
 118. K. Drescher, *et al.*, Architectural transitions in *Vibrio cholerae* biofilms at single-cell resolution. *Proc. Natl. Acad. Sci. U. S. A.* **113**, E2066–E2072 (2016).
 119. B. Qin, *et al.*, Cell position fates and collective fountain flow in bacterial biofilms revealed by light-sheet microscopy. *Science (80-.)*. **369**, 71–77 (2020).
 120. F. Beroz, *et al.*, Verticalization of bacterial biofilms. *Nat. Phys.* **14**, 954–960 (2018).
 121. F. Díaz-Pascual, *et al.*, Breakdown of *Vibrio cholerae* biofilm architecture induced by antibiotics disrupts community barrier function. *Nat. Microbiol.* **4**, 2136–2145 (2019).
 122. E. K. Chu, O. Kilic, H. Cho, A. Groisman, A. Levchenko, Self-induced mechanical stress can trigger biofilm formation in uropathogenic *Escherichia coli*. *Nat. Commun.* **9**, 1–10 (2018).
 123. M. Delarue, *et al.*, Self-driven jamming in growing microbial populations. *Nat. Phys.* **12**, 762–766 (2016).
 124. S. C. Chew, *et al.*, Mechanical signatures of microbial biofilms in micropillar-embedded growth chambers. *Soft Matter* **12**, 5224–5232 (2016).
 125. C. Douarche, J. M. Allain, E. Raspaud, *Bacillus subtilis* Bacteria Generate an Internal Mechanical Force within a Biofilm. *Biophys. J.* **109**, 2195–2202 (2015).
 126. M. Trejo, *et al.*, Elasticity and wrinkled morphology of *Bacillus subtilis* pellicles. *Proc. Natl. Acad. Sci. U. S. A.* **110**, 2011–2016 (2013).
 127. C. Zhang, B. Li, X. Feng, Experimental and theoretical studies on the morphogenesis of bacterial biofilms. 7389–7397 (2017).

128. C. Zhang, B. Li, X. Huang, Y. Ni, X. Q. Feng, Morphomechanics of bacterial biofilms undergoing anisotropic differential growth. *Appl. Phys. Lett.* **109**, 143701 (2016).
129. D. R. Espeso, A. Carpio, B. Einarsson, Differential growth of wrinkled biofilms. *Phys. Rev. E - Stat. Nonlinear, Soft Matter Phys.* **91**, 022710 (2015).
130. M. Ben Amar, M. Wu, Patterns in biofilms: From contour undulations to fold focussing. *EPL* **108**, 38003 (2014).
131. Q. Wang, X. Zhao, A three-dimensional phase diagram of growth-induced surface instabilities. *Sci. Rep.* **5**, 1–10 (2015).
132. J. Yan, *et al.*, Mechanical instability and interfacial energy drive biofilm morphogenesis. *Elife* **8** (2019).
133. C. Fei, *et al.*, Nonuniform growth and surface friction determine bacterial biofilm morphology on soft substrates. *Proc. Natl. Acad. Sci. U. S. A.* **117**, 7622–7632 (2020).
134. D. O. Serra, A. M. Richter, R. Hengge, Cellulose as an architectural element in spatially structured escherichia coli biofilms. *J. Bacteriol.* **195**, 5540–5554 (2013).
135. C. Okegbe, A. Price-Whelan, L. E. P. Dietrich, Redox-driven regulation of microbial community morphogenesis (Elsevier Ltd, 2014).
136. J. N. Wilking, *et al.*, Liquid transport facilitated by channels in *Bacillus subtilis* biofilms. *Proc. Natl. Acad. Sci.* **110**, 848–852 (2013).
137. C. P. Kempes, C. Okegbe, Z. Mears-Clarke, M. J. Follows, L. E. P. Dietrich, Morphological optimization for access to dual oxidants in biofilms. *Proc. Natl. Acad. Sci. U. S. A.* **111**, 208–213 (2014).
138. M. Whiteley, *et al.*, Gene expression in *Pseudomonas aeruginosa* biofilms. *Nature* **413**, 860–864 (2001).
139. J. Yan, C. D. Nadell, H. A. Stone, N. S. Wingreen, B. L. Bassler, Extracellular-matrix-mediated osmotic pressure drives *Vibrio cholerae* biofilm expansion and cheater exclusion. *Nat. Commun.* **8**, 1–11 (2017).
140. N. Rivera-Yoshida, J. A. Arias Del Angel, M. Benítez, Microbial multicellular development: mechanical forces in action. *Curr. Opin. Genet. Dev.* **51**, 37–45 (2018).
141. K. Drescher, C. D. Nadell, H. A. Stone, N. S. Wingreen, B. L. Bassler, Solutions to the Public Goods Dilemma in Bacterial Biofilms. *Curr. Biol.* **24**, 50–55 (2014).
142. R. Rusconi, S. Lecuyer, L. Guglielmini, H. A. Stone, Laminar flow around corners triggers the formation of biofilm streamers. *J. R. Soc. Interface* **7**, 1293–1299 (2010).
143. C. D. Nadell, D. Ricaurte, J. Yan, K. Drescher, B. L. Bassler, Flow environment and matrix structure interact to determine spatial competition in *Pseudomonas aeruginosa* biofilms. *Elife* **6** (2017).
144. T. Rossy, C. D. Nadell, A. Persat, Cellular advective-diffusion drives the emergence of bacterial surface colonization patterns and heterogeneity. *Nat. Commun.* **10** (2019).
145. M. Klausen, *et al.*, Biofilm formation by *Pseudomonas aeruginosa* wild type, flagella and type IV pili mutants. *Mol. Microbiol.* **48**, 1511–1524 (2003).
146. P. K. Singh, M. R. Parsek, E. P. Greenberg, M. J. Welsh, A component of innate immunity

prevents bacterial biofilm development. *Nature* **417**, 552–555 (2002).

147. S. Geisel, E. Secchi, J. Vermant, The role of surface adhesion on the macroscopic wrinkling of biofilms. *Elife* **11** (2022).
148. R. Martínez-García, C. D. Nadell, R. Hartmann, K. Drescher, J. A. Bonachela, Cell adhesion and fluid flow jointly initiate genotype spatial distribution in biofilms. *PLOS Comput. Biol.* **14**, e1006094 (2018).
149. T. Rossy, C. D. Nadell, A. Persat, Cellular advective-diffusion drives the emergence of bacterial surface colonization patterns and heterogeneity. *bioRxiv*, 434167 (2018).
150. M. E. Asp, *et al.*, Spreading rates of bacterial colonies depend on substrate stiffness and permeability. *PNAS Nexus* **1** (2022).
151. A. Seminara, *et al.*, Osmotic spreading of *Bacillus subtilis* biofilms driven by an extracellular matrix. *Proc. Natl. Acad. Sci. U. S. A.* **109**, 1116–1121 (2012).
152. A. Cont, T. Rossy, Z. Al-Mayyah, A. Persat, Biofilms deform soft surfaces and disrupt epithelia. *Elife* **9**, 1–22 (2020).
153. G. O'Toole, H. B. Kaplan, R. Kolter, Biofilm Formation as Microbial Development. *Annu. Rev. Microbiol.* **54**, 49–79 (2000).
154. T.-F. C. Mah, G. A. O'Toole, Mechanisms of biofilm resistance to antimicrobial agents. *Trends Microbiol.* **9**, 34–39 (2001).
155. R. M. Donlan, J. W. Costerton, Biofilms: Survival mechanisms of clinically relevant microorganisms. *Clin. Microbiol. Rev.* **15**, 167–193 (2002).
156. T. Bjarnsholt, *et al.*, The in vivo biofilm. *Trends Microbiol.* **21**, 466–474 (2013).
157. R. De Weirde, T. Van De Wiele, Micromanagement in the gut: Microenvironmental factors govern colon mucosal biofilm structure and functionality. *npj Biofilms Microbiomes* **1**, 15026 (2015).
158. J. Toyjanova, *et al.*, High resolution, large deformation 3D traction force microscopy. *PLoS One* **9**, e90976 (2014).
159. J. K. Teschler, *et al.*, Living in the matrix: assembly and control of *Vibrio cholerae* biofilms. *Nat. Rev. Microbiol.* **13**, 255–268 (2015).
160. F. H. Yildiz, G. K. Schoolnik, *Vibrio cholerae* O1 El Tor: Identification of a gene cluster required for the rugose colony type, exopolysaccharide production, chlorine resistance, and biofilm formation. *Proc. Natl. Acad. Sci. U. S. A.* **96**, 4028–4033 (1999).
161. M. J. Pestrak, *et al.*, *Pseudomonas aeruginosa* rugose small-colony variants evade host clearance, are hyper-inflammatory, and persist in multiple host environments. *PLOS Pathog.* **14**, e1006842 (2018).
162. E. R. Rojas, K. C. Huang, Regulation of microbial growth by turgor pressure. *Curr. Opin. Microbiol.* **42**, 62–70 (2018).
163. G. Charras, A. S. Yap, Tensile Forces and Mechanotransduction at Cell–Cell Junctions. *Curr. Biol.* **28**, R445–R457 (2018).
164. D. E. Discher, P. Janmey, Y. L. Wang, Tissue cells feel and respond to the stiffness of their substrate. *Science (80-.).* **310**, 1139–1143 (2005).

165. S. Lee, X. Tong, F. Yang, The effects of varying poly(ethylene glycol) hydrogel crosslinking density and the crosslinking mechanism on protein accumulation in three-dimensional hydrogels. *Acta Biomater.* **10**, 4167–4174 (2014).
166. A. D. Tischler, A. Camilli, Cyclic diguanylate regulates *Vibrio cholerae* virulence gene expression. *Infect. Immun.* **73**, 5873–82 (2005).
167. A. R. Harris, *et al.*, Characterizing the mechanics of cultured cell monolayers. *Proc. Natl. Acad. Sci. U. S. A.* **109**, 16449–16454 (2012).
168. S. Timoshenko, J. M. Gere, *Theory of elastic stability* (Dover Publications, 2009) (December 6, 2019).
169. C. Y. Wang, On the Buckling of a Circular Plate on an Elastic Foundation. *J. Appl. Mech.* **72**, 795–796 (2005).
170. D. O. Serra, G. Klauck, R. Hengge, Vertical stratification of matrix production is essential for physical integrity and architecture of macrocolony biofilms of *Escherichia coli*. *Environ. Microbiol.* **17**, 5073–5088 (2015).
171. E. S. Gloag, G. K. German, P. Stoodley, D. J. Wozniak, Viscoelastic properties of *Pseudomonas aeruginosa* variant biofilms. *Sci. Rep.* **8**, 1–11 (2018).
172. S. C. Bischoff, *et al.*, Intestinal permeability - a new target for disease prevention and therapy. *BMC Gastroenterol.* **14** (2014).
173. T. M. Bartlett, *et al.*, A Periplasmic Polymer Curves *Vibrio cholerae* and Promotes Pathogenesis. *Cell* **168**, 172-185.e15 (2017).
174. A. Swidsinski, *et al.*, Presence of a Polymicrobial Endometrial Biofilm in Patients with Bacterial Vaginosis. *PLoS One* **8**, e53997 (2013).
175. L. Hardy, *et al.*, A fruitful alliance: The synergy between *Atopobium vaginae* and *Gardnerella vaginalis* in bacterial vaginosis-associated biofilm. *Sex. Transm. Infect.* **92**, 487–491 (2016).
176. P. Engel, K. D. Bartlett, N. A. Moran, The Bacterium *Frischella perrara* Causes Scab Formation in the Gut of its Honeybee Host. *MBio* **6**, e00193-15 (2015).
177. C. Chelakkot, J. Ghim, S. H. Ryu, Mechanisms regulating intestinal barrier integrity and its pathological implications. *Exp. Mol. Med.* **50**, 1–9 (2018).
178. R. Ahmad, M. F. Sorrell, S. K. Batra, P. Dhawan, A. B. Singh, Gut permeability and mucosal inflammation: Bad, good or context dependent. *Mucosal Immunol.* **10**, 307–317 (2017).
179. V. Tremaroli, F. Bäckhed, Functional interactions between the gut microbiota and host metabolism. *Nature* **489**, 242–249 (2012).
180. J. C. N. Fong, K. Karplus, G. K. Schoolnik, F. H. Yildiz, Identification and characterization of RbmA, a novel protein required for the development of rugose colony morphology and biofilm structure in *Vibrio cholerae*. *J. Bacteriol.* **188**, 1049–59 (2006).
181. T. Takigawa, Y. Morino, K. Urayama, T. Masuda, Poisson's Ratio of Polyacrylamide (PAAm) Gels. *Polym. Gels Networks* **4**, 1–5 (1996).
182. K. Helene Thelin, R. K. Taylor, Toxin-coregulated pilus, but not mannose-sensitive hemagglutinin, is required for colonization by *Vibrio cholerae* O1 El Tor biotype and O139 strains. *Infect. Immun.* **64**, 2853–2856 (1996).

183. J. W. Hickman, D. F. Tifrea, C. S. Harwood, A chemosensory system that regulates biofilm formation through modulation of cyclic diguanylate levels. *Proc. Natl. Acad. Sci. U. S. A.* **102**, 14422–7 (2005).
184. M. T. Rybtke, *et al.*, Fluorescence-based reporter for gauging cyclic di-GMP levels in *Pseudomonas aeruginosa*. *Appl. Environ. Microbiol.* **78**, 5060–9 (2012).
185. M. Rybtke, *et al.*, The LapG protein plays a role in *Pseudomonas aeruginosa* biofilm formation by controlling the presence of the CdrA adhesin on the cell surface. *Microbiologyopen* **4**, 917–930 (2015).
186. J. C. N. Fong, K. A. Syed, K. E. Klose, F. H. Yildiz, Role of *Vibrio* polysaccharide (vps) genes in VPS production, biofilm formation and *Vibrio cholerae* pathogenesis. *Microbiology* **156**, 2757–2769 (2010).
187. J. C. N. Fong, F. H. Yildiz, The *rbmBCDEF* gene cluster modulates development of rugose colony morphology and biofilm formation in *Vibrio cholerae*. *J. Bacteriol.* **189**, 2319–2330 (2007).
188. A. Cont, J. Vermeil, A. Persat, Mechanoregulation of biofilm architecture promotes *P. aeruginosa* antibiotic tolerance. *bioRxiv*, 2022.02.16.480709 (2022).
189. M. D. Koch, E. Han, J. W. Shaevitz, Z. Gitai, *Pseudomonas aeruginosa* differentiates substrate rigidity using retraction of type IV pili. *bioRxiv*, 2021.08.26.457786 (2021).
190. Y. W. Chang, *et al.*, Architecture of the type IVa pilus machine. *Science (80-.)*. **351** (2016).
191. D. Davies, Understanding biofilm resistance to antibacterial agents. *Nat. Rev. Drug Discov.* **2**, 114–122 (2003).
192. S. Azimi, G. R. Lewin, M. Whiteley, The biogeography of infection revisited. *Nat. Rev. Microbiol.*, 1–14 (2022).
193. S. G. Ho, L. Bureau, K. John, D. Débarre, S. Lecuyer, Substrate stiffness impacts early biofilm formation via a modulation of twitching motility. *bioRxiv*, 2022.02.18.480999 (2022).
194. E. Rossi, *et al.*, *Pseudomonas aeruginosa* adaptation and evolution in patients with cystic fibrosis. *Nat. Rev. Microbiol.* **19**, 331–342 (2021).
195. R. J. Cannara, M. Eglin, R. W. Carpick, Lateral force calibration in atomic force microscopy: A new lateral force calibration method and general guidelines for optimization. *Rev. Sci. Instrum.* **77**, 053701 (2006).
196. J. E. Sader, J. W. M. Chon, P. Mulvaney, Calibration of rectangular atomic force microscope cantilevers. *Rev. Sci. Instrum.* **70**, 3967–3969 (1999).
197. H. Hertz, Ueber die Berührung fester elastischer Körper. *J. für die Reine und Angew. Math.* **1882**, 156–171 (1882).
198. , Surface energy and the contact of elastic solids. *Proc. R. Soc. London. A. Math. Phys. Sci.* **324**, 301–313 (1971).
199. M. S. Rehmann, *et al.*, Tuning and Predicting Mesh Size and Protein Release from Step Growth Hydrogels. *Biomacromolecules* **18**, 3131–3142 (2017).
200. N. A. Peppas, P. Bures, W. Leobandung, H. Ichikawa, Hydrogels in pharmaceutical formulations. *Eur. J. Pharm. Biopharm.* **50**, 27–46 (2000).

201. J. Bruzaud, *et al.*, Flagella but not type IV pili are involved in the initial adhesion of *Pseudomonas aeruginosa* PAO1 to hydrophobic or superhydrophobic surfaces. *Colloids Surfaces B Biointerfaces* **131**, 59–66 (2015).
202. J. A. Beamish, J. Zhu, K. Kottke-Marchant, R. E. Marchant, The effects of monoacrylated poly(ethylene glycol) on the properties of poly(ethylene glycol) diacrylate hydrogels used for tissue engineering. *J. Biomed. Mater. Res. Part A* **9999A**, NA-NA (2009).
203. B. W. Holloway, A. F. Morgan, Genome Organization in *Pseudomonas*. *Annu. Rev. Microbiol.* **40**, 79–105 (1986).
204. J. J. Bertrand, J. T. West, J. N. Engel, Genetic analysis of the regulation of type IV pilus function by the Chp chemosensory system of *Pseudomonas aeruginosa*. *J. Bacteriol.* **192**, 994–1010 (2010).
205. M. J. Kirisits, L. Prost, M. R. Parsek, Characterization of Colony Morphology Variants Isolated from. *Am. Soc. Microbiol.* **71**, 4809–4821 (2005).
206. B. S. Tseng, *et al.*, Quorum sensing influences *Burkholderia thailandensis* biofilm development and matrix production. *J. Bacteriol.* **198**, 2643–2650 (2016).
207. B. V. Slaughter, S. S. Khurshid, O. Z. Fisher, A. Khademhosseini, N. A. Peppas, Hydrogels in Regenerative Medicine. *Adv. Mater.* **21**, 3307–3329 (2009).
208. E. Caló, V. V. Khutoryanskiy, Biomedical applications of hydrogels: A review of patents and commercial products. *Eur. Polym. J.* **65**, 252–267 (2015).
209. R. Yoda, Elastomers for biomedical applications. *J. Biomater. Sci. Polym. Ed.* **9**, 561–626 (1998).
210. D. Ajdic, Y. Zoghbi, D. Gerth, Z. J. Panthaki, S. Thaller, The relationship of bacterial biofilms and capsular contracture in breast implants. *Aesthetic Surg. J.* **36**, 297–309 (2016).
211. M. Steinacher, A. Cont, H. Du, A. Persat, E. Amstad, Monodisperse Selectively Permeable Hydrogel Capsules Made from Single Emulsion Drops. *ACS Appl. Mater. Interfaces* **13**, 15601–15609 (2021).
212. T. E. Brown, K. S. Anseth, Spatiotemporal hydrogel biomaterials for regenerative medicine. *Chem. Soc. Rev.* **46**, 6532–6552 (2017).
213. M. B. Browning, T. Wilems, M. Hahn, E. Cosgriff-Hernandez, Compositional control of poly(ethylene glycol) hydrogel modulus independent of mesh size. *J. Biomed. Mater. Res. - Part A* **98 A**, 268–273 (2011).
214. F. Alam, S. Kumar, K. M. Varadarajan, Quantification of Adhesion Force of Bacteria on the Surface of Biomaterials: Techniques and Assays. *ACS Biomater. Sci. Eng.* **5**, 2093–2110 (2019).
215. K. E. Kasza, *et al.*, The cell as a material. *Curr. Opin. Cell Biol.* **19**, 101–107 (2007).
216. J. T. Groves, Membrane Mechanics in Living Cells. *Dev. Cell* **48**, 15–16 (2019).

Curriculum Vitae

Alice Cont

alice.cont@epfl.ch | +41 786599077
 Chemin de Grand-Vennes 19, CH-1010 Lausanne
 Date of birth: 03/06/1992 | Nationality: Italian

WORKING AND RESEARCH EXPERIENCES

11/2017-Present Lausanne, Switzerland	PhD candidate École Polytechnique Fédérale de Lausanne (EPFL) Research unit: <i>Laboratory of microbial mechanics</i> Supervisor: Alexandre Persat <u>Title</u> : Biofilm morphogenesis on soft hydrogels
01/2017-03/2017 Singapore	Visiting researcher Nanyang Technological University (NTU) Research unit: <i>Laboratory for Biological and Biomimetic Materials</i>
02/2016-08/2016 Lausanne, Switzerland	Master thesis and research assistant École Polytechnique Fédérale de Lausanne (EPFL) Research unit: <i>Soft Materials Laboratory</i> Supervisor: Esther Amstad <u>Title</u> : 2D colloidal crystals made from hydrogel microparticles
08/2015 – 01/2016 St. Gallen, Switzerland	Research intern Swiss Federal Laboratories for Materials Science and Technology (EMPA) Research unit: <i>Laboratory for biomimetic membranes and textiles</i>

EDUCATION

11/2017-Present Lausanne, Switzerland	PhD in materials science École Polytechnique Fédérale de Lausanne (EPFL)
09/2014 – 07/2016 Lausanne, Switzerland	MSc in materials science and engineering - 5.62/6 École Polytechnique Fédérale de Lausanne (EPFL) Orientation: Materials for biotechnological and medical applications
10/2011 - 07/2014 Padova, Italy	BSc in materials science - 110/110 cum Laude Università degli Studi di Padova
09/2006 - 07/2011 Trento, Italy	Scientific high school diploma - 100/100 cum Laude Liceo Scientifico e Linguistico Leonardo Da Vinci

LANGUAGES AND IT

- Italian: native language
- English: fluent
- French: elementary
- German: elementary
- IT: MS Office, Python, ImageJ, OriginLab

PUBLICATIONS

Cont A., Vermeil J., Persat A. *Mechanoregulation of biofilm architecture promotes *Pseudomonas aeruginosa* antibiotic tolerance*. bioRxiv, 2022

Steinacher M., **Cont A.**, Du H., Persat A., Amstad E. *Monodisperse Selectively Permeable Hydrogel Capsules Made from Single Emulsion Drops*. ACS Applied Materials & Interfaces, 2021

Cont A., Rossy T., Al-Mayyah Z., Persat A. *Biofilms deform soft surfaces and disrupt epithelia*, eLife, 2020

Faccio G., **Cont, A.**, Mailand E., Zare-Eelanjegh E., Innocenti Malini R., Maniura-Weber K., Rossi R. & Spano F. *Complete inclusion of bioactive molecules and particles in polydimethylsiloxane: a straightforward process under mild conditions*. Scientific reports, 2019

Du, H.†, **Cont, A.**†, Steinacher, M., Amstad, E. *Fabrication of hexagonal-prismatic granular hydrogel sheets*. Langmuir, 2018 (†Equally contributed)

PRESENTATIONS

EDMX Research Day, 2022, Lausanne, Switzerland: poster (awarded best poster)

ASCB | EMBO Meeting: CELL BIO virtual, 2021: talk.

EDMX Research Day, 2021, Lausanne, Switzerland: talk

The 8th ASM Conference on Biofilms, 2018, Washington, DC: poster

EMBO | EMBL Symposium: New Approaches and Concepts in Microbiology, 2019, Heidelberg, Germany: poster

PERSONAL INTERESTS

- Pottery
- Gardening